Departamento de Computación

Tumor growth analysis using cellular automata based on the cancer hallmarks

PhD Thesis

Tese de doutoramento

Ángel Monteagudo Insua

2015

UNIVERSIDADE DA CORUÑA

PHD THESIS

Tumor growth analysis using cellular automata based on the cancer hallmarks

Ángel Monteagudo Insua

PhD supervisor:
Dr. José Santos Reyes

Thesis committee:

Dr. Amparo Alonso Betanzos
Dr. Rafael Lahoz Beltrá
Dr. Miguel Angel Fernández Graciani

D. José Santos Reyes, Profesor Titular de Universidad en el área de Ciencias de la Computación e Inteligencia Artificial de la Universidade da Coruña

CERTIFICA

Que la presente memoria titulada **Tumor growth analysis using cellular automata based on the cancer hallmarks** fue realizada bajo su dirección y constituye la Tesis que presenta **D. Ángel Monteagudo Insua** para optar al grado de Doctor por la Universidade da Coruña.

A Coruña, diciembre de 2015

Firmado: Dr. José Santos Reyes
Director de la Tesis

"Modern biology encourages us to imagine the cell as a molecular machine. Cancer is that machine unable to quench its initial command (to grow) and thus transformed into an indestructible, self-propelled automaton."
Dr. Siddartha Mukherjee, The Emperor of all Maladies: A Biography of Cancer. 2010.

Acknowledgments

I would like to mention, in the first place, my supervisor José Santos Reyes for letting me have the opportunity to do this PhD thesis. Thanks for all the help, suggestions and supervision during these years.

I want to thank the staff at the *Oncology Center of Galicia* for the technical advice and discussions about all the aspects of the modeling performed in the thesis.

I especially thank the members of our Lab in the Computer Science Department, and specially those with which I have shared the Lab these years, Martín, Edu, Javier, Víctor, Rodrigo, Dani, as well as the rest of the members for all the help and good moments.

This research has been supported by grants from the Government of Spain (Projects TIN2013-40981-R and TIN2011-27294).

Finally, I would like to dedicate this work to my family and friends, who sail with me on this strange and wonderful journey.

Abstract

In this thesis we used computational models based on cellular automata and the abstract model of cancer hallmarks to analyze the emergent behavior of tumor growth at cellular level. Tumor growth is modeled with a cellular automaton which determines cell mitotic and apoptotic behaviors. These behaviors depend on the cancer hallmarks acquired in each cell as consequence of mutations. The presence of the cancer hallmarks defines cell states and cell mitotic behaviors. Additionally, these hallmarks are associated with a series of parameters, and depending on their values and the activation of the hallmarks in each of the cells, the system can evolve to different dynamics.

With the simulation tool we performed an analysis of the first phases of cancer growth. Firstly, we studied the evolution of cancer cells and hallmarks in different representative situations regarding initial conditions and parameters, analyzing the relative importance of the hallmarks for tumor progression; Secondly, we focused on the analysis of the effect of killing cancer cells, inspecting the time evolution of the multicellular system under such conditions and the possible behavioral transitions between the predominance of cancer and healthy cells.

Later, we analyzed the effect of treatment applications on cancer growth taking into account the presence of Cancer Stem Cells (CSCs) and their regrowth capacity. Finally, we used evolutionary computing to analyze the implications of treatment strategies in a CSC context. In this way, we determined the best strategies of treatment applications in terms of intensity, duration and periodicity considering the regrowth capacity of CSCs.

Table of contents

List of Tables

List of Figures

Chapter 1

Introduction

1.1 Motivation

The thesis deals with the modeling of tumor growth, considering this as an emergent consequence of the interactions between cells and their environment. The state of a cell will depend on a number of characteristic features of cancer and its immediate surroundings, which defines the state of a cell and its mitotic behavior.

Cancer is currently considered a very complex phenomenon consistent of numerous and different diseases, each of them with different and multifactorial causes (being the genetic ones only one type among others such as environmental, occupational, nutritional or even viral). Although there are more than 200 different types of cancer that can affect every organ in the body, they share certain features. Thus, Hanahan and Weinberg described the phenotypic differences between healthy and cancer cells in a landmark article entitled "The Hallmarks of Cancer" [39]. The six essential alterations in cell physiology that collectively dictate malignant growth are: self-sufficiency in growth signals, insensitivity to growth inhibitory signals, evasion of programmed cell death (apoptosis), limitless replicative potential, sustained angiogenesis, and tissue invasion and metastasis, that are detailed later.

This thesis will consider this model of hallmarks, thus placing us in the study of the multicellular system behavior at the cellular level, without the need of a detailed knowledge of the molecular, genetic or epigenetic lower levels. That is, our modeling considers this abstract scheme that takes into account the presence of the hallmarks acquired by the cells. This abstract model is sufficient for our aim focused on the analysis of the behavior of the multicellular system at that cellular level. But given the interrelations among the hallmarks and their dependence on their defining parameters (like hallmark mutation probability, initial telomere length, ... described later), the behavior obtained in the multicellular system is impossible to infer intuitively or analytically. This modeling can help us to test novel hypotheses, confirm *in vitro* experiments and simulate the dynamics of complex systems in a relatively fast time without the enormous costs of laboratory experiments.

One of the traditional approaches to model cancer growth was the use of

differential equations to describe avascular, and indeed vascular, tumor growth [76]. For example, the kinetic models of clonal expansion [7][21][103] allowed to include and analyze specific cancer conditions. As indicated by Wodarz and Komarova [102], referring to the modeling with ordinary differential equations (ODE) "Among the advantages is its simplicity. The disadvantages include the absence of detail. For instance, no spatial interactions can be described by ODEs, thus imposing the assumption of mass-action-type interactions". Moreover, as indicated by Enderling et al. [24] these approaches tend to represent tumor cells collectively by a single proliferation term and a death term, including more optional specialized functionalities like interaction of tumor cells with their local environment [24]. Also, many models presuppose that all cancer cells have acquired the same hallmarks. Moreover, if partial differential equations (PDE) are used, as the again Wodarz and Komarova state "there is one obvious limitation of PDEs which comes from the very nature of differential equations: they describe continuous functions. If the cellular structure of an organ is important, then we need to use a different method" [102].

Cancer can be viewed, from the standpoint of the Artificial Life discipline [2][52], as an ecological system in which cells with different mutations compete for survival [94]. Moreover, tumor growth in multicellular systems is an example of emergent behavior, which is present in systems whose elements interact locally, providing global behavior which is not possible to explain from the behavior of a single element, but rather from the "emergent" consequence among the interactions of the group [2][52]. In this case, it is an emergent consequence of the local interactions between the cells and their environment. Emergent behavior was studied in Artificial Life and Complex Systems Theory [2][52] using models like Cellular Automata (CA) and Lindenmayer Systems [46][51][52]. CA have been the focus of attention because of their ability to generate a rich spectrum of complex behavior patterns out of sets of relatively simple underlying rules and they appeared to capture many essential features of complex self-organizing cooperative behavior observed in real systems [46].

The advantage of the CA models is that these can directly incorporate the rules that define the mitotic and apoptotic behaviors from the direct definition of the hallmarks. As indicated by Basanta et al. [11] "CA models allow the study of emergent processes in which space is an important feature and in which the behavior of individual agents can be described by rules". This is the case in the modeling of the rules of apoptotic and mitotic behaviors based on the presence of cancer cell hallmarks. There are also hybrid approaches in which the automaton combines discrete and continuous fields (modeled with ODEs), such as the work by Ribba el al. [82] using a hybrid cellular automaton, which incorporates nutrient and drug spatial distribution (these modeled with differential equations). As our aim is to model cell behavior at cellular level based on the presence of the hallmarks in each individual cell, we also used the CA approach.

1.2 Previous works using cellular automata for tumor growth modeling

There are several previous works using CA models for different purposes in the modeling of tumor growth. The work of Rejniak and Anderson [80] summarizes different alternatives, and here we comment some examples. Bankhead and Heckendorn [10] used a cellular automaton which incorporated a simplified genetic regulatory network simulation to control cell behavior and predict cancer etiology. Their simulation used known histological morphology, cell types, and stochastic behavior to specifically model ductal carcinoma in situ (DCIS), a common form of non-invasive breast cancer. The results of the authors showed that a contributing factor to the different pathology of hereditary breast cancer comes from the ability of progenitor cells to pass cancerous mutations on to offspring.

Ribba et al. [82] used a hybrid cellular automaton, "hybrid" because the automaton combines discrete and continuous fields, as it incorporates nutrient and drug spatial distribution together with a simple simulation of the vascular system in a 2-dimensional lattice model. The authors presented an application of the model for assessing chemotherapy treatment for non-Hodgkin's lymphoma (NHL). Alarcón et al. [5] used this model to study how blood flow and red blood cell heterogeneity influence the growth of systems of normal and cancer cells.

Gerlee and Anderson [30] presented a cellular automaton model of clonal evolution in cancer aimed at investigating the emergence of the glycolytic phenotype (cells uses an oxygen independent metabolic pathway, meaning that it does not use molecular oxygen for any of its reactions to produce ATP and lactic acid directly from glucose) and which acted in a two-dimensional grid. In their model each cell was equipped with a microenvironment response network that determined the behavior or phenotype of the cell based on the local environment. The response network was modeled using a feed-forward neural network, which was subject to mutations when the cells divided. This implies that cells might react differently to the environment and when space and nutrients are limited only the fittest cells survive. With this model they investigated the impact of the environment on the growth dynamics of the tumor. For low oxygen concentration they observed tumors with a fingered morphology, while increasing the matrix density gave rise to more compact tumors with wider fingers. The distribution of phenotypes in the tumor was also affected, as the glycolytic phenotype was most likely to emerge in a poorly oxygenated tissue with a high matrix density.

In the two-dimensional CA model of Ghaemi et al. [32] the authors determined thresholds for the nutrient concentration to establish the probabilities of a cancer cell remaining in that state or dying from necrosis, as well as for determining whether a healthy cell proliferates or it is replaced by a cancer cell. Gevertz et al. [31] adapted a previous CA model developed by the authors (designed to simulate spherically symmetric tumor growth) to study the impact of organ-imposed physical confinement and heterogeneity on tumor growth, that is, to incorporate the effects of tissue shape and structure. The results of the authors indicate that the impact is more pronounced when a neoplasm is

growing close to, versus far from, the confining boundary.

On the contrary to the diverse examples of CA for modeling tumor growth, there are very few previous works which have used the model of hallmarks. For example, in the work of Basanta et al. [11], the authors used a two-dimensional cellular automaton that modeled key cancer cell capabilities based on the Hanahan and Weinberg hallmarks. They focused their work on analyzing the effect of different environmental conditions on the sequence of acquisition of phenotypic traits. Their results showed that microenvironmental factors such as the local concentration of oxygen or nutrients and cell overcrowding may determine the expansion of the tumor colony. The results also showed that tumor cells evolve and that their phenotypes adapt to the microenvironment so environmental stress determines the dominance of particular phenotypic traits.

Abbott et al. [1] also investigated the dynamics and interactions of the Hanahan and Weinberg hallmarks in a CA model the authors called CancerSim. The main interest of the authors with their simulation was to describe the likely sequences of precancerous mutations or pathways that end in cancer. They were interested in the relative frequency of different mutational pathways (what sequences of mutations are most likely), how long the different pathways take, and the dependence of pathways on various parameters associated with the hallmarks. Using the same modeling, Spencer et al. [94] explored the timing of cancer onset, the order in which mutations are acquired, the diversity of tumours, and the competition and cooperation between cells in the tumor microenvironment, providing insight into how the sequence of acquired mutations affects the timing and cellular makeup of the resulting tumor.

Butler [14] studied the impact of hallmarks during the early growth stages of solid tumor development with a hybrid model that combines a discrete model of cancer cells using cellular automata, with a continuous model of blood flow using lattice Boltzmann methods. Hallmarks were removed in pairs, triplets and quadruplets in order to model combination therapies, abstracting drugs that target these properties as the removal of the hallmark from the system. It was found that not all combinations are equally effective, even if the individual treatments are effective. In fact, many combinations had no effect on tumor growth. However, in general, as more treatments were applied, cancer growth decreased.

We applied a 3D Cellular Automaton algorithm to model cancer growth behavior. This model mimics the development *in vitro* of multicellular spheroids of tumor cells. In vitro three-dimensional tumor spheroids are spherically symmetric aggregates of cells analogous to tissues, with no artificial substrate for cell attachment. Recently, these tumor spheroids have gained relevance as model of solid tumors. As indicated by Phung et al. [77], the three-dimensional spheroids exhibit many features of the tumor microenvironment and model the avascular region of tumors that is dependent on diffusion, and these models have begun to be included in toxicologic tests and evaluation of therapeutic strategies.

In our proposal the CA rules will be designed to model the mitotic and apoptotic behaviors in each cell from the information of the cell state and from its surrounding environment. We will define the rules from the main behavior

of the cells when the main hallmarks are present in the cells. As commented, Abbott et al.'s work [1], focused on possible pathways or sequences of hallmark mutations that end in cancer, and Basanta et al.'s work [11], focused on the influence of microenvironmental factors on tumor expansion, also used models based on the Hanahan and Weinberg hallmarks. Here, our aim is different, as our modeling and simulation will try to determine the dependence of the multicellular system behavior, at cellular level, on the presence of the different cancer cell hallmarks and their key defining parameters. We experimented with different conditions, not previously considered, that have implications for cell population dynamics and which are difficult to foresee without a model and associated simulating tool. We have focused our work on the study of possible behavioral regime transitions between states with predominance of one type of cells and on the dependence of the emergent tumor growth behavior on each individual hallmark, studying their relative importance in tumor development. The effects of Cancer Stem Cells are also included in the modeling, with their tumor regrowth capability. We have not considered in our study the effects of the concentration of oxygen or nutrients, as these factors are not relevant for our focus on the dependence of the cell behavior on the main hallmarks and in the avascular phase analyzed.

1.3 The biology of cancer

Cancer is a group of diseases characterized by out-of-control cell growth. Thus, cancer cells divide without control and are able to invade other tissues causing metastasis. There are more than 200 different types of cancer, and each is classified by the type of cell that is initially affected as well as the affected organs. Normal body cells grow and divide and know to stop growing. Over time, they also die. Unlike these normal cells, cancer cells just continue to grow and divide out of control and do not die when they are supposed to.
The great majority of cancers (90–95% of cases) are due to environmental factors such as lifestyle, behavioral factors, pollution, etc. The remaining 5–10% are due to inherited genetics (the genetic predisposition is inherited from family members) [6]. That is, it is possible to be born with certain genetic mutations or a fault in a gene that makes one statistically more likely to develop cancer later in life.

There are six broad groups that are used to classify cancer [72].

- Carcinomas: characterized by cells that cover internal and external parts of the body such as breast, lung and colon cancer.
- Sarcomas: characterized by cells that are located in bone, cartilage, muscle, connective tissue, and other supportive tissues.
- Lymphomas: cancers that begin in the lymph nodes and immune system tissues.
- Leukemias: cancers that begin in the bone marrow and often accumulate in the bloodstream.

- Adenomas: cancers that arise in the thyroid, the adrenal gland, the pituitary gland and other glandular tissues.
- Mixed types: cancers with components that belong to different previous categories. Some examples are: carcinosarcoma (malignant tumor that is a mixture of carcinoma and sarcoma, which can affect to different organs like utero, stomach or lungs) or adenosquamous carcinoma (type of cancer that contains two types of cells: squamous cells and gland-like cells, which affect to different organs like lungs or pancreas).

1.4 The hallmarks of cancer

Hanahan and Weinberg described the phenotypic differences between healthy and cancer cells in an article entitled "The Hallmarks of Cancer" [39] and its update in 2011 [40]. The six essential alterations in cell physiology that collectively dictate malignant growth are: self-sufficiency in growth signals, insensitivity to growth-inhibitory (antigrowth) signals, evasion of programmed cell death (apoptosis), limitless replicative potential, sustained angiogenesis, and tissue invasion and metastasis. In other words, these alterations provide the cell with an advantage due to increased proliferation capabilities, decreased death, the ability to induce angiogenesis or enhanced migration and invasion. Once a cell has evolved a sufficiently aggressive phenotype, it can escape from homeostatic control mechanisms and initiate tumorigenesis. In a recent update [40] the authors included two more hallmarks: reprogramming of energy metabolism and evasion of immune destruction, that emerged as critical capabilities of cancer cells. Moreover, the authors described two enabling characteristics or properties of neoplastic cells that facilitate acquisition of hallmark capabilities: genome instability and tumor-promoting inflammation (mediated by immune system cells recruited to the tumor site).

Below the different hallmarks used in the modeling in the avascular phase are described.

- Self-sufficiency in growth signals (SG, Self-Growth): Normal cells need external growth signals called growth factors to grow and divide. When the growth signals are not present, they stop growing. However, cancer cells do not require stimulation from external signals to multiply. Thus, they can grow and divide without external growth signals. Actually, cells can either produce their own growth hormones or they have changed so that they behave as if growth factors were present even in the absence of growth hormones.
- Insensitivity to anti-growth signals (IGI, Ignore Growth Inhibit): This hallmark refers to the inability to respond normally to signals that regulate growth. In normal tissue, proliferation is blocked by powerful negative regulators that control cell division. These inhibitors act on the cell cycle clock, by interrupting cell division in the interphase (see section 1.5). Cancer cells become insensitive to these anti-growth signals. As the tumor expands, it squeezes adjacent tissue, which sends out chemical messages that would normally bring cell division to a halt. Malignant

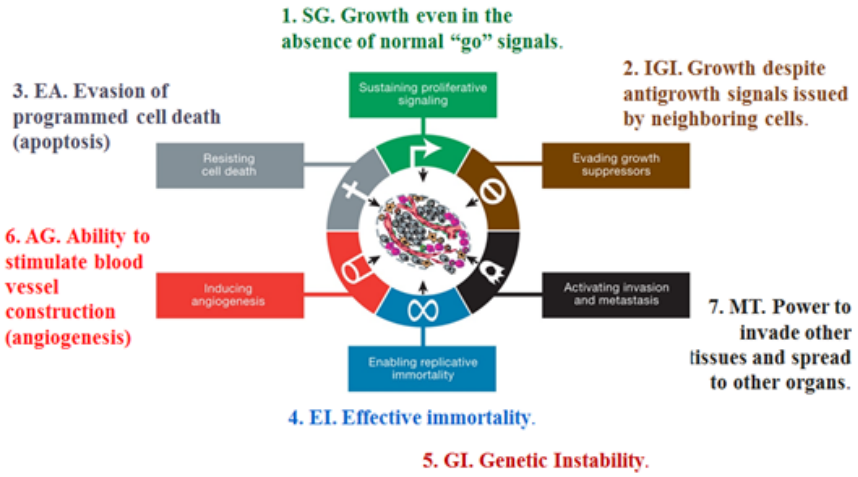

Figure 1.1: Schematic view of the initial hallmarks considered in [39][40]. Figure reprinted with permission from Elsevier.

cells ignore the commands, proliferating despite anti-growth signals issued by neighboring cells. This may be because tumor suppressor genes such as Rb, p53 or TP53 may be inactivated, or contact inhibition mechanisms may be evaded.

- Evading apoptosis (EA): Apoptosis is a form of programmed cell death, the mechanism by which cells are programmed to die in the event they become damaged. Cancer cells must overcome apoptosis to progress. The p53 tumor suppressor protein and gene elicits apoptosis in response to DNA damage, and is a major mechanism of cancer control. In order for cancer to progress, it must overcome p53, and p53 is mutated in more than 50 percent of cancers.

- Limitless replicative potential (EI, Effective Immortality): Healthy cells can divide no more than several times (< 100). The Hayflick limit [41] is the number of times a normal human cell can divide until cell division stops. The limited replicative potential arises because, with the duplication, there is a loss of base pairs in the telomeres (chromosome ends which protect the bases), so when the DNA is unprotected, the cell dies. Malignant cells overproduce the telomerase enzyme, avoiding the telomere shortening, so such cells overcome the reproductive limit.

- Genetic instability (GI): It is an additional factor that accounts for the high incidence of mutations in cancer cells [1]. It is an enabling characteristic of cancer [40] since, while not necessary in the progression from neoplasm to cancer, makes such progression much more likely [11].

- Sustained angiogenesis (AG): Angiogenesis is the process by which new

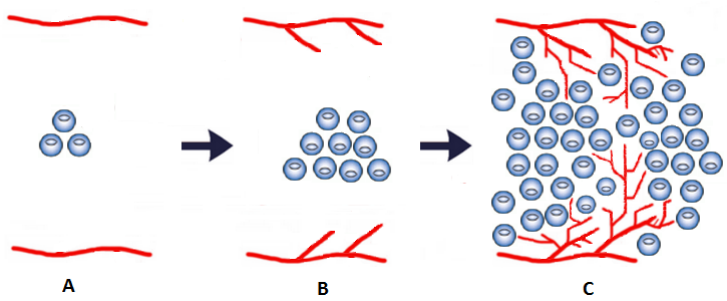

Figure 1.2: The effect of angiogenesis in tumor growth. A: When a tumor is small, cancer cells obtains oxygen and nutrients from surrounding blood vessels. B: As the tumor grows beyond the capacity of local blood vessels, soluble pro-angiogenic growth factors are released which promote the sprouting of new vessels (neovascularization) from local pre-existing blood vessels. C: The new vessels provide a blood supply for the tumor enabling tumors to grow beyond 2–3mm^3 in size.

blood vessels are formed. Cancer cells initially lack angiogenic ability, limiting their capability to expand. In order to progress, they must develop blood supply for ensuring that such cells receive a continual supply of oxygen and other nutrients (Figure 1.2). They obtain them by co-opting nearby blood vessels with growth induction of new branches that run throughout the growing mass. Angiogenic capability is the result of a balance between pro-angiogenic (VEGF, acidic and basic fibroblast growth factors) and anti-angiogenic factors (trombospondin-1).

- Tissue invasion and metastasis: Although uncontrolled cell growth and division is what most people associate with cancer, tissue invasion and metastasis (spreading) are what make many cancers lethal. In order for cancer to spread, cells must acquire mutations that turn on genes which allow them to break free from the primary tumor, travel through the blood stream, and establish a new colony of cells at another site in the body.

Different hallmarks are associated with different therapeutic agents as Figure 1.3 shows. The rapidly growing of targeted therapeutics can be categorized according to their respective effects on one or more hallmark capabilities. In fact, the observed efficacy of these drugs represents, in each case, a validation of a particular capability: if a capability is truly important for the biology of tumors, then its inhibition should harm tumor growth. Drugs that gum up with each of the acquired capabilities necessary for tumor progression have been developed and are in clinical trials or, in some cases, approved for clinical use in treating certain forms of human cancer [40].

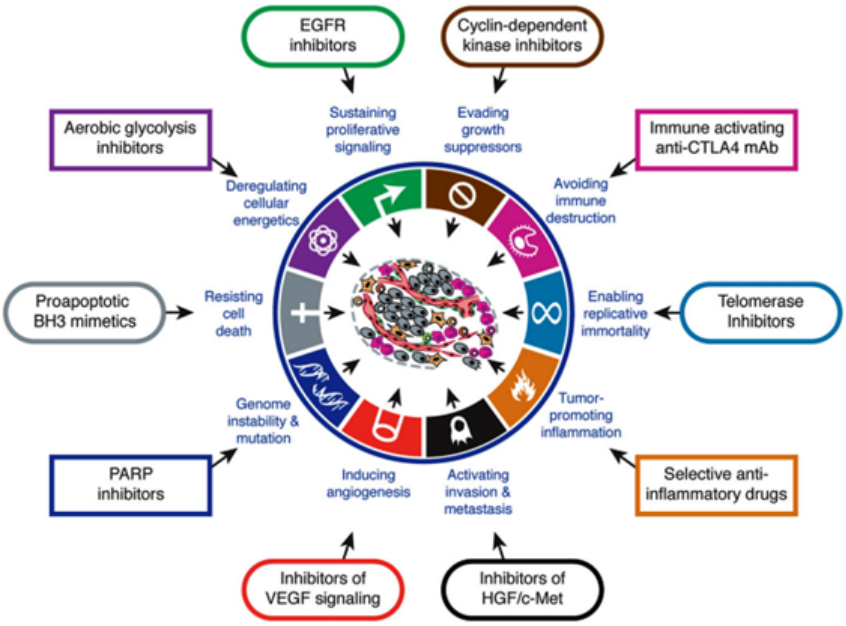

Figure 1.3: Terapeutic Agents. Figure from [40], reprinted with permission from Elsevier.

1.5 Cell cycle

The cell cycle is an ordered set of events that take place in a cell leading to its division and duplication. In cells with a nucleus the cell cycle can be divided in three periods: quiescent (G0 phase), interphase and the mitotic phase:

- The G0 phase is a resting phase where the cell has left the cycle and has stopped dividing.
- In the interphase, the cell is constantly synthesizing RNA, producing proteins and growing in size. Interphase can be divided into 3 steps: Gap 1 (G1), S (synthesis) phase, Gap 2 (G2).
  - The G1 phase: Cells increase in size in Gap 1, produce RNA and synthesize proteins. An important cell cycle control mechanism activated during this period (G1 Checkpoint) ensures that everything is ready for DNA synthesis.
  - The S phase: To produce two similar daughter cells, the complete DNA instructions in the cell must be duplicated. DNA replication occurs during this S (synthesis) phase.
  - In the G2 phase the cell continues to grow and to produce new proteins. At the end of this gap there is another control checkpoint (G2 Checkpoint) to determine if the cell can now proceed to enter phase M (mitosis) and divide.

- The mitotic phase consists of nuclear division. Cell growth and protein production stop at this stage in the cell cycle. All of the cell's energy is focused on the complex and orderly division into two similar daughter cells. Mitosis is much shorter than interphase, since it is a relatively short period of the cell cycle. There is a Checkpoint in the middle of mitosis (Metaphase Checkpoint) that ensures the cell is ready to complete cell division.

Figure 1.4 shows a schematic view of the cell cycle.

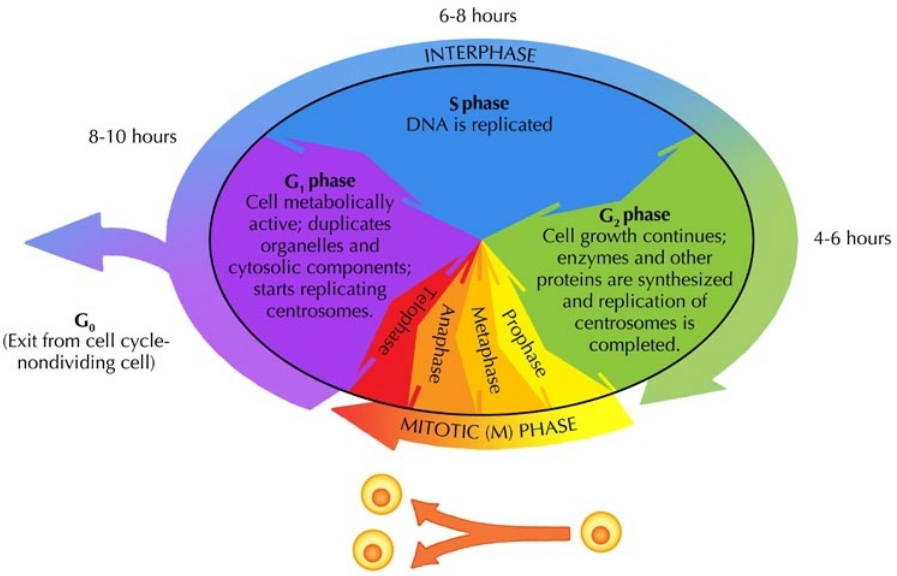

Figure 1.4: Phases of the cell cycle. Figure reprinted with permission by Siyavula Education and made available at `www.everythingscience.co.za` under the terms of a CC-BY 3.0 license [60].

1.6 Cell pathways

Many genes can be involved in a single cellular process. These genes are often organized into pathways. A pathway is the coordinated interaction of several proteins that are responsible for a particular component of a cell function. A pathway can be viewed as an electrical circuit. The pathway passes a signal in a particular order between proteins like a pulse of electricity traveling down a wire (passing on a phosphate group from one protein to another). When a protein is bound to a phosphate group, it is able to bind to the next protein in the pathway. It then hands off its phosphate group, and now this second protein is able to bind to the next protein in the series, and so on. This process is called phosphorylation.

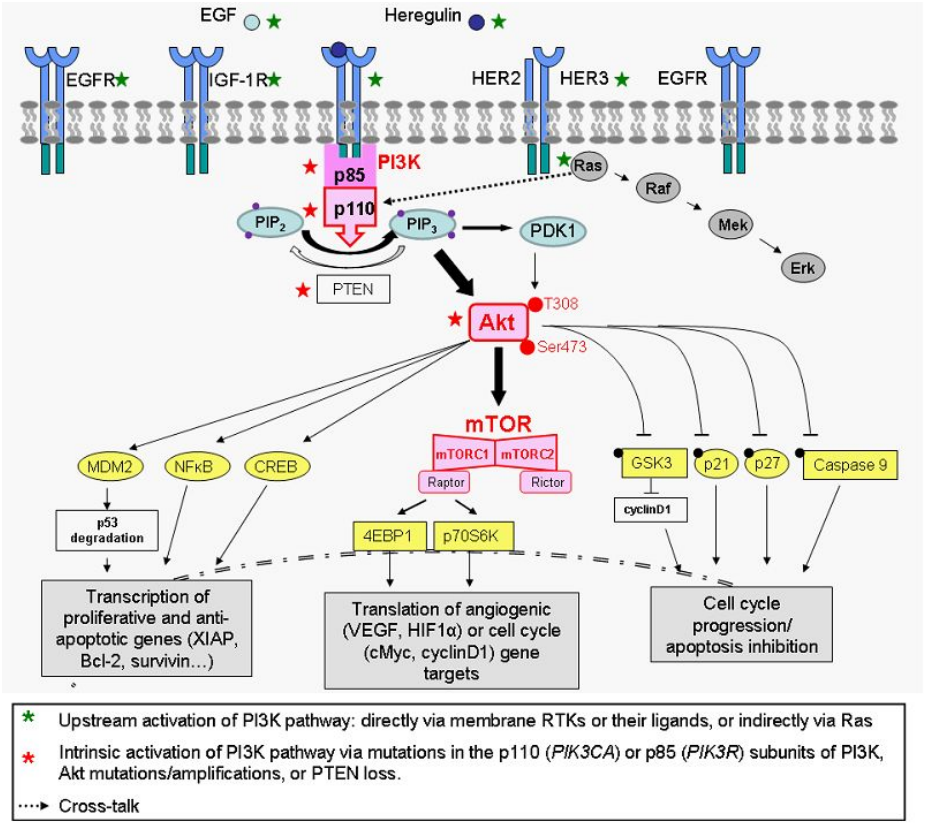

Figure 1.5: The PI3K/Akt/mTOR signaling pathway [54]. This pathway is up-regulated in a significant proportion of ovarian cancers. Figure reprinted with permission from InTech.

Many solid cancers exhibit a deregulation of different oncogenic pathways. In the last years, many genes responsible for the genesis of different cancers have been discovered, their mutations identified, and the pathways through which they act characterized. A single mutated protein in a pathway can cause uncontrolled growth and cause cancer. "Targeted" cancer drugs are designed to block abnormal pathways. By blocking an overactive pathway, the drugs can slow a cancer's growth and order malignant cells to self-destruct. Unfortunately, cancer cells can "learn" to activate other pathways, so that the original target drug is no longer effective by itself. Thus, the next step is to try to fight back by using combinations of drugs that attack multiple broken pathways.

In Figure 1.5 an example of cancer pathway called PI3K/Akt/mTOR pathway [54] is illustrated. This is is an intracellular signaling pathway important in regulating the cell cycle. It is directly related to cellular quiescence, proliferation, cancer, and longevity. PI3K activation phosphorylates and activates AKT, localizing it in the plasma membrane. AKT can have a number of

downstream effects such as activating mTOR which regulates cell growth by controlling mRNA translation, ribosome biogenesis, autophagy, and metabolism [35]. Several studies have identified this pathway as the most frequently altered in different types of cancer [45][75][100].

As we indicated in the subsections about motivation and hallmarks, a hallmark is an abstraction which can be activated as consequence of different malfunctions in the components of a pathway or pathways. Since our aims are focused on the study of the multicellular system behavior depending on the hallmarks acquired in the cells we will not consider the details of genes and proteins in the associated pathways.

1.7 Cancer stem cells

The cancer stem cell theory suggests that tumor cells include a minority population of cells responsible for the initiation of tumor development, growth, and tumor's ability to metastasize and reoccur [25][34]. Cancer stem cells (CSCs) are cancer cells that possess features associated with normal stem cells, specifically the ability to give rise to all cell types found in a particular cancer sample. Such cells are proposed to persist in tumors as a distinct population and cause relapse and metastasis by giving rise to new tumors [8].

Therefore, development of specific therapies targeted at CSCs holds hope for improvement of survival and quality of life of cancer patients, especially for patients with metastatic disease. The existence of CSCs has several implications in terms of future cancer treatment and therapies. These include disease identification, selective drug targets, prevention of metastasis, and development of new intervention strategies. Thus, different works tried to simulate their behavior, taking into account their main characteristics, such as their capacity to divide indefinitely [103]. If current treatments of cancer do not properly destroy enough CSCs, the tumor will reappear, so it is important to understand their behavior and effects.

There are two models when considering the origin of cancer cells: The hierarchical model assumes that tumors are originated from CSCs that give rise to progeny with self-limited proliferative capacity where most of the cells in the tumor are genetically homogeneous. The second model is the stochastic model or clonal evolution model, which postulates that tumorigenesis is a multi-step process that leads to progressively genetic alterations with the transformation of healthy cells into malignant phenotypes [104]. Thus, two models have been considered for explaining the origin of cancer cells: In the hierarchical CSC model, CSCs can divide either symmetrically to yield two CSCs, or asymmetrically to produce a CSC and a non-stem cancer cell with limited proliferation capacity (Differentiated Cancer Cell, DCC). These concepts will be exposed in better detail in chapter 4.

Figure 1.6 illustrates the problem with the presence of CSCs. If a standard treatment do not destroy the CSC population, there will be a regrowth of the tumor. This problem will be considered in chapters 5 and 6.

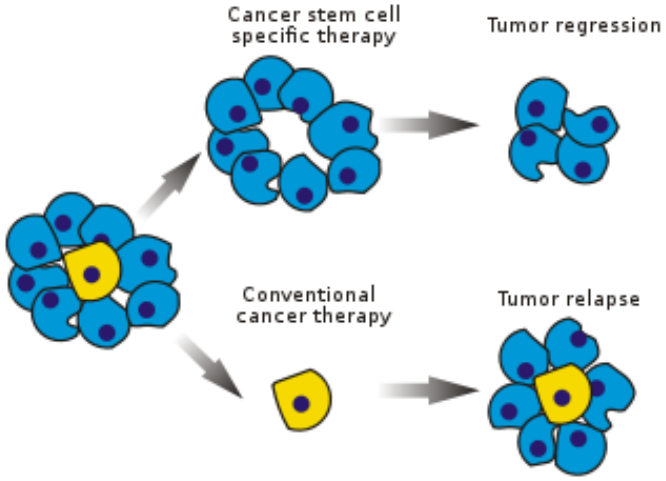

Figure 1.6: In the Cancer Stem Cell (CSC) model these cells can divide symmetrically or asymmetrically to produce Differentiated Cancer Cells (DCCs) with limited proliferative capability.

1.8 Organization of the thesis

This thesis describes the cancer growth model developed and the analysis of the simulation results. In the following paragraphs a short summary of each chapter is provided.

Chapter 2 describes the event model used for simulating the behavior of the multicellular system through time. The simulation algorithm is explained and different exploratory initial simulations using the event model are presented.

In Chapter 3 the relevance of hallmarks is studied in different representative situations of the first phases of cancer growth. Moreover, potential behavior transitions in tumor growth dynamics are analyzed when a treatment is applied in different scenarios defined by the relative prevalence of different hallmarks.

Chapter 4 focuses on the simulation of the behavior of cancer stem cells to inspect their capability of regeneration of tumor growth in different scenarios. The analyses of the capabilities of the hallmarks to promote tumor growth serve also to test their capabilities in a cancer stem cell context.

In Chapter 5 the effect of cancer treatments in a cancer stem cell context is analyzed. The application of a standard treatment in a cancer stem context has consequences on tumor regrowth behavior. Therefore, different strategies when a treatment is applied will be analyzed by taking into account the implications of CSC presence.

In Chapter 6 evolutionary computing is used to optimize a treatment in terms of intensity, duration and periodicity taking into account the presence and effects of cancer stem cells. We selected for our objective Differential Evolution as a robust evolutionary method.

Finally, in Conclusions we discuss and summarize the main conclusions,

together with ideas about possible future research lines related with the work of this thesis.

Chapter 2

Event model for tumor growth simulation

2.1 Event model

We used an event model for simulating the behavior of the multicellular system through time, which is oriented to the modeling of the cell cycle taking into account the presence of the hallmarks in the cells. We used the event model introduced by Abbott et al. [1], which uses an event queue for storing possible future mitotic events. Moreover, each cell resides in a site in a 3D grid environment. In the modeling, each cell genome indicates if any hallmark is activated as consequence of mutations.

On the contrary to Abbott et al.'s work [1], in our case metastasis and angiogenesis are not considered, as we are interested in the first avascular phases of tumorigenesis. So, every cell has its "genome" which consists of five hallmarks with a binary representation indicating if each one of the hallmarks (Self Growth-SG, Ignore Growth Inhibit-IGI, Evade Apotosis-EA, Effective Inmortality-EI and Genetic Instability-GI) is activated, in addition to some parameters particular to each cell. These parameters are related with each of the hallmarks considered and the behavior of the cells when the hallmarks are acquired in a cell.

The parameters are briefly defined in Table 2.1, whereas in next subsections the implications of the parameters in the multicellular system behavior will be explained.

In the simulation of the cell life cycle, most elements do not change observably each time step. The only observable changes to cells are apoptosis and mitosis. In a tissue, only a fraction of all cells are undergoing such transitions at any given time. The different phases of the cell cycle explained in Section 1.5 are simulated in a simple way. The G0 phase is triggered by contact inhibition. Thus, cells with a full set of neighbors normally do not attempt to replicate. Cells next to empty space within the tissue's natural extent automatically enter the G1 phase. G1 is modeled by the passage of time; each cell occupies equal volume, and the physical enlargement of cell growth is not simulated. DNA replication occurs in the S phase. The replication of DNA

Table 2.1: Definition of the parameters associated with the hallmarks

Parameter name	Default value	Description
Grid size		The number of cells in the 3D lattice for the simulation.
Hallmark mutation rate ($1/m$)	10^5	Each gene (hallmark) is mutated (when the cell divides) with a $1/m$ chance of mutation.
Telomere length (tl)	50	Initial telomere length in each cell. Every time a cell divides, the length is shortened by one unit. When it reaches 0, the cell dies, unless the hallmark EI is ON.
Evade apoptosis (e)	10	A cell with n hallmarks mutated has an extra n/e likelihood of dying each cell cycle, unless the hallmark EA is ON.
Genetic instability (i)	10^2	There is an increase of the hallmark mutation rate by a factor of i for cells with this mutation (GI).
Ignore growth inhibit (g)	30	Cells with the hallmark "Ignore growth inhibit" (IGI) activated have eliminated the inhibition by contact. For the modeling, as in [1][94], these cells have a probability $1/g$ of killing off or replacing a neighbor to make room for mitosis.
Random cell death (a)	10^3	In each cell cycle every cell has a $1/a$ chance of death from several causes.

occasionally introduces a mutation that will be inherited by daughter cells. Then, at the G2 checkpoint, cells undergo a check for genetic damage. Apoptosis is triggered in cells found to contain genetic defects. The G1 checkpoint is not modeled separately, because it is similar (This checkpoint prevents preparation for DNA replication until the detected DNA damage has been removed). Finally, the cell undergoes mitosis in the M phase. One of the daughter cells occupies the grid location of its parent, while the other fills an empty adjacent location.

Algorithm 2.1.1 summarizes the simulation, which takes into account the main aspects of the cell cycle from the application point of view, specifying the order for testing the implications of the different hallmarks in the simulated cell cycle (TESTS 1 to 5).

Figure 2.1 represents graphically the algorithm in order to explain the procedure more clearly. The process is simulated as a event model where a mitosis is scheduled several times in the future, being a random variable distributed uniformly between 5 and 10 time steps (see Figure 2.2). This is done to simulate the variable duration of the cell life cycle (between 15 and 24 hours). Taking into account these time intervals, each time iteration represents an average time of 2.6 hours, so, for example, 5000 iterations in the simulation imply an average time of 77.4 weeks (1.48 years). Moreover, in the simulation, a grid with 10^6 sites represents approximately 0.1 mm^3 of tissue. The main aspects of the model can be summarized in the following steps:

Start: The simulation can begin by initializing all elements of the grid to represent empty space, as in most previous works [1][11][25][80]. Then, the element at the center of the grid is changed to represent a single normal cell (no mutations). Mitosis is scheduled for this initial cell (push a mitotic event in the event queue between 5 and 10 time iterations in the future).

After the new daughter cells are created, mitoses are scheduled for each of them, and so on. Each mitotic division is carried out by copying the genetic information (the hallmark status and associated parameters) of the cell to an unoccupied adjacent space in the grid (a random free site among the 26 immediate neighbors in the 3D grid). Random errors occur in this copying process, so some hallmarks can be activated, taking into account that once a hallmark is activated in a cell, it will be never repaired by another mutation [1].

As an alternative, we will consider in our simulations an initial grid full of healthy cells, being the process the same but scheduling the mitoses for all the cells.

Pop event: The events are ordered on event time. Pop event from the event queue with the highest priority (the nearest in time) (see Figure 2.2).

Random cell death test (Test 1): Cells undergo random cell death with low probability ($1/a$ chance of death). In each cell cycle, each cell is subjected to a $1/a$ chance of death, where a is a tunable parameter. This might be due to mechanical, chemical or radiological damage, aging, or the immune system.

Genetic damage test (Test 2): The larger the number of hallmark mutations, the greater the probability of cell death. If "Evade apoptosis" (EA) is ON, death as consequence of the genetic damage is not applied. This corresponds with the G2 checkpoint of the cell cycle (see Section 1.5).

Mitosis tests:

1. **Replicative potential checking** (Test 3): If the telomere length is 0, the cell dies, unless the hallmark "Effective immortality" (Limitless replicative potential, EI) is mutated (ON).
2. **Growth factor checking** (Test 4): As in [1][11][94], cells can perform divisions only if they are within a predefined spatial boundary, which represents a threshold in the concentration of growth factor; beyond this area (95% of the inner space in each dimension in our simulations, which represents 85.7% of the 3D grid inner space) growth signals are too faint to prompt mitosis (unless hallmark SG is ON).
3. **Ignore growth inhibit checking** (Test 5): If there are not empty cells in the neighborhood, the cell cannot perform a mitotic division. As in [1][94], if the "Ignore growth inhibit" hallmark (IGI) is ON, then the cell competes for survival with a neighbor cell and with a likelihood of success $(1/g)$.

If the three tests indicate possibility of mitosis:

- Increase the hallmark mutation rate if genetic instability (GI) is ON. That is, if the cell has this factor (GI) acquired then its mutation rate is increase by a factor (i).
- Add mutations to the new cells according to the hallmark mutation rate $(1/m)$.
- Decrease telomere length in both cells.
- Push events. Schedule mitotic events (push in event queue) for both cells: Mother and daughter, with the random times in the future.

If mitosis cannot be applied:

- Schedule a mitotic event (in queue) for mother cell.

2.1.1 Comments about hallmark parameters

There are two particular parameters, *telomere length* and *hallmark mutation rate*, that can change their values in a particular cell over time, as explained in Table 2.1. The cell's genome is inherited by the daughter cells when a mitotic division occurs. The default values indicated in Table 2.1 are the same as those used in [1], except the initial telomere length and the higher value of g (which defines the probability of escaping the contact inhibition mechanism) used by us. In the case of the telomere length, we used the default value indicated in Spencer et al. [94] as it corresponds to the Hayflick limit [41]. Nevertheless,

Algorithm 2.1.1: EVENT MODEL FOR CANCER SIMULATION()

```
t ← 0    // Simulation time. Initial cell at the centre of the grid.
SCHEDULE A MITOTIC EVENT(5,10) // Schedule a mitotic event with a
        // random time (ts) between 5 and 10 time iterations in the future
        // (t+ts). The events are stored in an event queue. The events are
        // ordered on event time.
while event in the event queue
do {
    POP EVENT( ) // Pop event with the highest priority (the nearest in time).
    t ← popped event time
    TEST 1: RANDOM CELL DEATH( ) // The cell can die with a given
            // probability.
    TEST 2: GENETIC DAMAGE( ) // The larger the number of hallmark
                              // mutations, the greater the probability of cell
                              // death. If "Evade apoptosis" (EA) is ON, death
                              // is not applied.
    MITOSIS TESTS( ) :
       TEST 3: LIMITLESS REPLICATIVE POTENTIAL CHECKING( )// If
           // the telomere length is 0, the cell dies, unless the hallmark
           // "Effective immortality" (Limitless replicative potential, EI) is ON.
       TEST 4: GROWTH FACTOR CHECKING( ) // Cells can perform
           // divisions only if they are within a predefined spatial boundary which
           // sufficient growth factor; beyond this area cells cannot perform
           // mitosis, unless the hallmark "Self-growth" (SG) is ON.
       TEST 5: IGNORE GROWTH INHIBIT CHECKING( ) // If there are not
           // empty cells in the neighborhood, the cell cannot perform a mitotic
           // division. If the "Ignore growth inhibit" hallmark (IGI) is ON, then
           // the cell can perform the division with a given probability, replacing
           // one of the neighbor cells.
    if the three tests indicate possibility of mitosis
    then {
        PERFORM MITOSIS( )
          // Increase the hallmark mutation rate if "Genetic instability"
          // (GI) is ON.
          // Add mutations to the new cells according to the hallmark
          // mutation rate (1/m). Decrease telomere length in both cells.
        PUSH EVENTS( )
          // Schedule mitotic events (push in event queue) for both cells:
          // mother and daughter, with the random times in the future.
    }
    else PUSH EVENT( ) // Schedule a mitotic event in queue for mother cell.
}
```

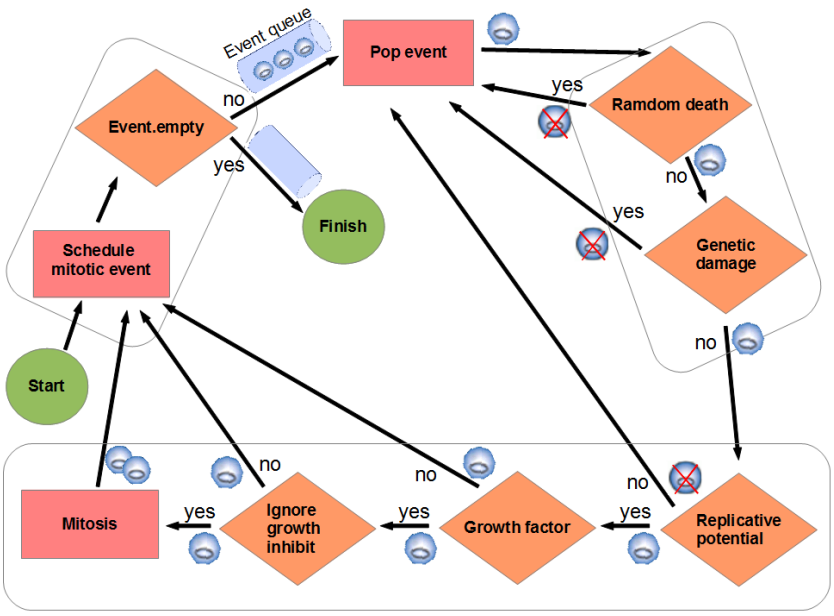

Figure 2.1: Diagram of the event model. The rectangles indicate an action, a rhomb indicates a check with an associated binary question, as explained in the text. This process is repeated to all the cells in the grid environment. Each cell is represented with a small circle. If the cell dies after a check it is represented with a crossed-circle.

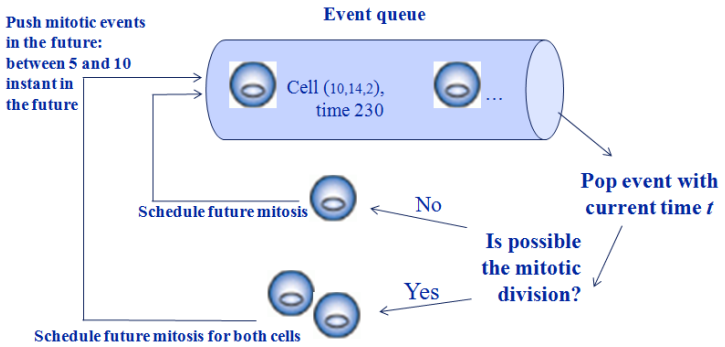

Figure 2.2: Event model used in the simulation. Mitoses are scheduled between 5 and 10 time iterations in the future. When a mitosis event is processed, several tests are performed to determine if the cell dies, continues quiescent or can perform the division (explained in Figure 2.1 and Algorithm 2.1.1).

the simulations can use greater values of the initial telomere length -as in [1]-, being in this case the main limits for cell proliferation the area with growth factors and the grid size.

Other parameters are more difficult to determine in order to have a direct analogy in nature. For example, as indicated by Spencer et al. [94], the parameters g, e and a were chosen via a sensitivity analysis such that the parameter plays an important role but does not dominate tumorigenesis or, as indicated in [1], the choice of parameter values "was guided by the observation that hallmarks only have meaningful interactions within some region of interest". We used a standard value of $g = 30$, a greater value than the one used in [1] ($g = 10$) and [94] ($g = 5$), implying a lower possibility of escaping the contact inhibition mechanism, although we will reason about the resultant behavior with different values.

The parameter m determines the probability of acquisition of a hallmark when the cell divides (hallmark mutation rate $1/m$). Bielas et al. [13] developed an assay to quantify random mutations in human tissue and their results showed that, in normal tissues, the frequency of spontaneous random mutations is exceedingly low, less than 10^{-8} per base pair. In contrast, tumors exhibited an average frequency of $210 \cdot 10^{-8}$ per base pair, an elevation of at least two orders of magnitude. Nevertheless, we must take into account that such values correspond to single-nucleotide mutations, while we are considering mutations or acquisitions in the abstract model of the cancer hallmarks. Moreover, as indicated in [1], with small cell population sizes in the simulations, large mutation rates are necessary to obtain the expected incidence of cancer. So, we used the same default value considered in Abbott et al. [1] and Spencer et al. [94] for the probability of acquisition of hallmarks in the mitotic divisions. Also, Basanta et al. [11] worked with parameters, such as hallmark mutation rate (10^{-5}) and mutation rate increase for cells with acquired genetic instability ($i = 100$), with the same default values.

For the grid size, we also used the same size of Abbot et al. [1] for most of the experiments (125000 cell sites). The reason is that "even with modern processor speeds, it is still not feasible to simulate a realistic number of cells using an individual-based approach in which each cell is represented explicitly" [1]. Moreover, as detailed in the next chapter, the emergent behavior will be independent of the grid size, provided that we use a sufficient number of cells to capture the emergent dynamics of the process with the interrelations of the hallmarks [65][85].

Regarding hallmark *self-growth* (SG), as in Abbott et al. [1] and Basanta et al. [11], cells can perform divisions only if they are within a predefined spatial boundary, which represents a threshold in the concentration of growth factor. These growth factors do no diffuse. The area is represented as an inner cube of the grid, defined by the 95% of the inner space in each dimension, so it represents 85.8% (0.95^3) of the 3D grid inner space. Beyond this area growth signals are too faint to prompt mitosis (unless hallmark SG is ON in a cell). Since the growth factors are present in the 95% of the inner space in each dimension, the cells with the hallmark *self-growth* activated have advantage in the most outer area of the grid environment, when the multicellular system growth has reached the limits with growth factors. The chosen value is arbit-

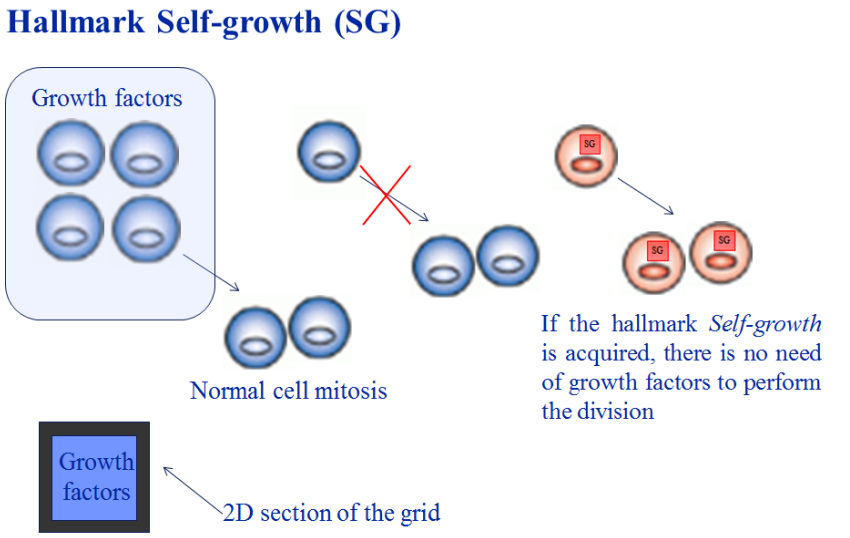

Figure 2.3: Self-Growth hallmark rule.

rary, as in the referenced works (Abbot et al. [1], Spencer et al. [94], Basanta et al. [11]), but reasonable to show the effect of the hallmark SG in such a stage. Changing the size of the area with growth factors would not change the conclusions, except that the situation when the system growth reaches the limits with growth factors would occur in a different time iteration.

Finally, in the simulation, there is not any boundary condition beyond the grid size and that the outer area of the grid is not filled with growth factor. That is, a cell cannot divide beyond the limits in each dimension and there are not neighborhood connections, for example, between the cells of the left-side limit and the right-side limit.

2.1.2 Hallmarks rules in a graphical way

As indicated in the simulation steps, frequently, cells are unable to replicate because of some limitation, such as contact inhibition or insufficient growth signal. Cells overcome these limitations through mutations in the different hallmarks. The different tests considered in the simulation of the mitotic and apoptotic behavior of the cells, taking into account the different hallmarks acquired, are a set of rules that are applied to each of the cells of the 3D environment. Therefore, we are using the classical concept of a cellular automaton where the rules are applied to a cell of the grid-like environment when an event is popped from the event queue regarding that cell and site. Figures 2.3 to 2.7 show, in a schematic view, the implications of the rules of the cellular automaton.

Figure 2.3 graphically illustrates the rule for the hallmark *self-growth*. As explained, a normal cell can perform divisions only if it is within a predefined spatial boundary area. However, if the hallmark SG is acquired (ON), the

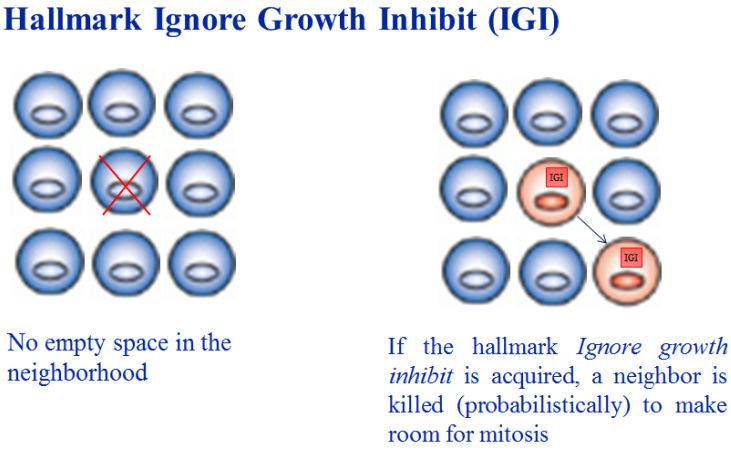

Figure 2.4: Ignore Growth Inhibit hallmark rule.

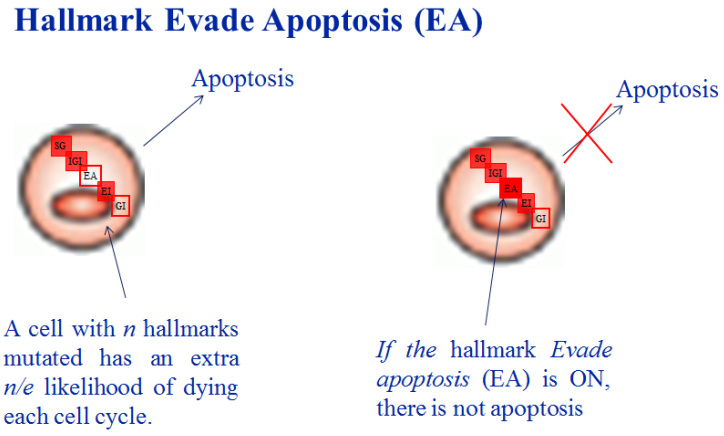

Figure 2.5: Evade Apoptosis hallmark rule.

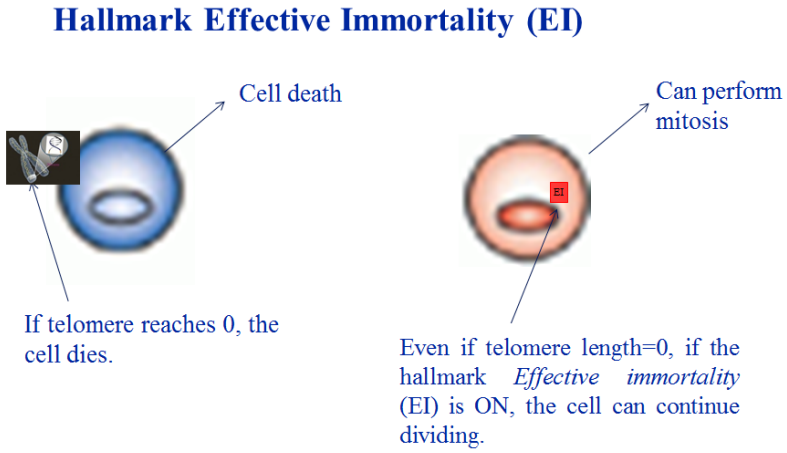

Figure 2.6: Effective Immortality hallmark rule.

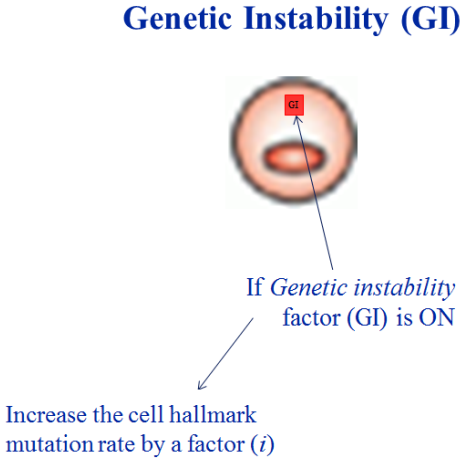

Figure 2.7: Genetic Instability hallmark rule.

cell can perform mitosis out of the predefined area with growth factor. In the Figure an example in 2D is shown but in the simulation a 3D space is used.

In Figure 2.4 the rule of the hallmark *ignore growth inhibit* is explained. A normal cell cannot perform mitosis if there is no empty space in its neighborhood, unless the hallmark IGI is ON. In this last case, a neighbor is killed probabilistically to make room for mitosis. These cells (hallmark IGI ON) have a probability $1/g$ of replacing a neighbor, as indicated in Table 2.1.

Figure 2.5 explains the rule of the hallmark *evade apoptosis*. A cell with the hallmark EA activated does not die by apoptosis.

Figure 2.6 illustrates the rule regarding hallmark *effective immortality*. A normal cell dies when its telomere length (decreased in every cell division) reaches the value 0, but a cell with the hallmark EI activated can continue dividing indefinitely.

Finally, Figure 2.7 graphically explains the rule of the hallmark *genetic instability*. A cell with this hallmark activated increases the hallmark mutation rate by a factor i, as indicated in Table 2.1.

2.2 Examples of simulation runs

This section illustrates exploratory initial simulations using the event model explained. Figure 2.8 shows the evolution over time of the number of healthy and cancer cells for two different values of the parameter m, which defines the hallmark mutation rate, maintaining the rest of the parameters in their default values and using the same grid size (125000, grid with 50 sites in each dimension) employed in [1]. The number of time iterations was 1000 in the different runs. A cell was considered as cancerous if any of the hallmarks was present. As expected, with increasing hallmark mutation rates ($1/m$), the increase in cancer cells becomes faster. For lower values of the hallmark mutation rate it is difficult to obtain rapid cancer progression, so we selected those two high values.

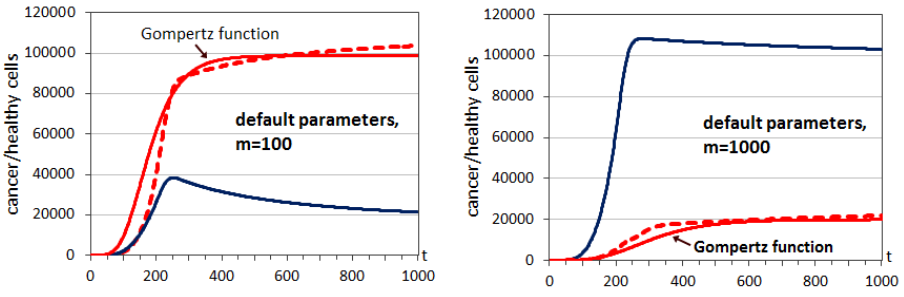

Figure 2.8: Evolution through time iterations of the number of healthy cells (continuous lines) and cancer cells (dashed lines) for two different hallmark mutation rates ($1/m$) and default parameters. It also appears in continuous red line the fit curve for cancer cells using a Gompertz function.

Rodriguez-Brenes et al. [84] analyzed tumor growth patterns and they classified them into five fundamentally different categories:

- The exponential growth is the simplest model used to describe tumor growth. Several leukemias and lymphomas exhibited exponential growth, most notably the L1210 leukemia [90]. Exponential growth has also been documented to describe the growth dynamics of certain non-solid cancers [27], but this law is not applicable to most solid tumors over long time periods.

- The surface growth suggests a linear relation between time and the diameter of a tumor. The models that follow this pattern use the basic idea that most of the growth activity is concentrated at the boundary of the tumor (cells near the surface divide more often than the cells in the core).

- The Sigmoidal growth is comprised by three distinct phases: the initial exponential phase, the linear phase, and the plateau where population size stabilizes (saturation). If the growth rate decays exponentially, we get the Gompertz law [84]. There is empirical evidence that tumor growth follows a Gompertz function in a lot of cancer types. In the 1960s, A.K. Laird [50], for the first time, successfully used the Gompertz curve to fit the growth of 19 tumor lines (ten mice, eight rats, and one rabbit) using the following equation: $V(t) = [V_0 e^{A/B(1-e^{Bt})}]$ where V represents the tumor size, in appropriate units, at any time t, V_0 is the initial tumor size, and A and B are constants that vary depending on the type of cancer. Since then, this equation has been extensively used in this context.

- Atypical growth corresponds to other data sets, of solid and non-solid tumors, that do not conform to the growth laws described so far. These data sets show sub-cubic growth for solid tumors and sub-exponential growth for non-solid tumors.

- Multistep growth is an irregular growth pattern based on the idea that the development of cancer is a multistep process in which cells gradually become malignant through a progressive series of alterations (random mutations and epigenetic changes) [62][70]. An irregular pattern of tumor growth generally incorporates plateaus or dormant periods separated by Gompertzian growth periods.

In the runs of Figure 2.8, using the standard parameters, the tumor growth follows a Gompertz curve since we have the three distinct phases: exponential phase, the linear phase and the saturation. In this figure a Gompertz growth curve is included for comparison with respect to the growth curve of the simulations (cancer cells). Depending on the parameters of the simulation the different phases are more o less pronounced. The inserted curve with a Gompertz type growth in Figure 2.8 with m=100 has the following constants of the Gompertz function: V_0=1, A=0,1845 and B=0,016. For the case of m=1000 the constants are: V_0=1, A=0,087 and B=0,00879. Nevertheless, we

are not interested in this thesis in the tuning of the model parameters to fit a particular cancer type, since we focus our aims on the hallmarks implications and their relevance on the resultant behavior, as analyzed in the next chapters.

Chapter 3

Relevance of hallmarks

In this chapter we study the evolution of hallmarks in different representative situations of the first phases of cancer growth, regarding initial conditions and parameters, analyzing the relative importance of the hallmarks for tumor progression. The presence of the cancer hallmarks defines cell states and cell mitotic behaviors. As previously explained, these hallmarks are associated with a series of parameters, and depending on their values and the activation of the hallmarks in each of the cells, the system can evolve to different dynamics. Such possible dynamics are analyzed here. Moreover, we study possible behavior transitions in tumor growth dynamics when a treatment is applied in different scenarios defined by the relative predominance of different hallmarks.

3.1 Dependence on hallmark parameters

In this section we show the capability of the simulation tool for obtaining different dynamic behaviors. Figures 3.1, 3.2 and 3.3 (left part) show the evolution over time of the number of healthy and cancer cells for different values of the parameter m, which defines the hallmark mutation rate, maintaining the rest of the parameters in their default values and using the same grid size (125000). As in the previous initial examples in previous chapter, the simulations began with only one healthy cell at the center of the grid. A cell was considered cancerous if any of the hallmarks was present. The graphs are an average of 5 different runs, given the stochastic nature of the problem. The number of time iterations was 1000 in the different runs.

The central graphs of Figures 3.1, 3.2 and 3.3 show the time evolution of the cells with a given hallmark and such standard parameters. With the highest mutation rate ($m = 100$, Fig. 3.3), despite the rapid and initial cancer cell progression, two hallmarks present an advantage for cancer cell proliferation: *evade apoptosis* (EA) and *ignore growth inhibit* (IGI). The first one dominates in the cancer cell population because, as there are many mutations in the cells, the apoptosis mechanism eliminates many of the mutated cells, except those that have the hallmark EA acquired, which escape that control so they proliferate in the cell population. The second hallmark is necessary when the space is full, because in this situation there are no vacant sites for cell proliferation,

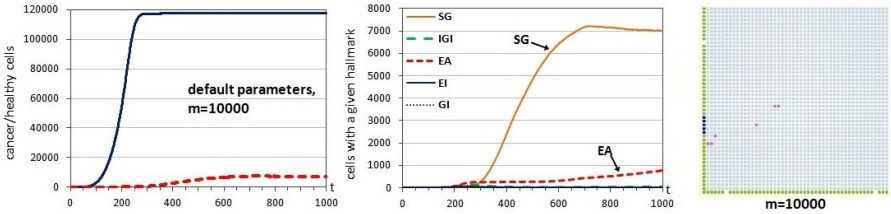

Figure 3.1: Left: Evolution through time iterations of the number of healthy cells (continuous line) and cancer cells (dashed line) with $m = 10000$ and parameter default values. Center: Time evolution of the number of cells with a hallmark acquired. All the graphs are an average of 5 independent runs. Right: Example of a 2D cross-section of a final configuration at the end of the temporal evolution (at $t = 1000$). Healthy cells are shown in bright gray whereas the other colors correspond to different combinations of hallmarks acquired.

except for those with hallmark IGI acquired (the free space limitation can be ignored by such cells). It should be remembered that these hallmarks, that allow the cells to escape those limits, are acquired by the offspring, so the daughters can continue proliferating. Using a lower hallmark mutation rate ($m = 1000$, Fig. 3.2), the hallmark *self-growth* (SG) is initially more predominant than IGI, as cells with hallmark SG acquired proliferate rapidly when the cells have reached the limits of the area filled with growth factor. With the lowest mutation rate ($m = 10000$, Fig. 3.1), the hallmark *self-growth* (SG) is the most predominant since, when the cells have reached the limits with growth factor, the cells with that mutation can proliferate rapidly in the small area without growth factor. In this case, the hallmark *evade apoptosis* (EA) is less predominant, as there are fewer mutations in cells, so the apoptosis mechanism is less important as a limit to cell proliferation. Table 3.1 includes statistical information of these simulation runs, with the final information of healthy and cancer cells at the end of the simulation at $t = 1000$, to know the variability involved in the different runs. We must take into account that the variability depends on the particular iteration at which the simulation is ended. For example, with simulations that end with the whole grid practically full of one type of cells, the variability of the runs is logically lower ($m = 10000$ in Fig. 3.1).

In Figures 3.1, 3.2 and 3.3, the subfigures at the right correspond to 2D cross-sections of final configurations at $t = 1000$, corresponding to a plane that crosses the centre of the 3D grid. These 2D cross-sections give information about the inner distribution of the cells which is useful to understand the resultant behavior. The colors correspond to different combinations of hallmarks acquired, whereas healthy cells are shown in bright gray. With the highest mutation rate ($m = 100$), most of the cells have acquired all the hallmarks (color dark blue), whereas with lower mutation rates there is a combination of two factors: i) mutations can be acquired randomly in any cell, so there are cells randomly located with some hallmark acquired and ii) when one cell acquires a hallmark, such as IGI, that cell can proliferate in its immediate surrounding (where the new cells can acquire new hallmarks in the mitotic di-

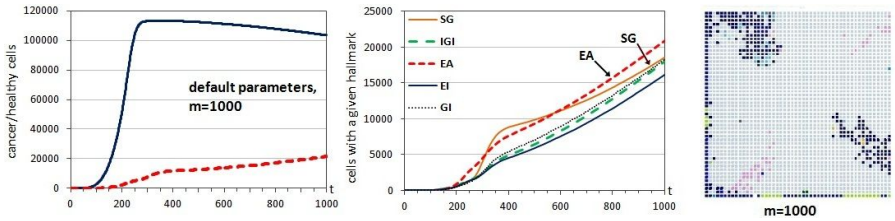

Figure 3.2: Left: Evolution through time iterations of the number of healthy cells (continuous line) and cancer cells (dashed line) with $m = 1000$ and parameter default values. Center: Time evolution of the number of cells with a hallmark acquired. All the graphs are an average of 5 independent runs. Right: Example of a 2D cross-section of a final configuration at the end of the temporal evolution (at $t = 1000$).

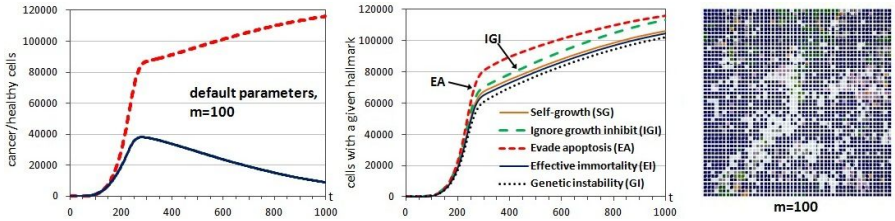

Figure 3.3: Left: Evolution through time iterations of the number of healthy cells (continuous line) and cancer cells (dashed line) with $m = 100$ and parameter default values. Center: Time evolution of the number of cells with a hallmark acquired. All the graphs are an average of 5 independent runs. Right: Example of a 2D cross-section of a final configuration at the end of the temporal evolution (at $t = 1000$).

vision), so there are clusters of concentrated or localized cells with hallmarks acquired.

These first tests serve to check the difficulty of appearance of a cancer growth with such default parameters, requiring high values of the hallmark mutation rate. Note that most of the m values imply fixed dynamics in terms of complex systems, as the dynamics ends with most of the cells in healthy or cancerous states. Note also that we finished the runs when the emergent behavior is obtained as consequence of the first appearance of acquired hallmarks, without explaining the next multicellular system evolution, which in most cases ends with the cells dying after their maximum number of divisions.

To see the effect of other hallmarks, we can inspect tumor growth appearance with low hallmark mutation rates and parameters different from the default values. Figure 3.4 is a very representative case, where we repeated the simulations but using a parameter set that facilitates the appearance of cancer cells, again with a grid size of 125000. We selected values as the ones used by Abbott et al. [1] (m=100000, tl=35, e=20, i=100, g=10, a=400) for the determination of possible mutational pathways, that is, the sequences of appearance of hallmarks that end in tumor growth. For example, the lower

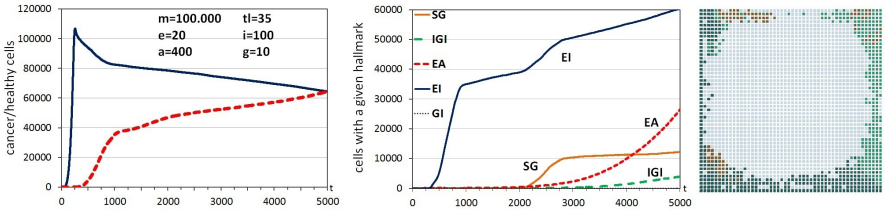

Figure 3.4: Left: Time evolution of the number of healthy cells (continuous line) and cancer cells (dashed line) with a parameter set which facilitates cancer growth. Center: Time evolution of the number of cells with a hallmark acquired. All the graphs are an average of 5 independent runs. Right: 2D cross-section of a final configuration at the end of the temporal evolution (at $t = 5000$).

value of tl implies fewer mitoses in healthy cells, and the lower value of a facilitates that more vacant sites are available for cancer cells to propagate, in connection with the higher probability of replacing neighbors to make room for mitosis (lower value of g). As in the previous case, Figure 3.4 corresponds to an initialization of the grid consistent of only one healthy cell at the center.

Table 3.1: Summary of statistics regarding Figures 3.1 - 3.4

			Average	**Standard deviation**
Figs. 3.1-3.3	m=10000	Cancer cells	7315	323
		Healthy cells	117284	146
	m=1000	Cancer cells	21570	3159
		Healthy cells	103414	3399
	m=100	Cancer cells	116099	3729
		Healthy cells	8896	3728
Figure 3.4	m=100000	Cancer cells	64409	508
		Healthy cells	64386	490

The left part of Figure 3.4 shows the evolution of the number of healthy and cancer cells, whereas the central part of Figure 3.4 shows the time evolution of the cells with a given hallmark and that parameter set. The dominant hallmark in that tumor growth is *effective immortality* (EI), allowing the progression of the cells with that mutation even when the telomere length reaches its limit. We must take into account that the original cell at the center of the grid has only 35 opportunities to divide, whereas the descendants (which acquire shortened telomeres) have even fewer mitotic opportunities. Thus, the cells which have acquired the mutation EI have no such a limit to proliferate, which represents a clear advantage with respect to healthy (non-mutated) cells, which die after the maximum number of 35 divisions. This explains the rapid proliferation of the hallmark EI, before iteration 1000, when the healthy cells have performed their maximum number of mitotic divisions.

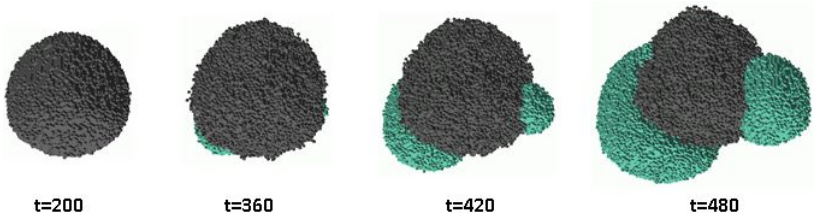

Figure 3.5: Snapshots of the cellular system at different time steps using the parameter set of Figure 3.4 (Grid size=10^6).

When there is a high number of cells with the hallmark EI acquired, other limits to cell proliferation begin to be important. The first limit is again the apoptotic process when the cells have acquired more mutations. Hence, around time iteration 2000, cells that acquired the hallmark *evade apoptosis* (EA) tend to increase in number, as its acquisition represents again an advantage against the proliferation limit. The other limit is when the cells have reached the extremes of the area with growth factor, so cells that have acquired the hallmark *self-growth* (SG) begin to proliferate beyond the area with growth factor. The hallmark *ignore growth inhibit* (IGI) does not proliferate rapidly as in the previous case (Figure 3.3, $m = 100$), because now there are more vacant sites since many cells provide free sites after their maximum number of divisions, together with the higher value of random cell death (parameter a). The right part of Figure 3.4 shows again a cross-section of the final configuration in one of the runs, which shows a clear localized pattern of cells with the hallmark EI acquired (green cells), which is clearly advantageous in that scenario. Note that the proliferation begins in areas of the outer part of the growth, when the healthy cells performed the maximum number of divisions. As the mutation rate is low, in the inner part practically there are not cells with hallmarks acquired.

Figure 3.5 shows snapshots at different time states of the multicellular system in a run with the previous parameters, depicting the beginning of tumor progression. The grid was initialized with only one healthy cell at the center. In this run a grid size of 10^6 was used, with the aim of achieving better visualization of tumor growth. Again, the cancer cells are shown in different colors (depending on which hallmarks are activated) whereas the healthy cells are depicted in dark gray. The predominant hallmark is EI in the initial cancer cell proliferation (green cells), showing the advantage of this hallmark when there is still free space in the grid. This is also an example that shows that the emergent behavior is independent of the grid size, since in both cases (Figures 3.4 and 3.5) the same parameters were used, showing how the proliferation of cancer cells with the hallmark EI acquired begins in the outer area.

3.1.1 Dependence of the emergent behavior on initial conditions

The previous examples and graphs correspond to initial situations with only one healthy cell at the center of the grid. This is the strategy used in most simulations found in previous works. To check if the initial condition determines

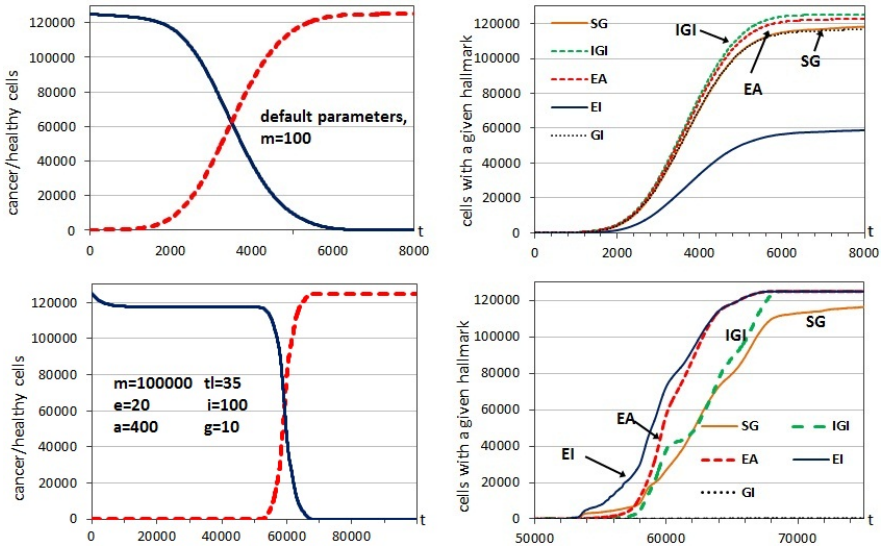

Figure 3.6: Evolution through time iterations of the number of healthy cells (continuous lines) and cancer cells (dashed lines) using an initial grid full of healthy cells (left), together with the evolution of the different hallmarks (right). The upper graphs correspond to the emergent behavior with parameter default values and $m = 100$, whereas the bottom graphs correspond to the behavior obtained with the parameters of Figure 3.4. All the graphs are an average of 5 independent runs.

the results in terms of emergent behavior obtained, we repeated the analysis but using an initial situation where the grid was initially full of healthy cells. Figure 3.6 shows the emergent behaviors obtained with two of the previous cases, using default parameters and $m = 100$ (Figure 3.3) and using the same parameter set of Figure 3.4.

In all cases, the final results are the same independently of the initial condition, except that this second and more realistic strategy needs more time iterations to reach a stable number in both types of cells. This is because there are fewer vacant sites in the grid to perform mitotic divisions, which does not allow the rapid progression of the cells as in the first strategy. The upper graphs of Figure 3.6 show the time evolution of healthy and cancer cells with parameter default values and $m = 100$, together with the time evolution of the hallmarks. This graph shows practically the same evolution of the hallmarks with respect to the case of beginning with only one healthy cell at the center of the grid, except the higher predominance of IGI with respect to EA, since the grid was (practically) full from the beginning. The bottom part of Figure 3.6 corresponds to the emergent behavior obtained with the parameters of Figure 3.4 but using again an initially full grid of healthy cells. For example, with this second strategy, the 100000 time iterations shown in the graphs correspond approximately to an average time of 29.7 years taking into account the corresponding biological time explained in the previous chapter.

The bottom graph on the right shows only the time interval of the transition between healthy and cancer cells, which begins after time iteration 52000, for a better visualization of the evolution of the hallmarks. Again, the hallmarks show the same evolution pattern of Figure 3.4, with a first predominance of EI with respect to EA, which is progressively reduced in next iterations.

3.2 Coupling between parameters

The previous examples correspond to specific scenarios with selected parameters in order to show representative situations regarding the emergence of different growth behavioral regimes and their dependence on hallmarks and hallmark parameters. Additionally, the simulations can visualize the coupling between parameters, that is, the resultant behavior can be inspected when the values of two parameters are changed, maintaining the rest at fixed values. Figure 3.7 corresponds to different examples changing two parameters, showing the final number of cancer cells after 1000 time iterations. Moreover, these examples in Figure 3.7 help to understand the main implications of the parameter values. In Figure 3.7.a the parameters g (which controls the hallmark IGI) and e (which controls the hallmark EA) were changed around their default values while the rest of parameters were set at their default values, except $m = 1000$. Figure 3.7.a shows that, when the value of g is decreased, as expected, the number of cancer cells tends to increase given the higher probability of invasion $(1/g)$ of the cells that acquired the hallmark *ignore growth inhibit* (IGI). When the parameter e is increased, the number of cancer cells also increases given the lower probability of cell death by the apoptotic process $(n/e$, see Table 2.1). However, this effect with the parameter e is lower with respect to the fast increase of cancer cells with a small change of the parameter g, as it can be seen in the upper graph with the rapid increase of the number of cancer cells with values of g around 10.

Figure 3.7.b corresponds to a sweep of the parameters i, which controls the hallmark *Genetic Instability* (GI) and e, again with the rest of parameters at their default vales and $m = 1000$. The increase in the orders of magnitude of i implies a slow increase in the final number of cancer cells, since the parameter only affects the cells that acquired the hallmark GI. As in the previous case, the increase of the value of e implies a low increase of the number of cancer cells, given the lower probability of apoptosis as consequence of the acquired hallmarks. Finally, Figure 3.7.c shows the results when the parameters m and g are changed while the rest were fixed at their default values. As remarked before, a decrease in the value of g means that the cells with the hallmark IGI acquired have a higher invasion potential in the surrounding tissue, as it is shown in the bottom graph, where the fast increase in the cancer cells with low values of g begins earlier. Nevertheless, the increase of the hallmark mutation rate $(1/m)$ has a greater effect on the number of final cancer cells after the limited number of time iterations considered.

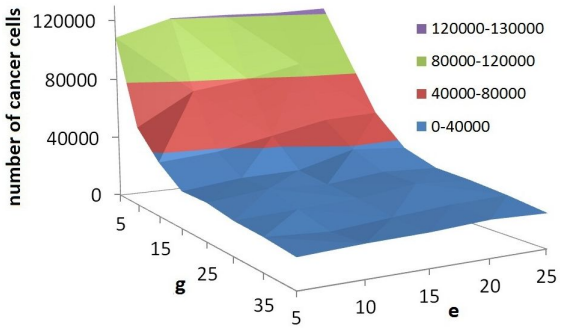

(a)

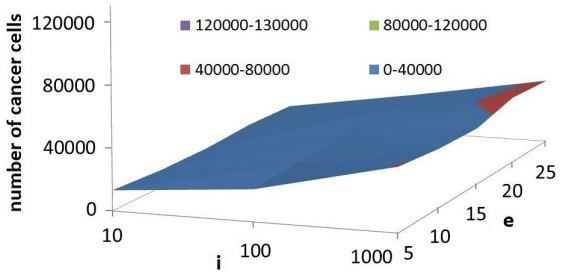

(b)

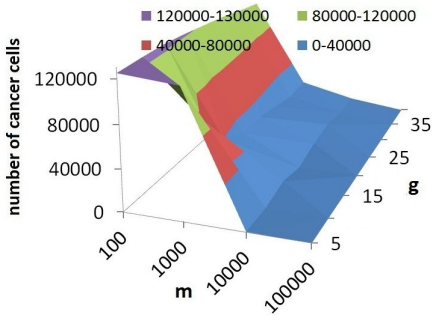

(c)

Figure 3.7: Number of final cancer cells when two parameters are changed, while the rest of parameters are set at their default values, except $m = 1000$ (a and b). The z axis shows the final number of cancer cells after 1000 time iterations in the simulation. a) Change of parameters e (which controls EA) and g (IGI). b) the parameters e (EA) and i (GI) were changed. c) the parameters m (hallmark mutation rate) and g (IGI) were changed. All the graphs are an average of 5 independent runs.

3.3 Relative importance of hallmarks

The aim in this section is to inspect the relative importance of each hallmark in the emergent behavior of tumor growth. To answer this, we can analyze the growth behavior when the individual hallmarks are not present or do not imply any effect on the cellular behavior. This is the same as considering that mutations do not activate a particular hallmark. We selected two representative cases to study the effect of not considering the individual hallmarks, that is, to inspect the relative importance of each hallmark in the cancer growth behavior. Note that this analysis can be very useful to establish the most appropriate therapeutic targets. As pointed out by Hanahan and Weinberg [40] "rapidly growing armamentarium of targeted therapeutics can be categorized according to their respective effects on one or more hallmark capabilities", although, as the same authors state, "each of the core hallmark capabilities is regulated by partially redundant signaling pathways. Consequently, a targeted therapeutic agent inhibiting one key pathway in a tumor may not completely shut off a hallmark capability" [40], although different drugs can act against specific hallmarks, as indicated for example with the categorization of therapeutic agents attacking specific hallmarks detailed by Luo et al. [56].

First, Figure 3.8 (Left part) shows the evolution across time iterations of the number of cancer cells (grid size=125000), using the default parameters with $m = 100$, when all the hallmarks are considered (previously shown in Figure 3.3), and when a particular hallmark is not taken into account in the rules of apoptotic and mitotic behaviors. As seen in Figure 3.8, the most important hallmark regarding the growth of cancer cells is *evade apoptosis* (EA), since its elimination implies a high decrease in the number of cancer cells. This is because, without the consideration of EA, all the cancer cells have a probability of death by apoptosis, so cancer cell proliferation is highly decreased.

The next most important hallmark is *ignore growth inhibit* (IGI), since its elimination implies also an important decrease in the number of cancer cells. This is because when the grid is almost full of healthy or cancer cells, after time iteration 200, the main limit for the mitotic divisions is the available free space. In this situation, the cancer cells with the hallmark IGI activated have an advantage, as they can replace (with a given probability) a neighbor cell to replicate. So, if this advantage does not exist when hallmark IGI is not considered, the cancer cells tend to remain stable in number, even with this very high hallmark mutation rate ($1/m$). A hallmark with similar relevance is *genetic instability* (GI), as without its consideration there are fewer mutations or acquisition of hallmarks. The previous effects are not present with the elimination in the simulation of the other hallmarks, as it implies a smaller decrease in the number of cancer cells.

The right part of Figure 3.8, in an alternative and similar analysis, shows the same evolution when only one particular hallmark is considered. As the Figure denotes, hallmarks EA and IGI are again the most relevant, and because the same reasons exposed. Note that now, when only *genetic instability* (GI) is considered, the number of cancer cells with only such a mutation cannot growth across time iterations. This is because GI only increases the

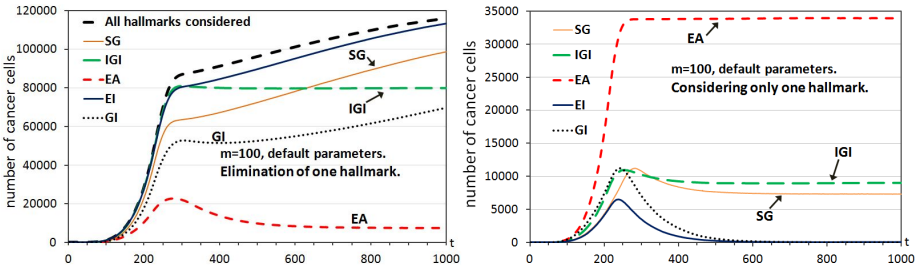

Figure 3.8: Left: Effect of elimination of an individual hallmark. Right: Number of cancer cells when only one hallmark is considered. Simulations with parameter default values and $m = 100$, averaged with 5 independent runs.

mutations in such cells for the acquisition of the other hallmarks that have a possible effect on the proliferation of cancer cells. Note also the difference between the hallmark relevance and the number of cells with a given hallmark (Fig. 3.3), since the relative relevance between EA and other hallmarks is not reflected in Figure 3.3.

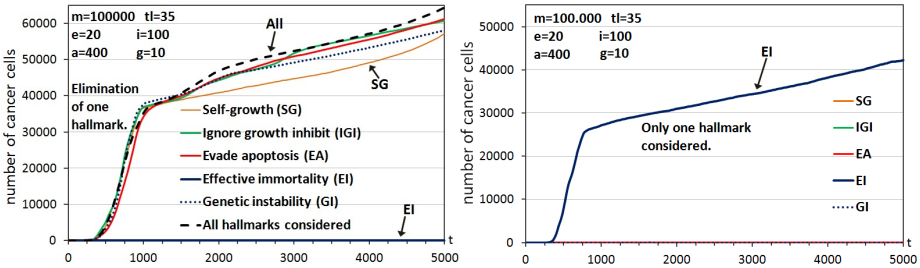

Figure 3.9: Number of cancer cells when an individual hallmark is not considered (Left) and when only one hallmark is considered (Right). Simulations with parameter values of Figure 3.4, averaged with 5 independent runs.

In Figure 3.9 we repeated the same analysis with the parameter set previously used in Fig. 3.4, which facilitates the appearance of cancer cells. As the Figure shows, when we do not consider the hallmark *effective immortality* (EI) in the simulation, the number of cancer cells is maintained to a minimum (close to 0, dark blue line). This is because, in this case, the great advantage of the limitless replicative potential is never present, so all cells have the same limit of replications imposed by the initial telomere length. The other hallmarks do not have relevance except the low relevance of *self-growth* (SG), as not considering it eliminates the final possible progression of cancer cells in the area without growth factor. It should be noted again that the relative relevance is not directly inferred from the evolution of the cancer hallmarks (Figures 3.4 and 3.6).

Table 3.2: Drugs that target specific hallmarks

Drug	Hallmark targeted	Comments
Bevacizumab	Angiogenesis	It blocks the potent angiogenic factor VEGF (Vascular Endothelial Growth Factor) to stop the angiogeneic ability of cancer.
Paclitaxel	Self growth	Inhibits mitosis to stop cancer cells from dividing. Cancer cells with self growth hallmark can divide without growth factors but this drug blocks their division.
GV1001	Effective immortality	It is a therapeutic peptide cancer vaccine targeting telomerase. Telomerase is an attractive target antigen for cancer immunotherapy because it is expressed almost universally in human cancers. This vaccine sensitizes immune cells to tumor cells expressing telomerase peptides as surface antigens. This causes an expansion of telomerase-specific cytotoxic T lymphocytes, directing the patient's own immune system to target and kill telomerase positive tumor cells.
Imatinib	Evade apoptosis	It is a tyrosine-kinase inhibitor used in the treatment of multiple cancers, especially leukemia. Imatinib blocks the BCR-ABL enzyme in cells with an abnormality of chromosome 22 and, as a result, these cells stop growing and even die by apoptosis.
Gendicine	Evade apoptosis	A drug that activates normal p53, this is used to treat head and neck cancers by activating normal p53 function (DNA repair, the induction of apoptosis,...) [14].
Flavopiridol	Ignore growth inhibit	It is an inhibitor of several cyclin-dependent kinases (CDKs), a family of proteins that regulate the cell cycle. It targets over expressed cyclins that allow cells to evade RB signals (RB protein is a tumor suppressor) and over-grow.

As indicated recently by Hanahan and Weinberg [39], in addition to providing a solid basis for cancer research, the hallmarks have served to identify certain cell functions that have become therapeutic targets. However, the utility of such attempts has been limited because tumor cells have demonstrated an ability to develop resistance to drugs that disrupt a single pathway. This adaptability of cancer cells suggests to Hanahan and Weinberg that simultaneous targeting of two or more hallmark pathways may be a more effective approach to therapy. So, our study indicates the importance of targeting therapies to the genetic networks and molecular pathways that control such most relevant hallmarks in each environmental and multicellular system situation. In fact, in modern therapeutic approaches most of cancer drugs are deliberately developed for specific molecular targets that involve the hallmarks. Following this philosophy, in the last years drugs interfering with the hallmarks of cancer have been developed. Some of them have already been approved, while others are still being tested in clinical trials [9][40]. In Table 3.2 examples of drugs that target each of the hallmarks are presented [14], whereas in Luo et al. [56] more details are shown about therapeutics selected based on the diversity of their chemical structures, the hallmarks they attack and their cellular targets.

Butler [14], in her PhD thesis in The University of Western Ontario (Canada), with this work as baseline, has continued our work in this line. In her work, hallmarks were removed in pairs, triplets and quadruplets in order to model combination therapy, abstracting drugs that target these properties as the removal of the hallmark from the system. It was found that many combinations had no effect on tumor growth. In some cases combinations even increased growth, selecting for the most aggressive hallmarks since weaker hallmarks were unavailable. However, in general, as more treatments were applied, cancer growth decreased [14].

3.4 Analysis of behavior transitions

The aim of this section is to inspect the change in behavioral regimes between states with predominance of one type of cells, especially when a target acts against cancer cells. Our objective is to analyze the growth behavior transitions in different circumstances. As in the previous study, the objective is not to mimic any particular cancer type, but to show how the simulation tool can provide knowledge to understand the implications and interrelations of the hallmarks, in this case to analyze possible behavior transitions, and selecting representative scenarios like in the previous sections.

Within this objective, Figure 3.10 shows a test of the decrease in cancer cells when a possible target acts against such cancer cells, killing them. We are supposing a perfect therapy in the sense that a drug only kills the cancer cells. The x axis is interpreted as the probability of eliminating cancer cells in the mitotic average time during the simulation. The mitotic events are scheduled between 5 and 10 iterations in the future, so the average time for a mitosis is 7.5. In practice, we applied, in each iteration or simulation time, the killing probability shown in the x axis divided by 7.5. The y axis indicates the number of final cancer cells. The graphs are an average of 5 different runs with each killing probability. The only reason for this definition of the probability

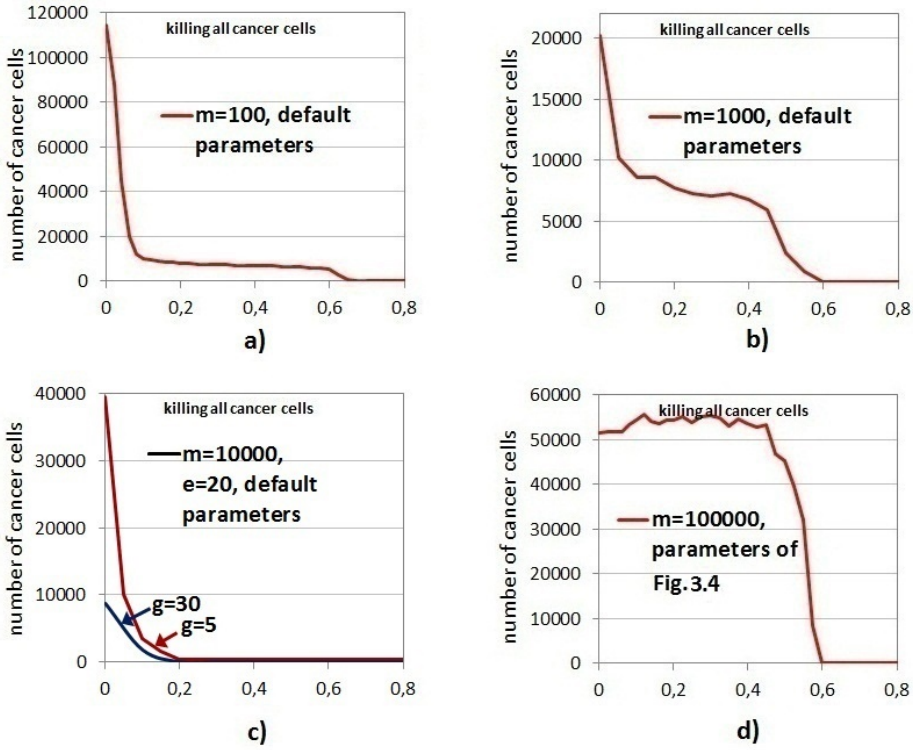

Figure 3.10: Effect of killing cancer cells during tumor growth for different killing probabilities and using four parameter sets. The x-axis is interpreted as the probability of eliminating cancer cells in the mitotic average time during the simulation, whereas the y-axis represents the final number of cancer cells.

is because it is better to think in the probability of cancer cell elimination in the average time of the mitosis (15-24 hours), being the results in terms of behavioral transitions independent of that interpretation.

Figures 3.10.a and 3.10.b include tests using two values of the parameter m, whereas the rest of parameters were set to their default values. In these two cases, the Figures show the final number of cancer cells after 1000 time iterations (y axis). As the Figures denote (Fig. 3.10.a and 3.10.b), it is easy to maintain the number of cancer cells to a minimum. In fact, there is a rapid decrease in the number of cancer cells (with probabilities < 0.2), which is similar to critical phase transitions of many emergent and complex systems, such as the Ising Model (Solé and Goodwin [92]), which present sudden shifts in behavior arising from small changes in circumstances.

The third case considered in Figure 3.10.c corresponds to a scenario with lower mutation rate ($m = 10000$) and different invasion potentials by ignoring the contact inhibition mechanism, since we used different values in parameter g. We used two values, the standard value ($g = 30$) and a lower value ($g = 5$) that confers a high invasion potential to the cells that acquire the hallmark

ignore growth inhibit (IGI). These parameters (with g=5) used in this scenario are the same used by Spencer et al. [94], in their case to study how the sequence of acquired mutations affects the timing and cellular makeup of the resulting tumor. Thus, cells that have acquired the hallmark IGI will have a high capability to invade the surrounding space. Cervical cancer is an example, whereas, on the contrary, the naked mole-rat displays hypersensitivity to contact inhibition which confers it an extraordinary resistance to cancer [89]. In this example, Figure 3.10.c shows again the final number of cancer cells after 1000 time iterations (y axis). As in the first example with a high mutation rate, there is a fast transition in the emergent behavior, again showing that a small increase of the killing probability can imply a fast decrease in the capability of cancer cells to propagate. Cells that acquired the hallmark IGI have such a high capability, but there are few because the lower mutation rate (with respect to the previous cases). So, the simulation shows how a little increase in the killing probability counteracts the high invasion capability of the few cells with IGI acquired.

Finally, we repeated the experiment using the parameter set in Figure 3.4, which facilitates the appearance of cancer cells (m=100000, tl=35, e=20, i=100, g=10, a=400). Figure 3.10.d shows again the final number of cancer cells after the simulation run, taking into account that the cancer cells in each simulation iteration are eliminated with a given probability. In this case the y axis indicates the number of final cancer cells after 3000 time iterations, since with this parameter set more iterations are needed to overtake the rapid and initial increase of healthy cells (as left part of Figure 3.4 denotes). With this parameter set, the sharp behavior transition happens at a higher frequency with respect to the previous cases, indicating the difficulty in maintaining the cancer cells under a low threshold when the conditions make their appearance easier. The small increase of cancer cells with low values of the killing frequency is because, with such values, healthy cells can perform more rapidly their limited number of mitoses (there are more available sites to complete the maximum number of mitoses). Thus, more vacant sites are appearing for the cancer cells with hallmark *effective immortality* (EI) acquired, so they propagate more rapidly. This effect is counteracted by the increasing killing frequency, until the final and critical behavior transition.

Nevertheless, this first strategy to inspect the behavior transitions, when killing cancer cells, could be valid in cells cultured as monolayers, but not in vitro three-dimensional tumor spheroids or in vivo solid tumors. As explained by Minchinton and Tannock [64], tumors are more resistant to therapy than cancer cells cultured as monolayers. This can be explained by "multicellular resistance", a mechanism for drug resistance attributed to cell-cell contacts, cell-matrix contacts, and the three-dimensional (3D) shape found in tissue. As Phung et al. also indicate [77] "the solid tumor microenvironment has several major characteristics, including hypoxia, large distances between blood vessels, high interstitial fluid pressure, structure and composition of the extracellular matrix, and cell-cell adhesion. Overall, these features of the tumor microenvironment limit the delivery of anticancer drugs to cancer cells that are situated far from blood vessels". Nevertheless, as the same authors comment [77], even with the simplifications of the in vitro multicellular spheroids,

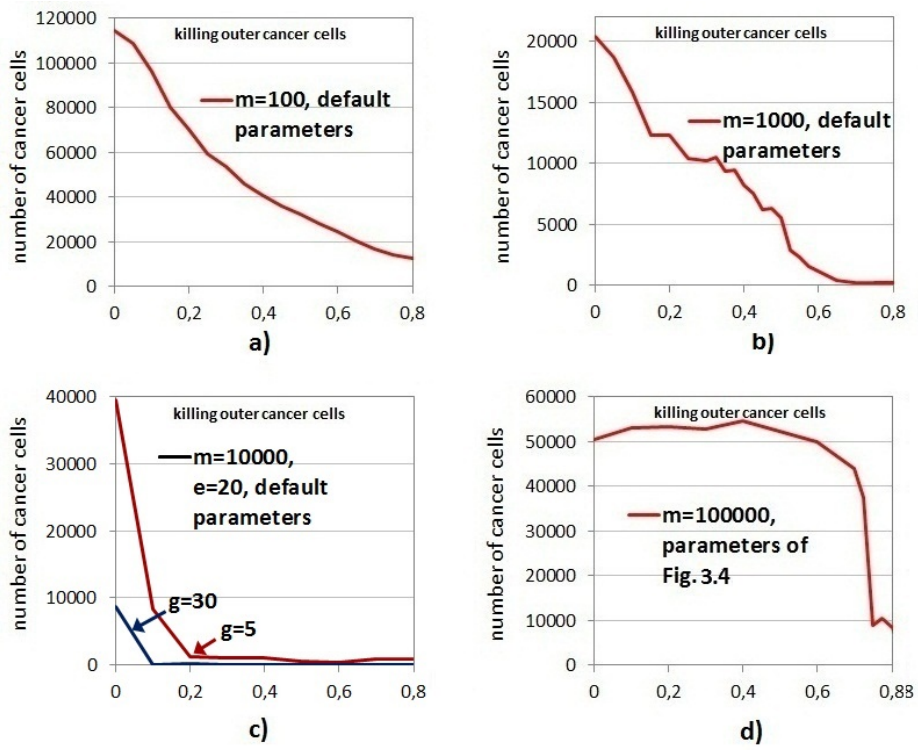

Figure 3.11: Effect of killing cancer cells during tumor growth for different killing probabilities and using four parameter sets. The x-axis is interpreted as the probability of eliminating cancer cells in the mitotic average time during the simulation, whereas the y-axis represents the final number of cancer cells. Only the most outer cells (distance of 3 or less to the boundary of the expanding tumor) are killed with the corresponding probability indicated in the x-axis.

these constitute a simple and relevant model of in vivo tumors "that allows for further investigations of the microenvironmental effects on drug penetration and tumor cell killing".

Ma et al. [57] applied a 3D imaging method of tumor spheroids to study the penetration behavior of doxorubicin, one of the most celebrated chemotherapeutics, commonly used to treat a wide range of cancers. When HeLa cells (human cervical adenocarcinoma) were grown in a monolayer, doxorubicin was absorbed rapidly during a short period of time. They compared the penetration of doxorubicin into monolayer cells versus spheroids and found that doxorubicin entered spheroids much more slowly than an equivalent number of monolayer cells. As the authors state, this demonstrates that HeLa cells in 3D structures provide a multicellular resistance model that mimics the chemotherapy resistance often found in solid tumors in vivo.

Therefore, we repeated the analysis but considering that only the outer cells are subject to be killed by the effect of a drug. We considered as targets the

cancer cells in the boundary of the tumor expansion or close to the boundary, at a Euclidean distance of 3 or less to the exterior of the expanding tumor. We are using again a grid with 125000 sites, thus each dimension has 50 sites or points with integer coordinates. So, the maximum distance of 3 represents, for example, a 6% of the total distance in each dimension.

Figure 3.11 shows again the same analysis with the four parameter sets considered before when killing all cancer cells. In the first case (Figure 3.11.a), using the highest mutation rate ($m = 100$), now there is not a fast transition in the number of cancer cells when increasing the probability of cancer cell killing. This is because the inner cells, with many hallmarks acquired given the high mutation rate (see cross-section of Figure 3.3), are the responsible to renew constantly the outer area of the expansion tumor. This effect is less clear with a lower mutation rate ($m = 1000$, Figure 3.11.b).

Considering the scenario of a high invasion potential, ignoring the contact inhibition mechanism when using a lower value of the parameter g (Figure 3.11.c), the transition is quite similar to the case when all cancer cells were killed (Fig. 3.10.c). The transition is practically as fast as in Fig. 3.10.c, requiring a very small increase in the killing probability to practically eliminate all the cancer cells. The reason is that there are few cells with the high invasion potential, cells that propagate only in the outer part of the growing tumor. So, the scenario is similar to consider the elimination of all the cancer cells. With the higher value of the parameter ($g = 30$), although the lower number of final cancer cells (with respect to g=5), the same comments can be made with respect to the previous case in Fig. 3.10.c

On the contrary, the cases in Figure 3.11.c are different to the previous cases with higher mutation rates, because in those previous cases ($m = 100$ and $m = 1000$, Fig. 3.11.a and 3.11.b), as indicated, a cancer cell in the inner area can propagate rapidly if only the most outer cells are eliminated. In those cases, the resultant vacant sites allow the easy replication of such cancer cells, acquiring also more hallmarks given the high mutation rate.

Finally, with the parameter set used in Fig. 3.4, which uses a low mutation rate ($m = 100000$) and short telomere lengths in all cells ($tl = 35$), there is also a critical phase transition (Figure 3.11.d). The reason is that, in this case, the increase in cancer cells begins in the boundary of the multi-cellular system expansion, when a cell or cells with the hallmark *effective immortality* (EI) acquired appear, so they are not limited in their number of possible replications as the healthy cells. This expansion in only the outer area was shown in the 2D cross-section of Figure 3.4 and in the temporal progression in 3D of Figure 3.5. As in this case the inner area does not provide cancer cells, then the transition is similar with respect to the case of killing all cells (Figure 3.10.d), although requiring a bit higher probability of killing the outer cancer cells for the fast transition.

Therefore, in this section, we focused on the analysis of the effect of killing cancer cells, inspecting the time evolution of the multicellular system under different conditions (defined by the relative prevalence of different hallmarks) and the possible behavioral transitions between the predominance of cancer and healthy cells. With high mutation rates and standard parameters, considering a scenario of cells cultured as monolayers, the cancer cells can be easily

controlled supposing that a target can kill all cancer cells, with the presence of rapid behavior transitions. When considering the growth of multicellular spheroids, killing only the outer cells, there are not rapid transitions but a progressive decrease of the number of cancer cells when increasing the killing frequency. On the contrary, in situations where cells at the tumor boundary drive tumor expansion, there are no significant differences between the consideration of killing all cancer cells and killing only cancer cells at the boundary or the tumor, such as the case considered with a high invasion potential when ignoring the contact inhibition mechanism. Also in this case, the study showed the difficulty in maintaining the number of cancer cells to a minimum when the hallmark *effective immortality* has an advantage with respect to the rest of the cells, and with the appearance of rapid behavior transitions between states with predominance of both types of cells. So, this analysis represents an alternative to the in-vitro experiments focused on the study of the comparative effects of different drugs or drug combinations [22][63], since it indicates that these in-vitro studies should also search for possible behavior transitions when drugs are applied.

Chapter 4

Simulation of Cancer Stem Cells

4.1 Cancer stem cell theory

A central question in cancer biology is which cells can be transformed to form tumors. The cancer stem cell theory suggests that among all cancerous cells, a minority of them called Cancer Stem Cells (CSC) act as stem cells that reproduce themselves and sustain the cancer. They are responsible for the initiation of tumor development, growth, and tumor's ability to metastasize and reoccur [25][34]. The transformation of a normal stem cell into a cancer stem cell is due to the accumulation of genetic modifications (mutations in oncogenes, suppressor genes and miss-match repair genes) and epigenetic alterations (abnormal methylation, histone modification) [34].

Vital studies of serial re-transplantation of harvested tumor cells into immunodeficient mice repeatedly reveal that large numbers of tumor cells, although apparently transformed, cannot initiate new tumors [4]. Initial growth phases are followed by remarkable decreases in tumor size up to complete remission and a burden-free survival of the animal. Al-Hajj et al. [4] using a model in which human breast cancer cells were grown in immunocompromised mice, found that only a minority of breast cancer cells had the ability to form new tumors. They were able to distinguish the tumorigenic (tumor initiating) from the nontumorigenic cancer cells based on cell surface marker expression.

Cancer stem cells have been shown to have various characteristics in common with stem cells. For example, they have the capacity to divide indefinitely [93]. Nevertheless, to avoid speculative comparison to somatic stem cells, alternative nomenclatures such as tumorigenic cells, tumor-initiating cells, tumor rescuing units, or stem-like cancer cells are common [12]. CSCs may generate tumors through the stem cell processes of self-renewal and differentiation into multiple cell types. So, departures from the classic view of cancer have recently emerged [25] since, if current treatments of cancer do not properly destroy enough CSCs, the tumor will reappear.

There are two models when considering the origin of cancer cells: The hierarchical model assumes that tumors are originated from CSCs that give rise to

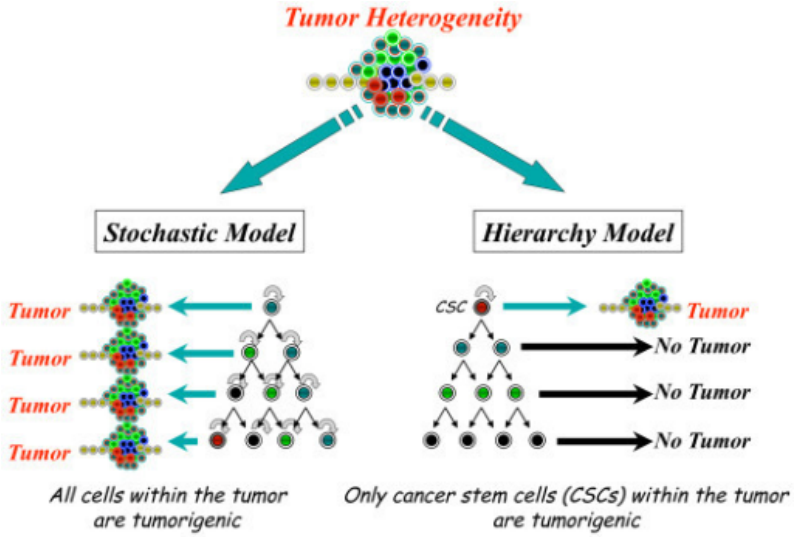

Figure 4.1: Different models for cellular origin of cancer. Two models have been proposed to explain the cellular heterogeneity in cancer: the stochastic model and the hierarchical model. In the first one, every tumor cell can stochastically generate a tumor. In the second one, only the CSCs can generate tumors. Figure from [16], reprinted with permission from BioMed Central.

progeny with self-limited proliferative capacity where most of the cells in the tumor are genetically homogeneous. The second model is the stochastic model or clonal evolution model, which postulates that tumorigenesis is a multistep process that leads to progressively genetic alterations with the transformation of healthy cells into malignant phenotypes [104]. Figure 4.1 shows the difference between these two models.

In the hierarchical model, such CSC cells are proposed to persist in tumors as a distinct population and cause relapse and metastasis by giving rise to new tumors. So, different works tried to simulate their behavior, taking into account their main characteristics, such as their capacity to divide indefinitely [103]. Since CSCs can cause regrowth of the tumor, it is important to understand their behavior and effects.

4.1.1 Previous works about cancer stem cell simulation

Enderling and Hahnfeldt [25] used a hybrid mathematical-cellular automaton model that simulated growth of a heterogeneous solid tumor comprised of cancer stem cells and non-stem cancer cells, adopting a parameter-minimalist approach, focused on cell proliferation, cell migration and cell death. Unlimited proliferation capability, immortality and symmetric division define their CSC modeling. While two non-stem cancer cells are always the result of non-stem cancer cell proliferation, CSCs can divide either symmetrically to yield two CSCs, or asymmetrically to produce a CSC and a non-stem cancer cell (Differentiated Cancer Cell, DCC) with limited proliferation capacity. This is

similar to the behavior of adult stem cells in their aim for maintaining and renewing a given tissue, where the division of adult stem cells is thought to be asymmetric. Their model showed how the introduction of cell fate heterogeneity paradoxically influences the tumor growth dynamic in response to apoptosis, to reveal yet another bottleneck to tumor progression potentially exploitable for disease control. Moreover, in [71], the authors showed that although CSCs are necessary for progression, their expansion and consequently tumor growth kinetics are surprisingly modulated by the dynamics of the non-stem cancer cells. Their simulations revealed that slight variations in non-stem cancer cell proliferative capacity can result in tumors with distinctly different growth kinetics.

Vainstein et al. [98] used a 2D CA model which emphasized the distinction between CSCs and DCCs (Differentiated Cancer cells, which do not divide and have a limited lifespan) and assumed that CSC fate is governed by quorum sensing, i.e., the ability of a stem cell to decide whether to differentiate, on the basis of the number of stem cells in its neighborhood. They analyzed how tumor progression is affected by differentiation therapy and by standard (cytotoxic or antiproliferative) therapy, both alone and in combination. Their simulation results showed that only treatment which simultaneously prevents CSC proliferation and promotes differentiation can effectively eliminate CSCs and lead to tumor eradication.

Sottoriva et al. [93] presented a mathematical model of malignancies to investigate how a hierarchical organized cancer cell population affects the fundamental properties of solid malignancies. Their results indicated that tumors modeled in a CSC context more faithfully resemble human malignancies and show invasive behavior, whereas tumors without a CSC hierarchy do not. Moreover, their results showed that the CSC model allows for significantly higher tumor heterogeneity, which may affect therapy resistance, showing also that therapy which fails to target the CSC population is not only unsuccessful in curing the patient, but also promotes malignant features in the recurring tumor.

4.1.2 Cancer stem cell modeling

For the simulation of the hierarchical CSC model we considered the scheme that distinguishes between CSCs and Differentiated Cancer Cells (DCCs). The CSCs have two defining properties: no limit in their proliferation capacity and resistance to apoptosis [34]. In our model it is easy to incorporate these properties, as they imply that CSCs have acquired the hallmarks *effective immortality* (EI) and *evade apoptosis* (EA). In the simulations, we will introduce a low number of CSCs in the inner area with growth factor to check their effect on the behavior of the multicellular system evolution.

We followed the simulation used by Enderling and Hahnfeldt [25] regarding CSC differentiation. Thus, CSCs will divide symmetrically, with a low probability ($p_s = 0.01$ in [25]) or asymmetrically (with probability $1 - p_s$) to produce a CSC and a non-stem cancer cell (Differentiated Cancer Cell - DCC). Moreover, in our simulation, in the asymmetric division, the differentiated non-stem cancer cell acquires (randomly) one of the hallmarks considered in our modeling

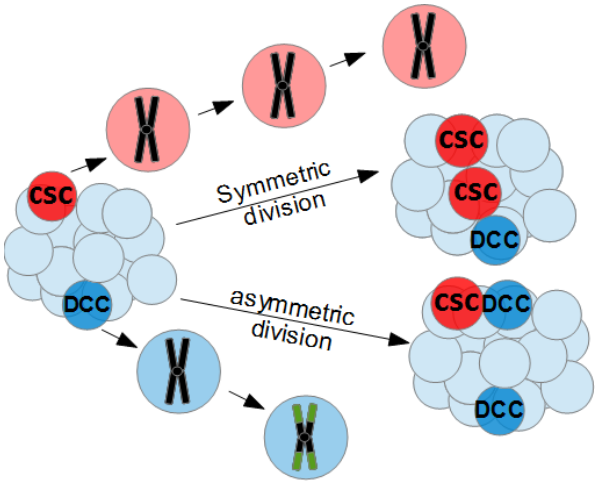

Figure 4.2: In the Cancer Stem Cell (CSC) model these cells can divide symmetrically or asymmetrically to produce Differentiated Cancer Cells (DCCs) with limited proliferative capability.

as well as the initial telomere length which defines its finite replicative potential. So, our model is more general as it considers in the CSC scheme the different capabilities of hallmarks acquired in the cells. Thus, our model does not consider both models about the origin of cancer cells as mutually exclusive, since DCCs are genetically heterogeneous given the different hallmarks acquired in such cells. As indicated by Yap et al. [104], there is a high degree of convergence between the two models as shown, for example, in leukemia [104].

Figure 4.2 summarizes the behavior of these cells. Cancer stem cells can divide either symmetrically to yield two CSCs, or asymmetrically to produce a CSC and a non-stem cancer cell (DCC). The probability of symmetric division is very low, which reflects the correspondingly low fraction of cancer stem cells reported throughout the literature. For example, as commented, Enderling and Hahnfeldt [25] considered a probability $p_s = 0.01$ to determine symmetric CSC division.

Finally, a CSC can only divide when it has available space in its immediate neighborhood. This is the same condition considered by Morton et al. [71] or Vainstein et al. [98]. For example, Morton et al. [71] stated that "the probability of symmetric and asymmetric CSC division is constant and stochastic, and cells require adjacent available space to migrate or proliferate". Similarly, in Vainstein et al. [98] the authors assumed that each CSC is either "non-cycling" (quiescent) or "cycling", i.e., the cell progresses through the cell cycle and after a fixed time period divides into two CSCs. Their non-cycling CSCs can enter the cell cycle at any time and it depends on the total cell density in the CSC's vicinity: the more vacant (i.e., unoccupied by other cells) space available, the greater the probability that the CSC will enter the cell cycle. Nevertheless, we did not use their model of a "quorum sensing" control mech-

anism (direct stimulation of differentiation of a stem cell by its neighboring stem cells), as we used the commented model of CSC differentiation taking into account a probability of symmetric and asymmetric division, as in [25] and [93].

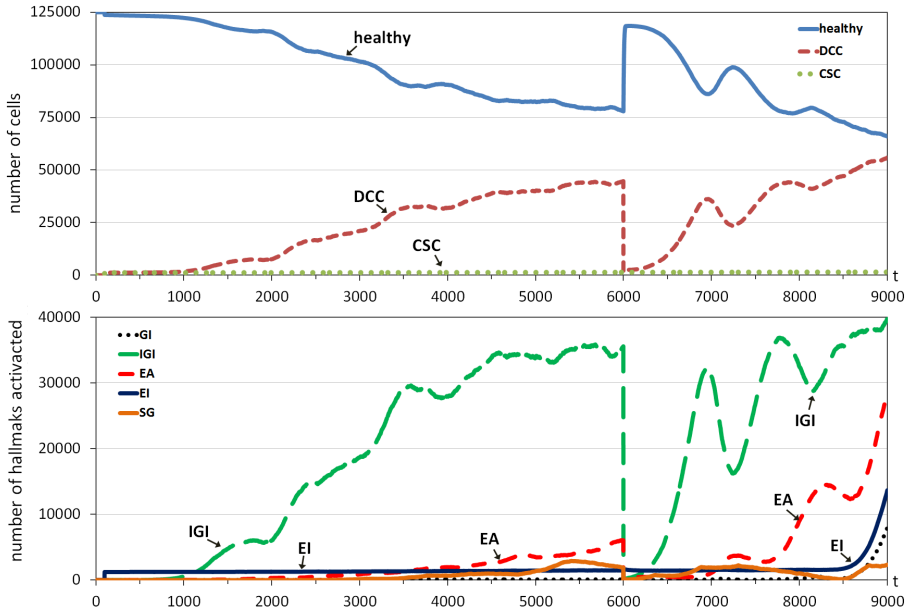

Figure 4.3: Upper graph: Evolution through time iterations of the number of healthy cells (continuous line), non-stem or differentiated cancer cells (DCCs, dashed line) and Cancer Stem Cells (CSCs) (pointed line). CSCs are introduced at time iteration 100 (1% of the grid size) in the grid initially full of healthy cells. Standard hallmark parameters were used except g=5. At time iteration $t = 6000$ the 100% of DCCs is killed. Bottom graph: Evolution through time iterations of the different hallmarks in the cancer cells.

4.2 Cancer stem cells simulation

In the previous chapter we have analyzed the capabilities of the hallmarks, with their main interrelations with other hallmarks, to promote tumor growth. These previous analyses serve us to test now their capabilities in a cancer stem cell context.

In their work, Enderling and Hahnfeldt [25] considered a probability p_s to determine symmetric CSC division. As the authors indicate [25], in a model based on cancer stem cells hypothesis, only a minority of cells are presumed to be CSCs, the rest being non-stem cancer cells with a finite proliferation capacity (maximum number of mitoses). The authors assumed that cancer stem

cells divide symmetrically with probability $p_s = 0.01$, reflecting the correspondingly low fraction of cancer stem cells reported throughout the literature.

Our simulated CSCs will have always the hallmark *effective immortality* acquired, so they will have no limit in their proliferation capacity, in addition to the resistance to apoptosis [34]. The CSCs will divide symmetrically, with the same probability used in [25] ($p_s = 0.01$) or asymmetrically to produce a CSC and a non-stem cancer cell and with probability $1 - p_s$. As explained, in the asymmetric division, the differentiated non-stem cancer cell acquires (randomly) one of the 5 hallmarks considered in the simulation as well as the initial telomere length which defines its finite replicative potential (unless it acquires the hallmark EI). Note that this is different to the general symmetric division that copies all the genetic information to the daughter cell. When those non-stem cancer cells divide later, the resultant non-stem cancer cells can acquire more mutations or hallmarks.

For the simulation we introduce a number of CSCs in the growth area of the multicellular system evolution. Figure 4.3 includes a representative example with a run of the system evolution with this simulation. The Figure shows the evolution through time iterations of healthy cells, non-stem cancer cells (DCCs) and CSCs, when a number of CSCs corresponding to a 1% of the grid size (125000) was introduced at iteration 100 (1250 CSCs) in the inner area with growth factor, with the grid initially full of healthy cells. These incorporated CSCs are not subject to apoptosis [34], so their presence is maintained according to the cancer stem cell theory. The value of parameter g was set to 5 and the rest of the hallmark parameters were set to their standard values in the run.

Since there is not practically any free site, in this situation, most CSCs remain quiescent until they have free space to perform mitoses. Additionally, as the probability of symmetric division is very low, the number of CSCs remains stable during the 9000 iterations shown in Figure 4.3. However, the non-stem cancer cells begin to grow due to the asymmetric division of the CSCs and thanks to the acquisition of the hallmark *ignore growth inhibit* (IGI) in many of such non-stem cancer cells, which can proliferate in this situation with practically no free sites and until they reach the maximum number of divisions ($tl = 50$). The value of g used in the simulation example ($g = 5$) allows such a rapid proliferation thanks to their high capability to propagate in the surrounding tissue. As more mutations are appearing in this proliferation of non-stem cancer cells, then hallmark *evade apoptosis* (EA) also appears in many non-stem cancer cells to avoid the apoptotic process.

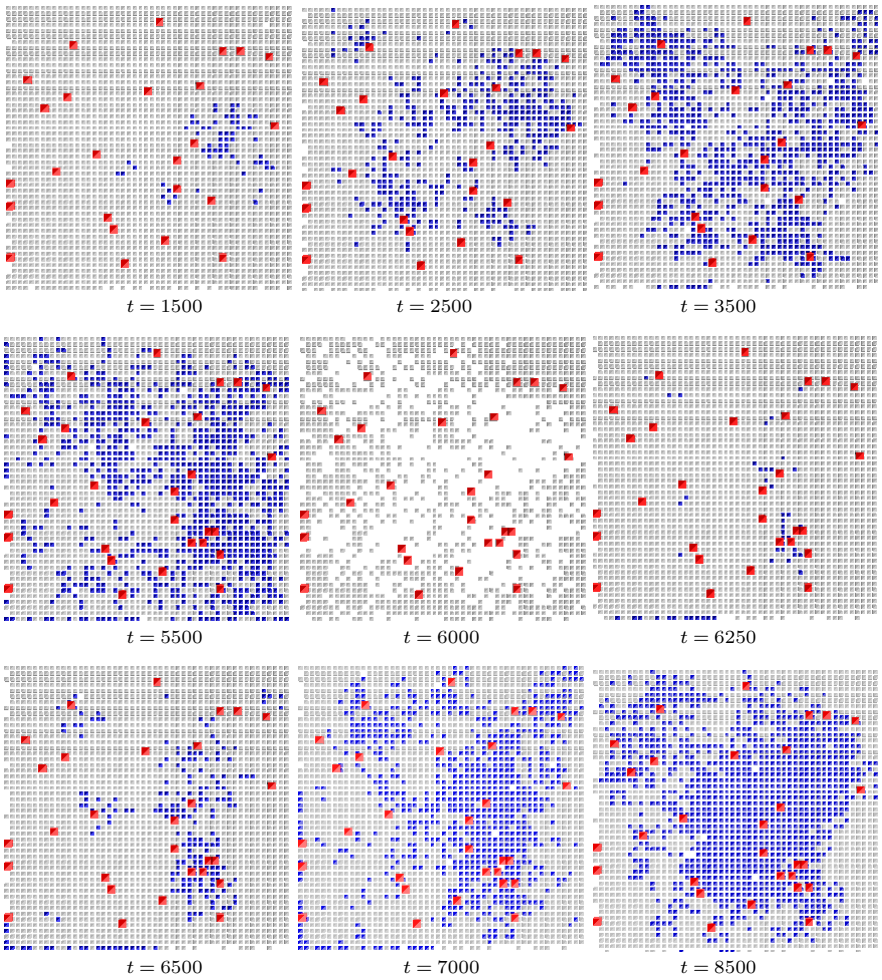

Figure 4.4: Snapshots of 2D central sections of the multicellular system evolution corresponding to different time iterations in Figure 4.3 (Colors: Gray - healthy cells, Blue - DCCs, Red-enlarged size - CSCs).

Figure 4.4 shows cross-sections of this multicellular system evolution at different time iterations. These cross-sections correspond to 2D sections of a plane that crosses the center of the grid. These 2D cross-sections show the progressive expansion of the tumor cells (DCCs), with the colonization of many areas previously initialized with some DCCs and thanks to the continuous presence of CSCs (shown with enlarged sizes in the cross-sections).

CSCs have been suggested to be more resistant to therapeutic interventions such as chemotherapy or irradiation compared with their differentiated counterparts [93]. In fact, CSCs are relatively resistant to such standard cytotoxic and irradiation therapies since, for example, cytotoxic therapies affect rapidly proliferating cells, whereas evidence suggests that only a small fraction of CSCs actively proliferate. Hence, at time iteration 6000 the 100% of non-stem cancer cells is killed, simulating a cancer therapy, causing the drastic drop of the non-stem cancer cells. The healthy cells that have not performed the maximum number of divisions fill rapidly the space (see the cross-section at t=6250), but the non-stem cancer cells recover quickly because the CSCs not killed produce again non-stem cancer cells, repeating a similar evolution pattern like the one at the beginning of the simulation. Nevertheless, note that this second proliferation on non-stem cancer cells is faster. This is because, after killing the DCCs, there is one important detail to take into account: The CSCs had more opportunities to differentiate in the small amount of time until the grid is completely filled with mostly healthy cells. So, the few non-stem cancer cells, after the differentiation, can produce the faster proliferation of cancer cells. The fluctuations in the expansion of these cells (and consequently in healthy cells) are because the cells with IGI acquired proliferate faster when they are surrounded by healthy cells. However, when the concentrations or clusters of cells with IGI acquired reach a certain size, then the apoptotic process can decrease their size for a small time, until reaching another lower size where the proliferation continues again.

We repeated the same analysis with another conditions. In Figure 4.5 we introduced again the same number of CSCs at $t = 100$ in the inner area of the grid with the same size (125000), being this initially full of healthy cells. In this case, all the parameters were set to their standard values except a higher mutation rate ($m = 1000$). Figure 4.6 shows cross-sections of the multicellular system evolution at different time iterations. Now, given the higher mutation probability, the hallmark *evade apoptosis* (EA) becomes the most predominant to avoid the apoptotic process. Its combination with *ignore growth inhibit* (IGI) allows the cells with both hallmarks acquired to begin to proliferate after many iterations (around time iteration 3900). These two hallmarks are co-acquired since they are necessary to overcome two different barriers to cancer growth: EA is necessary to avoid the barrier of the apoptotic process, given the high mutation rate, whereas IGI is necessary to escape the second barrier to cancer cell proliferation, since practically there is no free space.

The growth begins in most cases near the boundary of the grid, because cells that acquire the hallmark *self-growth* (SG) find an immediate advantage in the area without growth factor (most outer area of the grid). As in the previous case, at $t = 6000$, the non-stem cancer cells are killed. After that, the

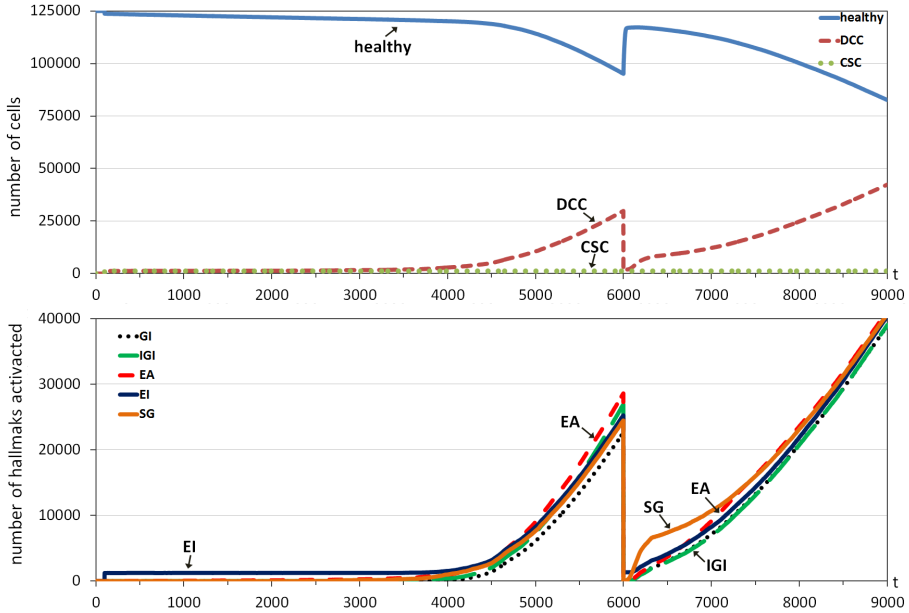

Figure 4.5: Upper graph: Evolution through time iterations of the number of healthy cells (continuous line), non-stem or differentiated cancer cells (DCCs, dashed line) and Cancer Stem Cells (CSCs) (pointed line). CSCs are introduced at time iteration 100 (1% of the grid size) in the grid initially full of healthy cells. Standard hallmark parameters were used except m=1000. At t=6000 the 100% of DCCs is killed. Bottom graph: Evolution through time iterations of the different hallmarks in the cancer cells.

same proliferation pattern happens but with a clear faster evolution, and for the same reason as in the previous case: The CSCs had the opportunity to differentiate just after killing the DCCs, thanks to the free sites that suddenly appear, although these are rapidly filled mostly with healthy cells (e.g., see cross-section at t=6100). Nevertheless, the few DCCs after the differentiation are sufficient to cause that rapid increase of cancer cells.

Note that even we had modeled the killing of only the cancer cells that are close to the boundary of the tumor expansion in the same sense considered in previous chapter, the conclusion would have been the same, being this that some CSCs (near the boundary) would have the opportunity to differentiate in non-stem cancer cells that can renew a tumor proliferation in advantageous scenarios, although needing more iterations. This second example (Figures 4.5 and 4.6) is also closer to this consideration, since most of the cancer cells are close to the boundary, as the cross-sections of Figure 4.6 show.

Since the application of a standard treatment in a cancer stem context has consequences on the tumor regrowth behavior, we can analyze in more detail different strategies to apply a standard treatment, with the aim of minimizing the effects of possible regrowth. This is the aim of the next chapter.

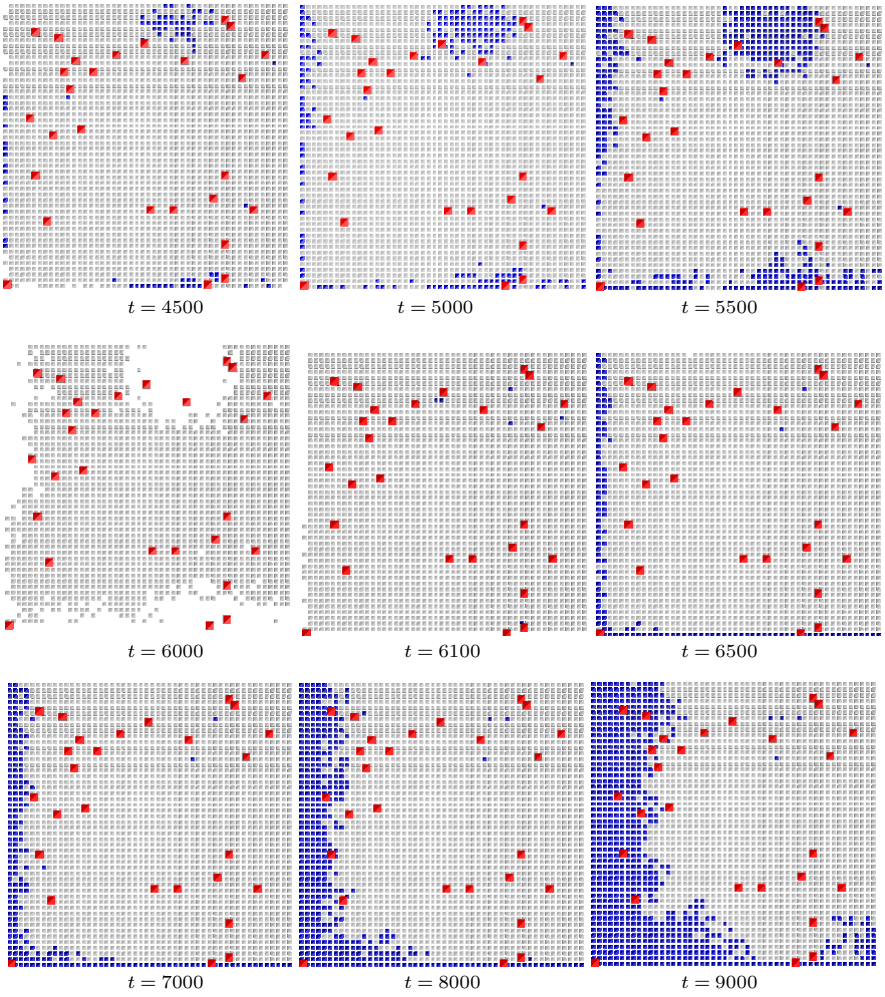

Figure 4.6: Snapshots of 2D central sections of the multicellular system evolution corresponding to different time iterations in Figure 4.5 (Colors: Gray - healthy cells, Blue - DCCs, Red-enlarged size - CSCs).

Chapter 5

Treatment strategies analysis in a cancer stem context

Designing successful cancer drugs is very challenging but equally challenging is the design of optimal treatment scheduling. Biologists, clinicians, mathematicians, computational scientists and engineers are working towards the goal of improving the treatment scheduling. As McGuire et al. [61] mentioned: "Researchers with different scientific backgrounds explored the topic of how to advance metronomic drug therapy for cancer from its experimental successes to general clinical acceptance for specific pathologies."

In this chapter the effect of cancer treatments in a cancer stem cell context is analyzed. The simulations can help to suggest which treatment strategies are better taking into account the regrowth capacity of cancer stem cells considered in the previous chapter. Most of the results considered here are described in our works [69][87].

There is no single treatment for cancer. Doctors use different treatments, or a combination of them, to achieve the best result depending on the concrete case. There are three major types of treatments:

- Surgery.
- Radiotherapy: uses high-energy rays to cure or control cancer. The high-energy radiation used during radiotherapy permanently damages the DNA of cancer cells, causing them to die.
- Drug therapies: this therapy can be divided in two subclasses:
  - Chemotherapy: uses cytotoxic drugs to kill cancer cells. There are many types of chemotherapy drugs that can be given individually or in combination. Usually, the drugs work by damaging the RNA or DNA that tells the cell how to copy itself in division. If the cells are unable to divide, they die. As with radiotherapy, the faster the cells are dividing, the more likely it is that drugs will kill the cells. In other words, chemotherapy destroys healthy and cancerous cells in the proliferative state but is most effective at killing cancer cells

because these have higher proliferative fractions than normal cells. This type of chemotherapy drugs are called cell-cycle specific (antimetabolites, vinca alkaloids, taxanes, epipodophyllotoxins, camptothecans), while other drugs that affect cells when they are at rest are called cell-cycle non-specific (antitumour antibiotics, Alkylating agents, Nitrosoureas). The scheduling of chemotherapy is set based on the type of cells, rate at which they divide, and the time at which a given drug is likely to be effective. This is why chemotherapy is typically given in cycles.

– Biological therapies: use substances that occur naturally in the body to destroy cancer cells. The main types of biological therapies are: monoclonal antibodies, cancer growth inhibitors, angiogenesis inhibitors, gene therapy, vaccines and interferon (a group of signaling proteins made and secreted by cells of the immune system in response to the presence of pathogens, such as viruses, bacteria, or tumor cells).

5.1 Previous works on cancer treatment simulation

The goal of standard therapies like chemotherapy and radiotherapy is to destroy the tumor cells, while maintaining adequate amounts of healthy tissue. Optimality in treatment might be defined in a variety of ways. Some studies have been carried out in which the total amount of drug administered, or the number of tumor cells, is minimized. For example, in the models considered in [96][97], the goal was to maximize the number of cancer cells killed by a chemotherapy agent, or to minimize the number of cancer cells at the end of the therapy session, while keeping the toxicity of the normal tissues acceptable.

In chemotherapy, the administration of one or more drugs is aimed to kill tumor cells in which the growth rate is faster than normal cells. Within this context, the mathematical modeling of anticancer chemotherapy has existed for more than four decades [23][95]. For example, the Norton-Simon model [74][91] states that the rate of cancer cell death in response to treatment is directly proportional to the tumor growth rate at the time of treatment. This model, for cell-cycle specific drugs, suggests that moderate early doses followed by later dose intensification would kill more tumor cells [74].

In the work of De Pillis and Radunskaya [20], the authors attempted to find equilibrium for a chemotherapy administration schedule that would kill off the tumor cells as effectively as possible, with the constraint that the treatment must not kill too many normal cells. Their optimal control algorithm dictates that a drug must be administered continuously over relatively long periods of time (on the order of days). Other authors have also applied techniques from optimal control theory to discover how chemotherapy and immunotherapy can best be combined for the effective treatment of cancer [47].

Several models predict that continuous infusion (in particular of cell-cycle phase specific drugs) is more effective than short pulses [53]. However, if the drug is applied too slowly by continuous infusion, drug resistance may develop [53]. Gardner [28] modeled this trade-off considering cell-cycle specific and

cell-cycle nonspecific drugs, and used his model to provide insight into how the chance of a cure is connected with the dose and type of infusion.

These representative examples are not an exhaustive list of the works related to *in silico* studies about treatments. This present study is related to them although it will analyze the effect of treatments in a cancer stem cell context.

5.2 Results

5.2.1 Simulation setup

In the simulations the effect of a cancer treatment taking into account the presence of CSCs is simulated. Generic cancer protocols in early avascular stages of cancer are considered, given that they are ideal treatments that only kill the cancer cells, although this simplification does not change the conclusions to be drawn here. For this study representative scenarios have been considered in order to analyze the behavior of the multicellular growth when a treatment is applied.

A grid of 125000 cell sites, as in [1] and [94], was considered again. For the simulation a number of CSCs in the inner area with growth factor (in random positions) was introduced at the beginning. The simulations begin with the grid full of cells all of which are healthy except the incorporated CSCs. Nevertheless, the emergent growth behaviors are independent of this initial condition (the initial number of healthy cells) as well as the grid size, as indicated in chapter 3.

As explained in chapter 4, CSCs will divide symmetrically, with the same probability used by Enderling and Hahnfeldt [25] ($p_s = 0.01$), or asymmetrically to produce a CSC and a non-stem cancer cell with probability $1 - p_s$. Regarding the number of CSCs introduced from the beginning, this corresponds to a small percentage of the grid size (1-5%) since the proportion of identified CSCs varies among different cancers. For example, Ricci-Vitiani et al. [83] showed that tumorigenic cells in colon cancer population (with CD133+ marker) accounts for about 2.5% of the tumor cells and Korkaya et al. [49] determined that CSCs comprise 1-5% of primary tumors in human mammary carcinomas.

5.2.2 Effect of treatments on regrowth behavior

In order to explain the effect of treatments in a CSC context, a scenario with high invasion potential where the value of parameter g was set to 5 and the rest of the hallmark parameters were set to their standard values in the runs was considered again. Nevertheless, the explanations and conclusions would be similar in other scenarios. This therefore corresponds to a scenario with a high invasion potential by ignoring the contact inhibition mechanism (with probability $1/g$), since such a low value in parameter g (5) was used. Thus, cells that have acquired the hallmark *ignore growth inhibit* (IGI) will have a high ability to invade the surrounding space.

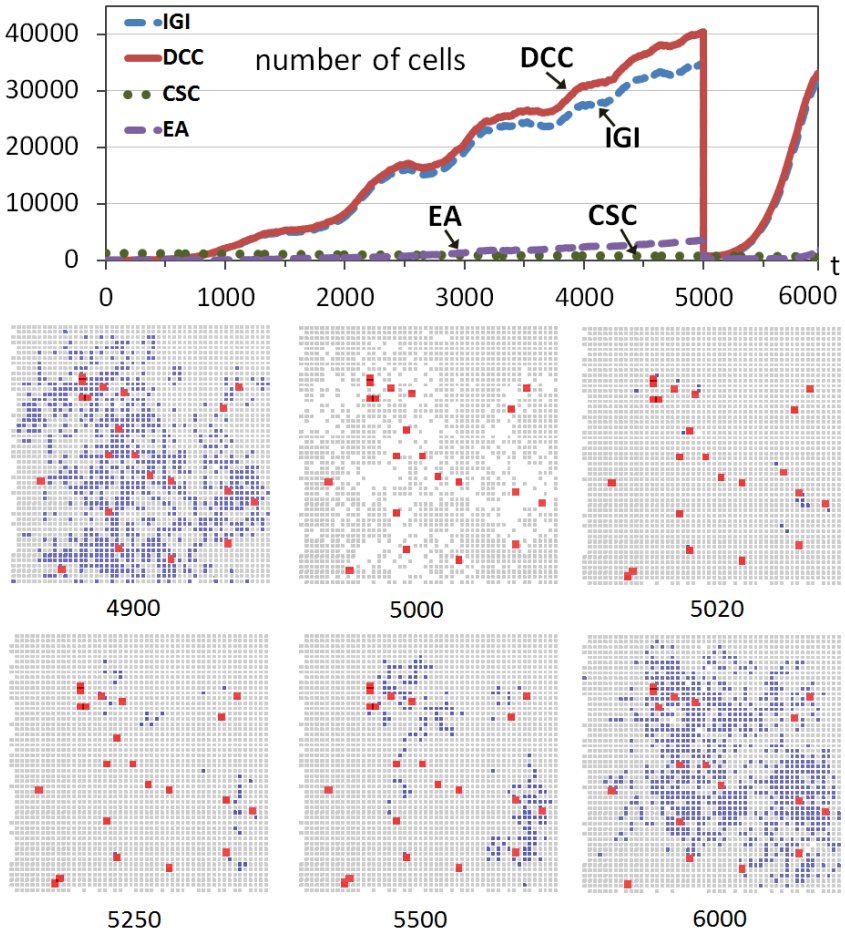

Figure 5.1: Tumor regrowth after a high-intensity treatment. The graph shows the evolution through time iterations of the number of Differentiated Cancer Cells - DCCs (continuous red line) with g=5 while the rest of the parameters were set to their standard values. A number of Cancer Stem Cells (CSCs) corresponding to 1% of the grid size is introduced from the beginning of the simulation (dashed green line). At iteration 5000 the 100% of DCCs is killed. The graph also shows the evolution of the two most predominant hallmarks acquired in cancer cells (IGI and EA). The bottom part shows snapshots of central sections of the multicellular system evolution corresponding to different time iterations (Colors: Gray - healthy cells, Blue - DCCs, Red-enlarged size - CSCs).

Fig. 5.1 includes an example of this scenario with a run of the system evolution, which is similar to the one previously used in the previous chapter. The upper part of Fig. 5.1 shows the evolution through time iterations of non-stem cancer cells (DCCs) and CSCs when the number of CSCs corresponds to 1% of the grid size (125000), CSCs that were introduced at the beginning in

random positions of the inner area with growth factor. As explained, the grid is initially full of cells which are practically all healthy except for the CSCs incorporated. Fig. 5.1 also shows the evolution of the two most predominant hallmarks (considering the hallmarks acquired in all cancer cells) during the multicellular system evolution.

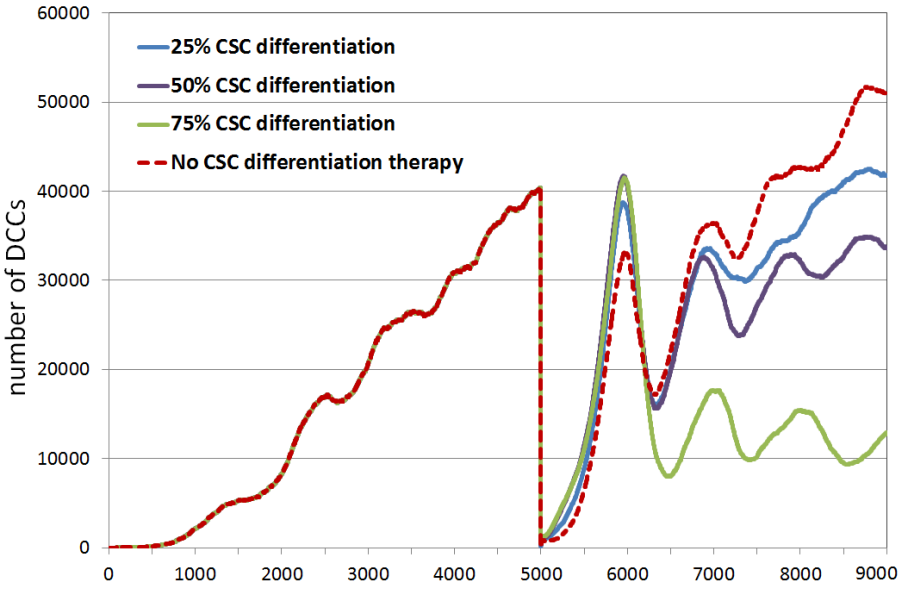

Figure 5.2: Evolution through time iterations of the number of DCCs with the same setup of Fig. 5.1 and including CSC differentiation. At $t = 5000$ a standard treatment is applied, killing the 100% of DCCs. After that, a CSC differentiation treatment is applied, with three different percentages of CSCs differentiated.

Since there is not practically any free site, most CSCs remain quiescent until they have free space to perform mitoses. Given the low probability of symmetric division the number of CSCs remains stable during the 6000 iterations shown in Fig. 5.1. However, as explained in the previous chapter, the non-stem cancer cells begin to grow due to the asymmetric division of CSCs and because of the acquisition of the hallmark *ignore growth inhibit* (IGI) in few of the DCCs, which can rapidly proliferate because of their advantage in this situation with practically no free sites (the daughters acquire the same hallmark). As more mutations appear in this proliferation of DCCs, the apoptotic process begins to be an important limit for their proliferation. Therefore, as an evolutionary and emergent consequence, the hallmark *evade apoptosis* (EA) also appears in many DCCs to avoid the apoptotic process.

At time iteration 5000 the 100% of non-stem cancer cells is killed, simulating a (perfect) cancer therapy and causing the drastic drop of the non-stem cancer cells. Nevertheless, as explained in previous chapter, since CSCs are more resistant to therapeutic interventions, such as chemotherapy or irradi-

ation, compared with their differentiated counterparts [93], the CSCs remain in the simulation.

The bottom part of Fig. 5.1 shows cross-sections of this multicellular system evolution at different time iterations. The snapshot at $t = 5000$ shows how these DCCs are eliminated by the effect of treatment. The next snapshots show how the healthy cells that have not performed the maximum number of divisions fill the space rapidly (see for example the cross-sections at t=5020 and 5250), but the non-stem cancer cells recover quickly because, as also explained in the previous chapter, the CSCs not killed produce non-stem cancer cells again. These DCCs produce an evolution pattern similar to the one at the beginning of the simulation, as shown in the cross-sections and in the upper part of Fig. 5.1.

Vainstein et al. [98] considered the stimulation of CSC differentiation. A "differentiation therapy" (like retinoic acids and drugs targeting tumor epigenetic changes) force CSCs to differentiate terminally and lose their self-renewal property [38]. Therefore, Vainstein et al. [98] proposed that, in clinical trials, CSC differentiation therapy should only be examined in combination with chemotherapy to substantially reduce the population sizes and densities of all types of cancer cells. We considered also this possibility, so, after the standard treatment against DCCs, a percentage of CSCs is differentiated. Figure 5.2 includes a comparison of DCC evolution using the previous scenario ($g = 5$ and default values in the rest of parameters) and differentiation therapy. This means that CSCs are transformed to DCCs, acquiring randomly one of the 5 hallmarks, so the number of CSCs is decreased and the number of DCCs is increased. We have considered three different percentages of CSC differentiation, where we simulated the differentiation in only one iteration, which does not affect the conclusions. When CSCs are differentiated, the slope of the DCC increase is a bit higher with respect to the case of no differentiation, as it is logical since more DCCs (some with the hallmark IGI acquired) are immediately present to begin the fast proliferation. However, in the long term, with fewer CSCs the number of DCCs is best controlled (note that the other limits for DCC proliferation are active, like the apoptotic process).

The experiment was repeated but this time by considering a situation where the treatment kills DCCs gradually and within a given period. Fig. 5.3 shows another run although now the treatment is applied between iterations 5000 and 6000, killing 1% of DCCs in each iteration. Now there is an important difference after the beginning of the treatment, because in the next iterations the healthy cells rapidly replace the free sites that are appearing as a consequence of the elimination of a limited number of DCCs. Most of the few CSCs are therefore immediately surrounded by cells, without the possibility of proliferation and differentiation as in the previous case. This can be observed in the snapshots corresponding to iterations 5000 and 5250.

At time iteration $t = 6000$ the treatment is ceased and DCCs begin to proliferate again. Nevertheless, the slope in the regrowth is not as high as in the previous case (Fig. 5.1) because the treatment strategy did not allow the differentiation of a significant number of CSCs as in that first case. This can be seen in the evolution graphs (Fig. 5.1 and Fig. 5.3) or in the snapshots. For example, the comparison of the snapshot of Fig. 5.1 at $t = 6000$ (1000 iterations

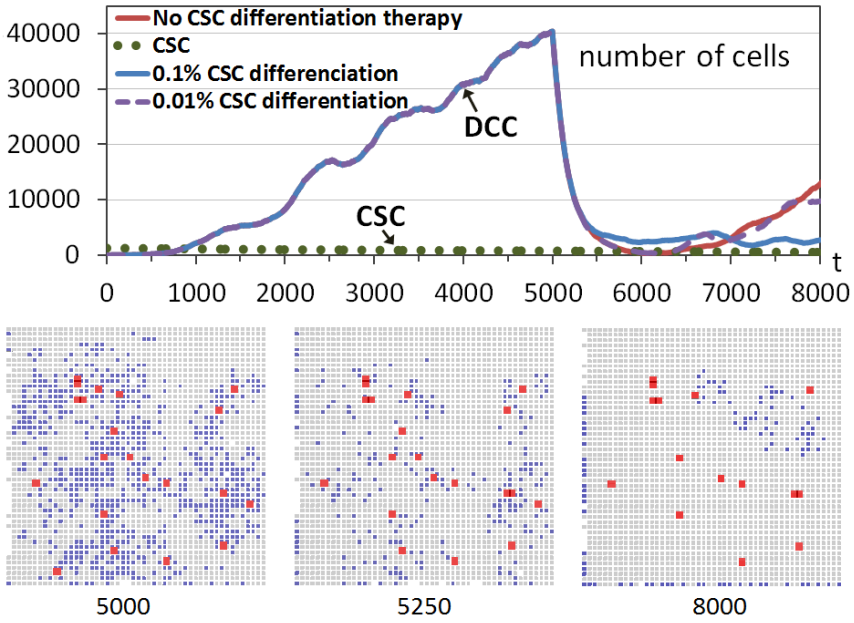

Figure 5.3: Tumor regrowth after a low-intensity treatment. The graph shows the evolution through time iterations of the number of Differentiated Cancer Cells - DCCs (continuous red line) with g=5 while the rest of the parameters were set to their standard values. A number of Cancer Stem Cells (CSCs) corresponding to 1% of the grid size is introduced from the beginning of the simulation (dashed green line). Between iterations 5000 and 6000 DCCs are killed with a probability of 1% in each iteration. The graph also includes the cases when, in the same interval, a CSC differentiation treatment is applied, differentiating 0.01% and 0.1% of CSCs in each iteration. The bottom part shows snapshots of central sections of the multicellular system evolution at three different time iterations corresponding to the first case (no differentiation therapy) (Colors: Gray - healthy cells, Blue - DCCs, Red-enlarged size - CSCs).

after the beginning of the regrowth) and the snapshot at $t = 8000$ of Fig. 5.3 (2000 iterations after the beginning of the regrowth since the treatment ceases at $t = 6000$), clearly shows the faster increase of DCCs using a high intensity treatment in a short period. This therefore indicates and explains that this strategy, the application of a treatment against non-stem cancer cells with low intensity and with a longer period, is better regarding the future regrowth of the tumor behavior. It should be noted that this conclusion is a consequence of the higher probability of CSCs proliferating and differentiating which is favored with treatments with high intensity. Moreover, this effect is independent of the particular advantage of DCCs proliferating, although in this example such a scenario, where cells with the hallmark IGI acquired are the most predominant, was chosen.

We also included the cases in which very low intensity CSC differentiation treatments are applied in the same interval ($t = 5000$ - $t = 6000$). With a

treatment that differentiates 0.01% of CSCs in each time iteration, practically there is not any difference with respect to not using a differentiation therapy since the key aspect is to block CSC proliferation. Meanwhile, using a treatment that differentiates 0.1% of CSCs in each time iteration, no CSCs remain at $t = 6000$ which could contribute to the continuous increase of DCCs. Moreover, in order to have effective treatments, the relative timing of the two treatment strategies is important, since the standard treatment must decrease the new DCCs generated by the CSC differentiation therapy.

5.2.3 Treatment scheduling

The objective of this part of the study is to analyze treatment scheduling in a CSC context by taking into account the effects of treatment intensity and application period in future tumor regrowth. Two representative scenarios were considered: the one previously used where the predominant hallmark is *ignore growth inhibit*, and another scenario dominated by the hallmark *evasion of apoptosis* when using an increased mutation rate.

Fig. 5.4 shows a multicellular system evolution with the same hallmark parameters used in Fig. 5.1; that is, using a high invasion potential scenario in which the parameter g was set to 5 and the rest of the hallmark parameters were set to their standard values. The number of incorporated CSCs is 5% of the grid size, a larger number with respect to previous cases to show better CSC implications. A treatment is started from the beginning, and considering the four cases shown in Fig. 5.4. In all cases the treatment is applied using a simple control: it is administered unless the number of DCCs is under a threshold value corresponding to 1% of the grid size. We use this so we can infer conclusions about tumor regrowth without considering the extreme case where the number of DCCs is reduced to zero, as in previous explanatory examples.

In the first case (Fig. 5.4.a) the treatment kills 1% of DCCs in each iteration. In the second case (Fig. 5.4.b) the treatment kills 10% of DCCs in each iteration, maintaining the treatment during 60 iterations (6.5 days) and repeating the strategy periodically every 100 iterations (10.8 days). In the third case (Fig. 5.4.c) the treatment is applied every 100 time iterations although now 50% of DCCs in such iterations are killed. The fourth case (Fig. 5.4.d) is similar although 75% of DCCs are killed when the treatment is applied every 100 time iterations. The bottom subfigures in the four cases show the number of CSC asymmetric divisions in every simulation iteration.

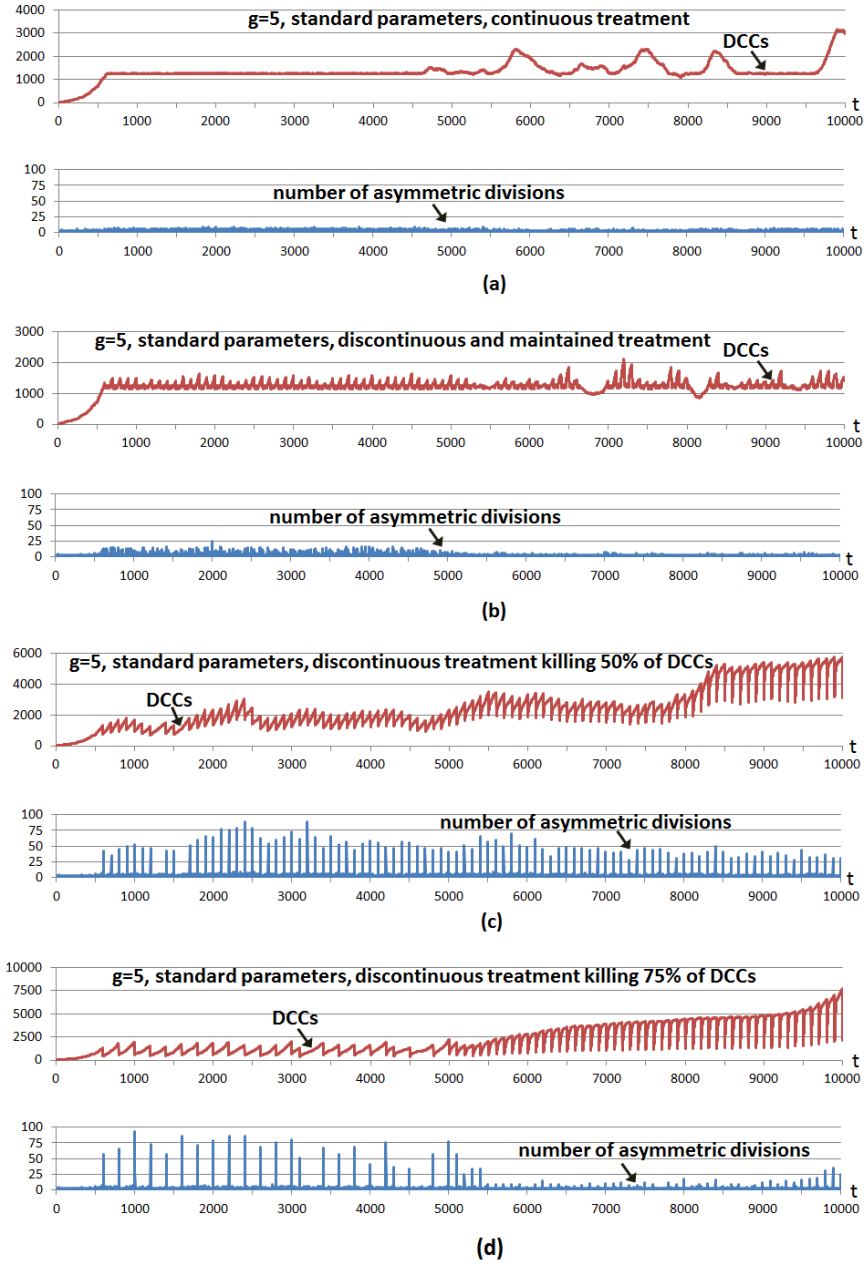

Figure 5.4: Different treatment strategies in a high invasion potential scenario. The graphs show the evolution of the number of DCCs (continuous red line) with g=5 (standard values in other parameters). A number of CSCs corresponding to 5% of the grid size is introduced from the beginning (not shown). The treatment is applied from the beginning only if the number of DCCs is equal or over a threshold value (1% of the grid size). a) Treatment applied continuously, killing 1% of DCCs. b) Treatment applied every 100 time iterations, continuously killing 10% of DCCs during 60 iterations. c) Treatment applied every 100 time iterations, killing 50% of DCCs. d) Treatment applied every 100 time iterations, killing 75% of DCCs. The bottom parts show the number of asymmetric divisions in CSCs.

In the first strategy (Fig. 5.4.a), the simple adaptive mechanism of treatment application maintains very close the number of DCCs to the threshold value, with very few CSC asymmetric divisions. The number of DCCs occasionally presents small increases and oscillations. The fluctuations in the expansion of DCCs are now because some cancer cells have acquired the hallmark *self-growth* (SG) in the outer part of the grid. In this area there is not growth factor, so empty sites appear quickly since only cells with SG acquired can perform mitosis. When a DCC with SG acquired appears in the outer area, a fast increase of DCCs occurs which is not controlled with the treatment. When these DCCs have colonized the outer area, other factors reduce their number, being the main reason that some cells have also acquired the hallmark *ignore growth inhibit* (IGI), given that rapid proliferation. Therefore the same reason for the oscillations in the number of DCCs in previous Figures appears again.

In the third case (Fig. 5.4.c), after 50% of DCCs have been killed, these recover again owing to the fast proliferation of the remaining DCCs and to the CSC proliferation and differentiation which is now favored by the fast DCC elimination. This last contribution has a higher importance when the number of remaining DCCs is lower. The run also indicates that it is not necessary to kill 100% of DCCs in order to show the fast increase of DCCs as a consequence of the greater CSC differentiation possibility. The fourth case is similar (Fig. 5.4.d), when the treatment kills 75% of DCCs in particular iterations, although in this case the treatment is applied fewer times with respect to the third case, since the threshold is reached in less occasions. As in the previous case, killing a considerable number of DCCs favors CSC differentiation, therefore DCCs recover again to obtain a larger number of DCCs. The second case (Fig. 5.4.b) is a mixture of both strategies, as it uses a lower intensity with respect to the last cases but it is maintained during a certain number of iterations.

It should be noted that after time iteration 5000, and since most DCCs are located in the outer area (cells with hallmark *self-growth*), when the treatment is applied it kills cells mostly in this area. The empty cells are therefore mostly located in that area and, consequently, only the few CSCs located there can perform the asymmetric divisions. This explains why there is a lower number of asymmetric divisions after time iteration 5000. This effect is clearer when many DCCs are killed, as when the treatment is applied every 100 time iterations killing 75% of DCCs (Fig. 5.4.d) and when the treatment is applied every 100 time iterations, continuously killing 10% of DCCs during 60 iterations (Fig. 5.4.b), whereas the effect is less clear when it is applied every 100 time iterations killing 50% of DCCs (Fig. 5.4.c).

The experiment was repeated with standard parameters and a higher hallmark mutation rate ($m = 1000$) with respect to the standard value ($m = 100000$). The parameter m sets the time scale of the simulation as it determines how fast tumor growth behavior can appear, although the onset of tumor growth depends on the parameter values of other hallmarks. As previously explained, given the increased hallmark mutation rate, the hallmark *evade apoptosis* (EA) is the most predominant in DCCs in evading the apoptotic process. Fig. 5.5 shows the same cases considered in the previous example, except that in this case the treatment continuously applied (Fig. 5.5.a) kills

5% of DCCs in each iteration. This higher killing frequency (with respect to the previous example) is because it is necessary to decrease the number of DCCs faster given the higher hallmark mutation rate. In all cases the number of incorporated CSCs is again 5% of the grid size. The cases considered in Fig. 5.5 show once more that the same conclusions can be inferred, given that with discontinuous treatments more number of asymmetric divisions are obtained, whereas with continuous treatment, such a number of asymmetric divisions is near zero and consequently fast regrowth of DCCs is not favored. This is also the case with a low intensity treatment maintained during an appropriate period (Fig.5.5.b) in order to decrease the number of DCCs at the same time that low intensity does not favor the proliferation and differentiation of CSCs.

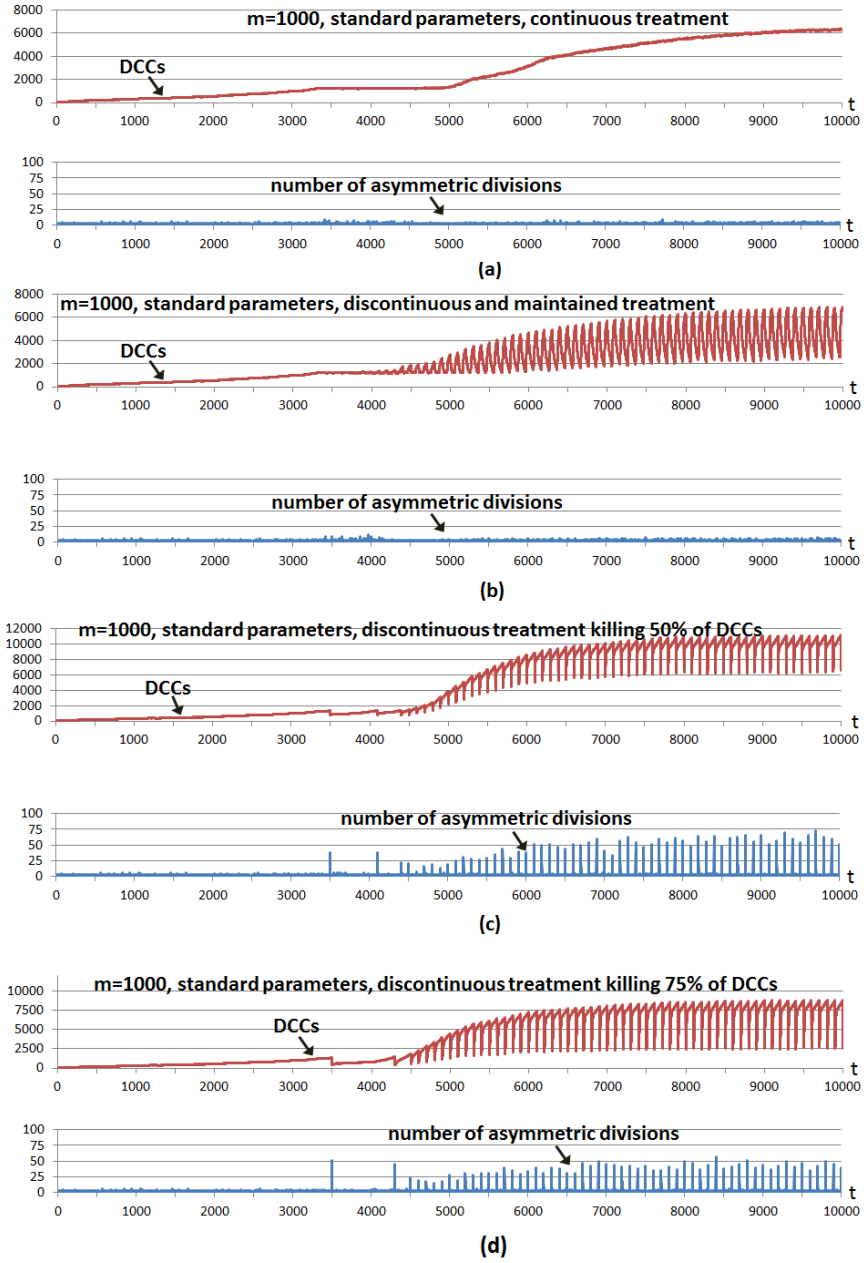

Figure 5.5: Different treatment strategies in a high hallmark mutation scenario. The graphs show the evolution of the number of DCCs (continuous red line) with m=1000 (standard values in other parameters). Same setup as in Fig. 5.4: a number of CSCs corresponding to 5% of the grid size is introduced from the beginning. A treatment is applied from the beginning only if the number of DCCs is equal or over a threshold value (1% of the grid size). a) Treatment applied continuously, killing 5% of DCCs. b) Treatment applied every 100 time iterations, continuously killing 10% of DCCs during 60 iterations. c) Treatment applied every 100 time iterations, killing 50% of DCCs. d) Treatment applied every 100 time iterations, killing 75% of DCCs.

5.3 Discussion

Different strategies when a treatment is applied were analyzed by taking into account the implications of CSC presence. These cells are resistant to usual present therapies, so these are the main cause responsible for tumor regrowth after treatments. As stated by Sottoriva et al. [93] "Therapy which fails to target the CSC population is not only unsuccessful in curing the patient, but also promotes malignant features in the recurring tumor. These include rapid expansion, increased invasion, and enhanced heterogeneity". This present analysis is therefore different to the studies focused on treatment applications to control non-stem cancer cells, given that its aims center upon future tumor regrowth in the long term as a consequence of the CSC behavior.

Vainstein et al. [98] employed a CSC simulation that takes into account a quorum sensing model (higher CSC density in the microenvironment promotes CSC differentiation). Their model considers "cycling CSCs" which are those CSCs that progress through the cell cycle and after a fixed time period divide into two CSCs, whereas the "non-cycling" CSCs are the quiescent CSCs that enter the cell cycle depending on the total cell density in the CSC's vicinity. Even the authors remark that their model's assumptions differ from those of other models of CSC dynamics, which either do not consider differentiation as a process triggered by environmental feedback or do not take into account the influence of neighboring cells on the differentiation decision (such as the model of Enderling and Hahnfeldt [25] and our study's model), they also showed that "accelerated death of DCCs (represented in their model by limited lifespan) decreased the number of DCCs, but increased the number of cycling CSCs". Although using a different model of CSC differentiation, this aspect of their model is similar to the results of our study regarding the relation between DCC elimination and CSC differentiation. Moreover, those authors [98] stated that neither stimulation of CSC differentiation or inhibition of CSC proliferation alone is sufficient for complete CSC elimination and cancer cure, since each of these two therapies affects a different subpopulation of CSCs.

Our results concerning the faster regrowth after a treatment are also in agreement with the results of Hillen et al. [42] when they comment regarding "tumor growth paradox". The authors define this paradox as an "accelerated tumor growth with increased cell death as, for example, can result from the immune response or from cytotoxic treatments". They showed that if DCCs compete with CSCs for space and resources, the first cells can prevent CSC division and drive tumors into dormancy. Conversely, if this competition is reduced by death of DCCs, as the authors state "the result is a liberation of CSCs and their renewed proliferation, which ultimately results in larger tumor growth". Their model only considers DCCs with limited proliferation capability, whereas the model employed in our study considers the different hallmarks that a DCC can acquire; therefore the different capabilities of the individual hallmarks can be analyzed in different situations. Nevertheless, the conclusions drawn here are the same in different scenarios characterized by the relative importance of the different hallmarks and clearly indicate that the treatments applied must not promote CSC division.

Finally, the effects of different treatment strategies were analyzed by using

continuous low-intensity treatments and periodic high-intensity treatments. The former presents an advantage as a continuous low-intensity treatment which does not favor CSC proliferation and differentiation, and therefore allows easy control of future tumor regrowth. On the contrary, the latter possibility of discontinuous periodic treatments with high intensity levels favors CSC proliferation and differentiation in the short term, and consequently favors future tumor regrowth. The inclusion of a CSC differentiation therapy in combination with a standard treatment can favor the control of future regrowth, although the possibility of the remaining CSCs to divide is the key point in the control.

Therefore, this analysis indicates that making CSC proliferation more difficult is an important point to consider, especially in the immediate period after a standard treatment for controlling non-stem cancer cell proliferation. As stated by Han et al. [38] "maintaining the cells in a quiescent state by blocking specific receptors and signaling pathways within the CSC niche can inhibit CSC functions of tumor initiation and metastasis". Nevertheless, the current attempts at CSC control are focused on alternatives for CSC elimination and induction of CSC differentiation [17][38].

Chapter 6

Evolutionary optimization of cancer treatments in a cancer stem cell context

In this chapter evolutionary computing for optimizing cancer treatments is used taking into account the presence and effects of cancer stem cells. When a standard treatment is applied against non-stem (differentiated) cancer cells, different effects are present depending on the strategy used to eliminate these non-stem cancer cells, as explained in the previous chapter. The treatment strategy implies aspects such as intensity of application, duration and periodicity, with interrelated effects in the regrowth capability when CSCs are present. Additionally, the best treatment would be the one that, with the less possible intensity minimizes to a great extent the future regrowth capability of CSCs. Therefore, it is an optimization problem in which the best treatment is difficult to foresee, but it can be subject to be optimized with any optimization procedure. We selected evolutionary computing as a global search method and Differential Evolution [79] as a robust evolutionary method. Thus, this chapter explores the use of Differential Evolution to optimize a treatment in terms of intensity, duration and periodicity in a CSC context.

6.1 Differential Evolution

Differential Evolution (DE) [79] is a population-based search method. DE creates new candidate solutions by combining existing ones according to a simple formula of vector crossover and mutation, and then keeping whichever candidate solution has the best score or fitness on the optimization problem at hand. The central idea of the algorithm is the use of difference vectors for generating perturbations in a population of vectors. This algorithm is specially suited for optimization problems where possible solutions are defined by a real-valued vector. The basic DE algorithm is summarized in the pseudo-code of Algorithm 6.1.1.

Differential Evolution needs a reduced number of parameters to define its

Algorithm 6.1.1: DIFFERENTIAL EVOLUTION(*Population*)

for each $Individual \in Population$
  do $\{Individual \leftarrow$ INITIALIZERANDOMPOSITIONS()
repeat
 for each $Individual \;\; x \in Population$
  do
  - $x_1, x_2, x_3 \leftarrow$ GETRANDOMINDIVIDUAL($Population$)
  - // must be distinct from each other and x
  - $R \leftarrow$ GETRANDOM$(1, n)$ // the highest possible value n is the
  - // dimensionality of the problem to be optimized
  - **for each** $i \in 1 : n$ // Compute individual's potentially new position
  - // $y = [y_1, ..., y_n]$
    - **do**
      - $r_i \leftarrow$ GETRANDOM$(0, 1)$ // uniformly in open range (0,1)
      - **if** $((i = R) \;||\; (r_i < CR))$
        - $y_i = x_{1_i} + F(x_{2_i} - x_{3_i})$
      - **else** $y_i = x_i$
  - **if** $(f(y) \leq f(x)) \quad x = y$ // replace x with y in Population

until TERMINATIONCRITERION()
return (GETLOWESTFITNESS($Population$)) // return candidate solution

implementation. The parameters are F or differential weight and CR or crossover probability. The weight factor F (usually in $[0, 2]$) is applied over the vector resulting from the difference between pairs of vectors (x_2 and x_3). CR is the probability of crossing over a given vector of the population (target vector x) and a "donor" or "mutant" vector created from the weighted difference of two vectors ($x_1 + F(x_2 - x_3)$) [19]. We used the "binomial" crossover (specified in the pseudo-code of Algorithm 6.1.1), for defining the value of the "trial" vector (y) in each vector component or position i [19]. Finally, the index R guarantees that at least one of the parameters (genes) will be changed in that generation of the trial solution.

Finally, the selection operator maintains constant the population size. The fitness of the trial vector ($f(y)$) and the target vector ($f(x)$) are compared to determine which one survives for the next generation: If the new trial vector yields an equal or lower (better) value of the objective function, it replaces the corresponding target vector in the next generation; otherwise the target vector is retained [19]. Thus, the fitness of the best solution of the population is improved or remains the same through generations.

By combining different mutation and crossover operators various schemes have been designed. The usual variants or schemes of DE choose the base vector x_1 randomly (variant $DE/rand/1/bin$, where 1 denotes the number of differences involved in the construction of the mutant or donor vector and bin denotes the crossover type) or as the individual with the best fitness found up to the moment (x_{best}) (variant $DE/best/1/bin$). To avoid the high selective pressure of the latter, we used a tournament to pick the vector x_1, which also allows us to easily establish the selective pressure by means of the tournament

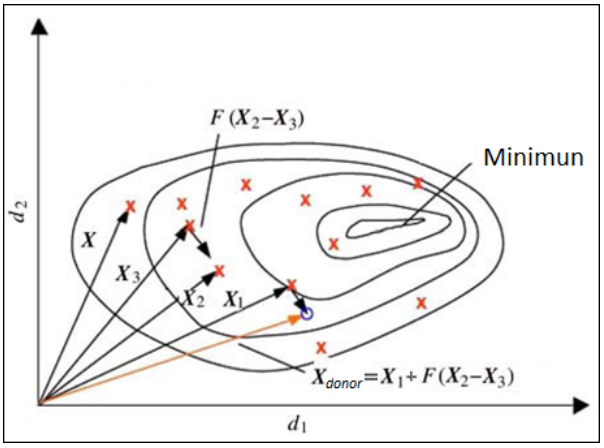

Figure 6.1: An example of a two-dimensional fitness landscape showing its contour lines and the process for generating the donor or mutant vector in Differential Evolution.

size.

Figure 6.1 shows a two dimensional example that illustrates the different vectors which play a part in the DE search algorithm. As Feoktistov [26] indicates, the fundamental idea of the algorithm is to adapt the step length ($F(x_2 - x_3)$) intrinsically along the evolutionary process. At the beginning of generations the step length is large, because individuals are far away from each other. As the evolution goes on, the population converges and the step length becomes smaller and smaller, providing this way an automatic balance in the search.

6.2 Examples of treatment strategies

We selected again different scenarios to show the implications of different treatment strategies when CSCs are present. We considered ideal treatments in the sense that these only kill (non-stem) cancer cells, although this does not change the reasoning and conclusions drawn from the experiments. The grid size was 64000 (40 sites in each dimension), the simulations begin with the grid full of healthy cells except the incorporated CSCs, from the beginning, in the inner area with growth factor. These CSCs correspond to a 5% of the grid size. We also selected a representative example in which differentiated tumor cells (DCCs) have a high invasion potential in the surrounding tissue, as we used $g = 5$, as in previous chapters. Moreover, since the parameter m determines the probability of acquisition of hallmarks and consequently the onset of a tumor behavior, we used $m = 1000$ to obtain tumor development behaviors without using a large number of iterations. Nevertheless, the conclusions and CSC implications commented here are independent of the particular scenario considered regarding the relevance of the hallmarks.

Figure 6.2 shows an example where continuous treatments are applied in

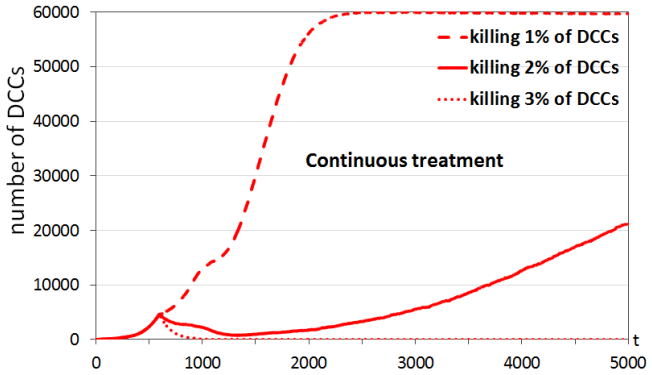

Figure 6.2: Evolution of the number of DCCs through time iterations when continuous treatments that (from time iteration 600) kill 1%, 2% and 3% of DCCs are applied in every time iteration.

every iteration. The treatments are applied from iteration 600, in order to give DCCs the opportunity to growth in number. When a treatment that kills 1% or 2% of DCCs is applied in every time iteration, the number of DCCs is not controlled enough, ending with an increase of DCCs that will cover the full grid. On the contrary, when a treatment that kills 3% of the DCCs is applied in every time iteration, the number of DCCs is controlled to a minimum through time.

As an opposite strategy, Figure 6.3 shows a run where a discontinuous and periodic treatment is applied. The treatment kills the 100% of the DCCs every 600 iterations. The problem with this strategy is that the regrowth of DCCs is faster with respect to a situation without treatment application, such as the initial increase of DCCs. The 2D snapshots shown at the bottom of Figure 6.3 explain again the reason. These snapshots correspond to a central plane that crosses the grid, and it should be noted that these provide more information than the 3D representation as these show the internal distribution of the cells. For example, at $t = 3000$, all DCCs are eliminated, so there are empty sites that are filled in few iterations with mostly healthy cells. Nevertheless, because of these empty sites, the few CSCs (shown with enlarged size) had more opportunities to proliferate and differentiate, generating a few DCCs (see snapshots at $t = 3020$ and $t = 3025$) that can produce a fast increase of a tumor bulk. In a normal situation, given the few possibilities for CSCs to proliferate (the grid is almost full), the increase of DCCs is slower. This fast increase is well documented in many cancer treatment applications [93][98]. So, this effect must be taken into account in treatment applications, trying to difficult CSC proliferation and differentiation.

Figure 6.4 now shows an "average" strategy between these two extreme cases. The treatment is applied periodically, again every 600 time iterations, but killing only 5% of DCCs in each time iteration. Moreover, the treatment is maintained during 150 time iterations. Figure 6.4 shows that now, when the treatment stops after such 150 iterations, the increase of the regrowth is slower with respect to the previous case. The reason can be guessed looking at the

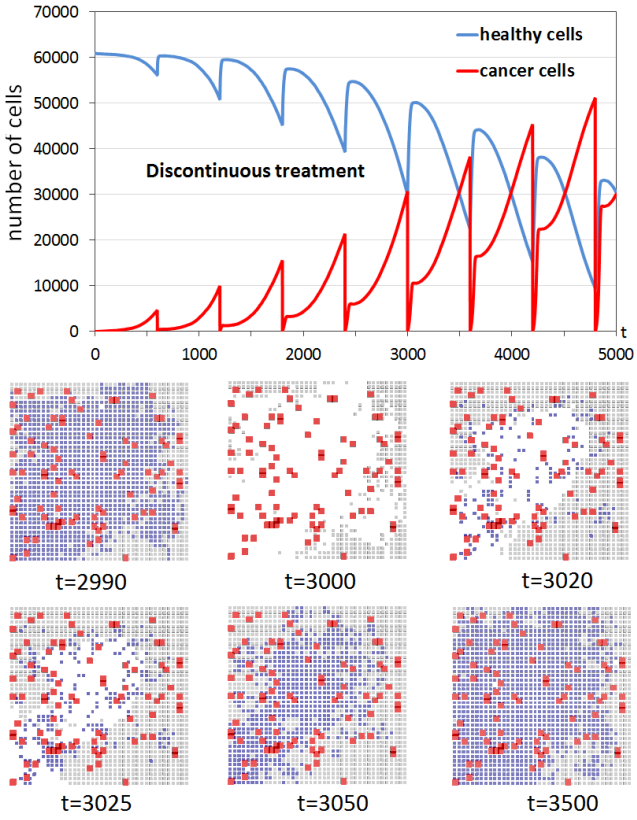

Figure 6.3: Evolution of the number of DCCs through time iterations when a periodic discontinuous treatment is applied (Every 600 time iterations killing the 100% of the DCCs in such iterations). The bottom part shows 2D snapshots of the central part of the grid at given time iterations (Colors: Gray - healthy cells, Blue - DCCs, Red-enlarged size - CSCs).

snapshots at the bottom of Figure 6.4. For example, the snapshot at $t = 3020$ shows that the CSCs are immediately surrounded by healthy cells, given the very few free sites produced as consequence of the low-intensity treatment, so CSCs had no so many opportunities to proliferate and differentiate as in the previous case (this behavior was explained in chapters 4 and 5). So, this seems a good strategy, trying to difficult CSC proliferation through low-intensity treatments.

Figure 6.5 illustrates the intensity used during each treatment application, measured as the percentage of DCCs killed in each iteration. This Figure shows the accumulative treatment intensity as consequence of the application of previous treatment strategies, that is, the summation of the intensity of the treatment during the intervals of its application. In Figure 6.5 we considered the intensities as probabilities of killing a DCC, so these are in the interval [0,1] in each iteration.

In the cases corresponding to the periodic treatments previously considered,

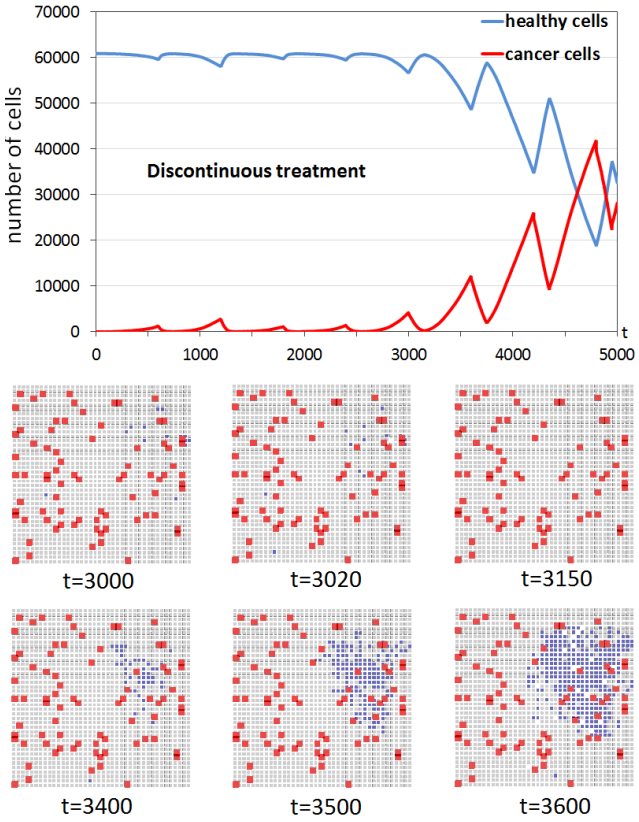

Figure 6.4: Evolution of the number of DCCs through time iterations when a periodic discontinuous treatment is applied (Every 600 time iterations killing the 5% of the DCCs during the next 150 iterations). The bottom part shows 2D snapshots of the central part of the grid at given time iterations.

logically the accumulative intensity follows a linear progression. With the discontinuous treatments, the accumulative intensity is increased in the particular iterations the treatments are applied. Figure 6.5 and previous Figures (Figs. 6.2 - 6.4) show the different behaviors in the two features considered (number of final DCCs and accumulative treatment intensity): The continuous treatment that kills 3% of DCCs in each iteration has the number of DCCs controlled at the cost of high treatment intensity. The discontinuous periodic treatment with high intensity (Figure 6.3) has a lower value in the accumulative treatment intensity but has a poorer control of the final number of DCCs (as consequence of the fast regrowth of DCCs). Finally, the periodic treatment that kills 5% of DCCs in each iteration, maintained during 150 time iterations (Figure 6.4) has a better control over the final DCCs (with respect to the previous case, Fig. 6.3) but a higher accumulative intensity. In order to find out what strategy would be the best regarding these objectives, we applied the evolutionary methodology to optimize the treatment taking into account such objectives or measures.

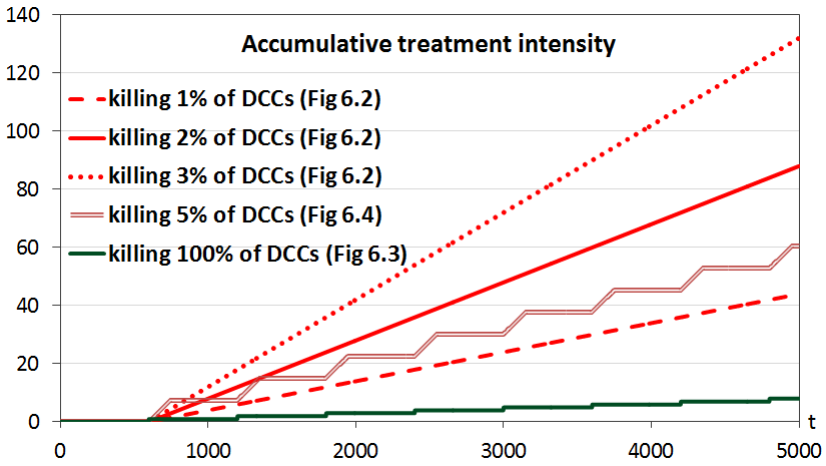

Figure 6.5: Accumulative treatment intensity across iterations with different treatment strategies of previous Figures.

6.3 Treatment strategy optimizations

We can first begin with the use of the evolutionary algorithm to try to optimize a single treatment application. The first test implies the optimization regarding the intensity of application of a conventional treatment (chemotherapy or radiotherapy) that kills DCCs as well as its duration. We used the previous scenario with high invasion potential of cells with the hallmark IGI acquired, with a 5% of incorporated CSCs. Treatments always begin at time iteration $t = 600$. The genotypes include the encoding of both parameters (intensity and duration) in the interval [-1,1], while the encoded values are decoded in the interval [0%,100%] for the intensity of the treatment, meaning that a number of DCCs corresponding to that percentage are killed in each iteration. The DCCs subject to be killed are randomly selected. For the duration of the treatment we used an ample range [0,600] (which corresponds to an interval [0,65 days]), meaning that the treatment with the encoded intensity of the first parameter is maintained that number of iterations.

For the fitness function we used a simple formula, which takes into account two terms: First, the final number of DCCs after a given number of iterations (100) once the treatment is stopped. Second, the intensity used during the treatment application. This second aspect is not easy to measure, but we can assume it is related to the summation of the percentage of DCCs killed in each iteration (as illustrated in previous examples and Figure 6.5). This means, for example, that a high-intensity treatment which kills 100% of DCCs in one iteration is equivalent (regarding the intensity measure) to a treatment that kills 1% of DCCs during 100 iterations. The fitness is a weighted summation of both terms (0.01·final number of DCCs + treatment intensity, with the weights tuned so that both terms have close values in best individuals). Finally, the fitness of each encoded parameter set is averaged with 5 independent runs of the multicellular system.

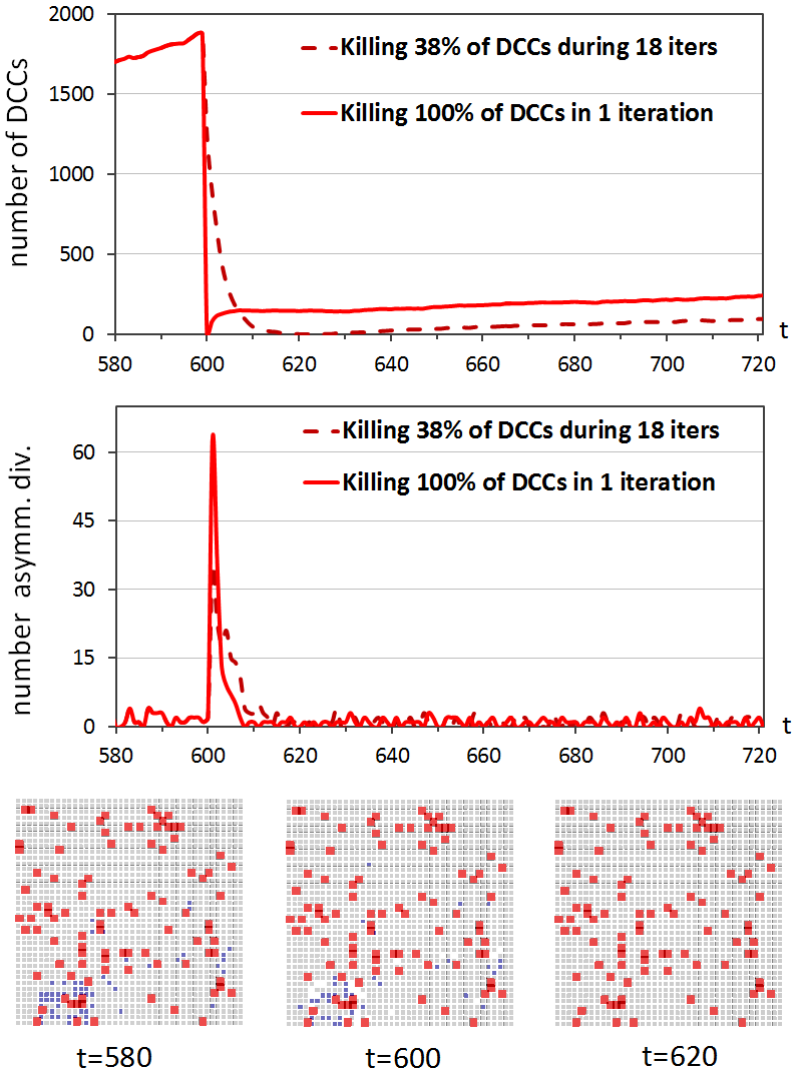

Figure 6.6: Multicellular system evolution when a best evolved treatment is applied, with its intensity and duration optimized. Treatments begin in time iteration $t = 600$. In the example, the best evolved treatment kills 38% of DCCs in the next 18 time iterations. A high-intensity treatment that kills the 100% of DCCs only at $t = 600$ is included for comparison. Upper part: Evolution of DCCs through time iterations. Middle part: Evolution of the number of CSC asymmetric divisions. Bottom Part: 2D snapshots of the central part of the grid corresponding to the multicellular system evolution at particular time iterations when the best evolved treatment is applied.

We used DE with a population of 50 individuals, with standard values for the other parameters in DE: $CR = 0.9$ and $F = 0.9$ [78], whereas the size of the

tournament to choose the base vector was 8% of the population, which implies a low selective pressure when selecting that vector to disturb (Section 6.1). The evolutions were run for 50 generations using again a grid size of 64000 sites. For this test we used the parameters previously commented ($g = 5$ and $m = 1000$ while the rest of hallmark parameters were set to their standard values) and, as indicated, the encoded treatments begin at time iteration $t = 600$. Because of the different duration of the encoded treatments, the simulation time of each treatment is variable. Given the high requirements in processing time for the simulation of the multicellular system, using an Intel Core i3 processor at 3.33 GHz and 4 Gytes of main memory, the average computing time for each DE generation was 36 minutes.

Figure 6.6 shows the behavior with one of the best strategies found by the evolutionary algorithm, with an intensity of 38% and duration of 18 iterations (1.95 days). The upper part corresponds to the evolution of the number of DCCs. We included a high-intensity treatment for comparison, which kills the 100% of DCCs only at time iteration $t = 600$. The middle graph illustrates the number of CSC asymmetric divisions in both cases, which is increased when CSCs have more opportunities to proliferate during the treatment administration. Finally, the bottom subfigures show again 2D snapshots of central sections of the grid at three time iterations when the best evolved treatment was applied. The snapshots show that, even with this treatment intensity that generates a few empty sites (see snapshot at $t = 600$) so the surrounding CSCs can take advantage for their proliferation and differentiation, the maintained treatment eliminates those DCCs in the next few iterations. All the best evolved treatments follow this pattern avoiding high intensities: the average intensity of the best evolved treatments was 32.3% (standard deviation 5.1) in 10 independent DE runs, while the average duration was 26.4 iterations (standard deviation 9.3).

In a second test we used DE for the optimization of three parameters of a treatment: the previous two (intensity and duration), together with the period of application of the treatment. As in the previous case, the treatment intensity, once decoded, can vary in the interval [0%,100%]. Now, the period of application can vary in the interval [0,600], meaning that the treatment is periodically repeated with the period indicated with the decoded value. The other parameter, the duration of the treatment in each application, is dependent on the period of application. This parameter is encoded again in the interval [-1,1], but decoded taking into account the encoded value of the period of application. For example, if the encoded value for the period represents 500 time iterations and the encoded value for the duration is 0 (middle value in the interval [-1,1]), then the duration is 250 time iterations in each application. The other DE parameters are the same as in the previous test. We used simulations of the multicellular system with a minimum of 3000 time iterations, so every encoded treatment strategy is applied several times to determine the fitness. Given the higher number of time iterations in the evaluation of each encoded solution, the average computing time per generation is now 237 minutes, using the same population size (50) and computing platform as in the previous test.

As in the previous case, the fitness is defined as the same weighted sum of

the intensity of the treatment and the final number of DCCs after 100 time iterations of its cessation. The first term is measured again as the intensity used across the whole period since the beginning of the treatment application, taking into account that all treatments are applied after time iteration $t = 600$ in order to have an initial and significant increase of DCCs.

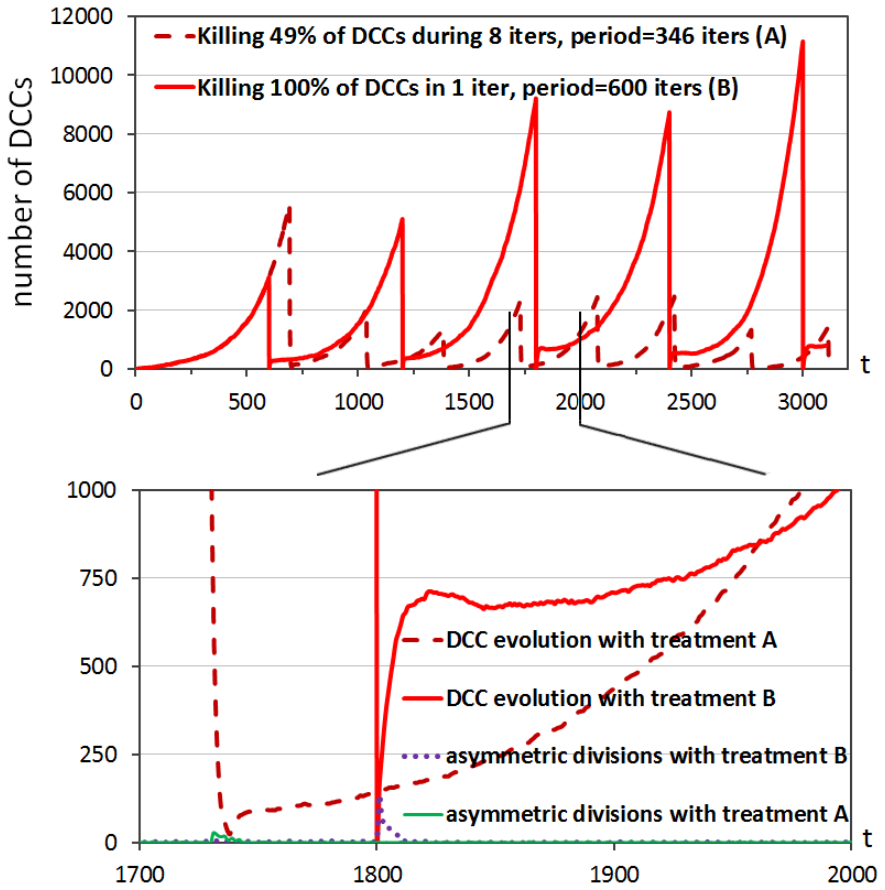

Figure 6.7: Multicellular system evolution when a best evolved treatment is applied, with its period, intensity and duration optimized. Treatments do not begin before time iteration $t = 600$. In the example, the best evolved treatment kills 49% of DCCs during 8 time iterations and a period of 346 iterations (treatment A). A high-intensity treatment that kills the 100% of DCCs every 600 iterations is included for comparison (treatment B). Upper part: Evolution of DCCs through time iterations. Bottom Part: Interval of time iterations enlarged for a more detailed view of the effect of the treatment strategies on next DCC progression. This bottom Figure also includes the number of CSC asymmetric divisions with the two treatments.

Figure 6.7 now shows the behavior with one of the best evolved strategies, with an intensity of 49%, a period of application of 346 (37.5 days) and a duration of 8 iterations (21 hours). Again, the graph includes, for comparison,

a high-intensity treatment that kills the 100% of DCCs in only one iteration, being periodically applied with a period of 600 time iterations. Figure 6.7 includes an enlarged view of a particular interval of the multicellular system evolution, between time iterations 1700 and 2000, which denotes the same effect previously explained: A high-intensity treatment promotes CSC proliferation and differentiation (as shown with the higher number of CSC asymmetric divisions in the bottom part of Figure 6.7), so there is a posterior high increase of DCCs. Note that this enlarged view shows that, after the fast increase of DCCs, their progression is more stable in next iterations. This is because in the CSC asymmetric divisions the new DCCs acquire randomly one of the five hallmarks and only the hallmark IGI provides an immediate advantage for fast proliferation. Thus, more time iterations are necessary so that a sufficient number of DCCs acquire that hallmark to begin again an increase in their number. On the contrary, the evolved periodic and discontinuous treatment makes more difficult CSC differentiation, so the future regrowth of DCCs is slower and consequently it is easier to control DCC increase.

6.4 Discussion

In this chapter we used the tumor growth model to analyze the implications of treatment strategies taking into account the presence of CSCs, using evolutionary computing to establish the best strategies of treatment applications considering the regrowth capacity of such CSCs. We emphasize the difference of our work and aim with respect to standard treatment strategies. For example, an usual treatment like FOLFOX4 protocol [43] demonstrated effectiveness against regrowth in phase II of colon cancer [18]. This is a chemotherapy treatment in which drugs are used to kill the cancer cells. Mostly two or more drugs are used in combination which proves to be more effective. In FOLFOX chemotherapy, drugs used are Fluorouracil 5FU, Folinic acid (Leucovorin) and Oxaliplatin. Typically the treatment is composed of 12 phases or cycles, each one 14 days length. These types of protocols were experimentally tested and tuned to shrink the tumor bulk. Nevertheless, no treatment analyses took into account, with an exhaustive study, the effect of possible future relapses (regrowths). So, computational experiments, even with the simplifications performed, can go a step ahead with respect to *in vitro* and *in vivo* analyses, and additionally allow explaining the reasons of the resultant behaviors.

Since we considered different terms in the fitness, it is obvious that we could use a multi-objective approach for searching the Pareto Set of non-dominated individuals regarding, for example, the treatments that minimize the total intensity applied and the treatments that minimize the final number of DCCs (with obvious optimal strategies). Nevertheless, we first tackled the problem with the mono-objective approach to analyze the implications of the presence of CSCs and the main aspects that can define a treatment strategy.

It is also obvious that other treatment strategies can be considered, such as applications with increasing or decreasing intensities through time. Although we used a particular scenario of relevance of hallmarks, and consequently the treatment parameters are optimized for that scenario, the implications of CSC presence are general: in contrast with the main current attempts to CSC

control focused on alternatives for CSC elimination and induction of CSC differentiation [17][38], our analyses show that treatments should be maintained during very few days, avoiding high intensities and, consequently, with longer periods than the ones used in standard treatments. This is always with the aim to make more difficult CSC proliferation and consequently their differentiation in order to minimize their future effect on a possible tumor regrowth.

Chapter 7

Conclusions

We used computational models based on cellular automata and the abstract model of cancer hallmarks to analyze the emergent behavior of tumor growth at cellular level. The emergent behavior of growing multiclonal tumors is almost impossible to infer intuitively, as commented by Rejniak and Anderson [80], so the simulation tools help to inspect the emergent behavior under different conditions. Or, as indicated by Kansal et al. [48], if tumors do not behave as random, disorganized and diffuse cell masses, then "the growing tumor and not only the single cell must be investigated and treated as a self-organizing dynamic system", which, according the authors cannot be done with currently available in vitro/in vivo models or common mathematical approaches. There is a need for novel computational models to simulate the mechanistic complexity of solid tumor growth and invasion, like CA, that can easily model the emergent nature of the process [48]. We used CA for the modeling because, given the interrelations among the different hallmarks, in addition to the dependence of the hallmarks on some parameters, the modeling at cellular level with CA makes easy the study of the final emergent behavior, which cannot be foreseen in many cases. Thus, we can easily analyze the dependence of the emergent behavior on hallmarks and defining parameters.

Another advantage of the "in silico" models is that we can run experiments that would be too expensive and time-consuming to carry out in the lab [88]. Moreover, as indicated by Savage [88] regarding the complexity of cancer "Researchers have tended to focus on genes and proteins, but to understand and fight the disease, it must be viewed as a system, rather than merely as a set of cellular activities". Thus, "the recent focus on genetics and pathways in individual cells has caused many researchers to neglect the systemic view" [88]. The simulations based on CA are within this idea emphasized by Savage [88], as the model permits an analysis and view of the system working with different levels of abstraction or with the focus on particular simulation aspects. Moreover, the abstract model of cancer hallmarks is the ideal one for the study of the multicellular system in terms of behavioral characterization, which was our objective, rather than particularizing in a cancer type and without the need of characterization of the molecular and gene pathways involved in the acquisition of the hallmarks.

We must point out a comment about the implications of the use of the hallmark abstract model considered here. Loeb and Loeb [55] indicated that "The mutator phenotype hypothesis proposes that the intrinsic genetic instability of cancer cells drives tumorigenesis by producing a pool of mutations, some of which confer a selective advantage, allowing cells to proliferate under adverse conditions. Others have suggested, however, that increased mutagenesis is not required to produce the multiple mutations observed in cancers, and hypothesize that selection pressures and clonal expansion are the major driving forces in tumorigenesis". We worked with the abstract model of the hallmarks, independently of those reasons for acquiring the corresponding hallmarks, as it can be an oncogene-induced mitotic stress [59]. But the hallmark abstraction does not take into account that, when a hallmark is acquired, there can be random mutations which were not selected (but can be advantageous in a posterior phase to confer resistance to treatments), or whether the mutations correspond to expanded mutations as result of ongoing selection to confer the cells with such mutations a growth capability. Our interest here was to isolate the hallmarks to study their effect in advantageous situations (that lead to tumor growth), and, with this knowledge, analyze the combined effect incorporating also a CSC context. These advantageous situations could be interpreted as clonal selection, but it is because the hallmarks provide the advantage in the scenarios chosen. However, the model does not provide insight about the different reasons to acquire the mutations that define the hallmarks.

As indicated by Rejniak and Anderson [80], "by necessity, many of the cancer models were general, phenomenological, and not specific to a type of cancer and therefore were plagued by a lack of experimental data to both parameterize and validate. That is not to say they were not useful". Given the simplifications, the modeling considered in the thesis was oriented to mimic the development of multicellular spheroids of tumor cells and not to a particular cancer type. As Spencer et al. point out "When modelling a complex biological process, it is always necessary to make simplifying assumptions" [94], so we can study cancer at the cell population level, modeling tumors as evolving ecosystems and without incorporating every known piece of molecular cell biology relating to cancer [94]. In the simulation, each cell has an associated genome which determines the different cancer hallmarks acquired by mutations. These hallmarks and their associated parameters define cell states and cell mitotic behaviors, so different dynamics can emerge in the multicellular system. We focused in the thesis on how the cellular automata simulating tool can provide a model for analyzing tumor growth behavior under different conditions, such as behavioral regime transitions between states with predominance of healthy or cancer cells and the dependence of the emergent tumor growth behavior on each individual hallmark, studying their relative importance in tumor development.

With the simulation tool we performed several tests. First, we tested whether the emergent behavior is independent of the initial conditions of the cellular environment, regarding its initial available free space (Chapter 3). The emergent behavior depended only on the parameters associated with the hallmarks, although the time iterations applied to obtain stable behaviors are dependent of the starting free space. Additionally, the experimentation per-

formed showed that the effect of elimination of hallmarks is different depending on the main advantage, with respect to healthy cells, of the cancer cells to propagate, allowing the quantitative analysis of the relevance of the hallmarks in different scenarios. As mentioned in Chapter 3, Hanahan and Weinberg [40] stated that, in addition to providing a solid basis for cancer research, the hallmarks have served to identify certain cell functions that have become therapeutic targets with the idea that simultaneous targeting of two or more hallmark pathways may be a more effective approach to therapy. Along this line, our study in Chapter 3 about the relative importance of the hallmarks in tumor cells proliferation indicates the importance of targeting therapies to the genetic networks and molecular pathways that control such most relevant hallmarks in each environmental multicellular system situation.

Moreover, we focused on the analysis of the effect of killing cancer cells, inspecting the time evolution of the multicellular system under such conditions and the possible behavioral transitions between the predominance of cancer and healthy cells (Chapter 3, Section 4). For example, the model shows that, in situations where cells at the tumor boundary drive tumor expansion, there are no significant differences between the consideration of killing all cancer cells and killing only cancer cells at the boundary or the tumor. As remarked in Chapter 3, that analysis represents an alternative to the "in-vitro" experiments focused on the study of the comparative effects of different drugs or drug combinations [22][63], since it indicates that these "in-vitro" studies should also search for possible behavior transitions when drugs are applied.

Later, the previously commented conditions defined by the relative prevalence of different hallmarks, were incorporated in the simulation of cancer stem cells (Chapter 4). The CSCs can regenerate the proliferation of cancer cells when the non-stem cancer cells, with the appropriate hallmarks acquired, find advantageous scenarios. The simulations showed how the increase of non-stem cancer cells is faster after a treatment that targets differentiated cancer cells, since CSCs have more opportunities to differentiate. This is in agreement with the clinical observations describing increased growth speed and enhanced invasion in the relapsing malignancy [93]. The importance of the simulations is that these provide the reason and an easy explanation of the faster regrowth behavior.

Moreover, the effects of different treatment strategies were analyzed by using continuous low-intensity treatments and periodic high-intensity treatments. The first alternative presents an advantage since continuous low-intensity treatment does not favor CSC proliferation and differentiation, allowing an easy control of a possible future tumor regrowth. On the other hand, the discontinuous periodic treatments with high intensity levels favor CSC proliferation and differentiation in the short term, and consequently favors a possible future tumor regrowth. Therefore, the analysis performed in the thesis indicates that making CSC proliferation more difficult is a key point to consider, especially in the immediate period after a standard treatment in order to prevent the spread of non-stem cancer cells.

The analyses of the treatment strategies applied in a cancer stem cell context (Chapter 5) indicate several key aspects:

1. Using only standard treatments, which only eliminate rapid prolifer-

ating non-stem cancer cells, not only do not stop possible future regrowths as consequence of the presence of CSCs, but facilitates that the regrowth is faster.

2. A differentiation therapy for CSCs in combination with a standard treatment can better control the future regrowth, but the relative timing of the two treatment strategies is determinant, since CSC differentiation produces non-stem cancer cells that can promote rapid tumor proliferations.

3. The ideal treatment should difficult CSC proliferation, especially after the immediate application of a standard treatment, and the analyses indicate that a low-intensity standard treatment is better for making more difficult CSC proliferation and differentiation. As stated by Enderling and Hahnfeldt [25] "If detected early, tumors could potentially be maintained at a non-advancing equilibrium by reinforcing the ability of non-stem cells to competitively suppress CSC proliferation". So, as indicated by Han et al. [38], targeting CSC niche and the quiescent state of CSCs is a therapeutic possibility since "Maintaining the cells in a quiescent state by blocking specific receptors and signaling pathways within the CSC niche can inhibit CSC functions of tumor initiation and metastasis". Our analyses show that this is one of the most important factors to control, which was not intensively considered.

Finally, we used evolutionary computing to analyze the implications of treatment strategies taking into account the presence of CSCs (Chapter 6). In this way, we determined the best strategies of treatment applications in terms of intensity, duration and periodicity considering the regrowth capacity of CSCs. We considered that the best treatment is the one that, with the less possible intensity minimizes to a great extent the future regrowth capability of CSCs. The intensity was measured as the summation of the percentage of DCCs killed in each iteration. The analyses showed that, in order to make more difficult CSC proliferation and consequently their differentiation, treatments with high intensities should be avoided. These ones promote CSC proliferation and differentiation, making more difficult the control of the final number of DCCs as consequence of the fast regrowth of these DCCs. The best evolved treatments follow this pattern avoiding high intensities, always with the objective to avoid CSC proliferation and therefore their differentiation in order to minimize their future effect on a possible tumor recurrence. Moreover, the optimized treatments correspond to those maintained during very few days and with longer periods than the ones used in standard treatments.

The work done in this thesis could be further developed in a number of ways. One of them is extending the computational model to consider angiogenesis and cell migration (translation of cells from one location to another). We have not considered these two aspects because we analyzed only the avascular phase. For example, the inclusion of metastasis and motility for CSCs could provide insights about other aspects, such as possible morphologies of the growing tumor, as studied, for example, in the work of Sottoriva et al. [93] in order to analyze the different infiltrative morphologies beyond the borders of the main tumor mass.

Another topic to explore in more detail is the use of evolutionary multi-objective algorithms for treatment optimization, as explained in Chapter 6. In this chapter we used mono-objective optimization for optimizing cancer

treatments in terms of intensity, duration and periodicity in a CSC context. This can be improved using a multi-objective approach for searching the Pareto Set of non-dominated individuals regarding the treatments that minimize the total intensity applied as well as the final number of DCCs.

Finally, little is known about the theoretical aspects of the behavior of the multicellular system, in terms of information theory. Studies should be performed on the situation once a tumor growth behavior has been obtained, at its origin, and at the intermediate stages. The characterization of the different behaviors could be done using a qualitative and quantitative study of the time evolution of cell colonies in the different behavioral regimes. For the quantitative analysis, classic information theory measures could be used, such as entropy and mutual information, through the study of the time evolution of the cells in the lattice environment, taking into account the state distribution (related to the presence of hallmarks) of cells in the lattice and the time evolution of such distributions. This analysis will be especially interesting under the threshold conditions that determine the outcome of different behavioral regimes, that is, these conditions will determine the presence or not of a tumor. So, this analysis would allow us to thoroughly study the dynamic process in the frontier conditions that lead to cancer.

Appendix A

Publications of the thesis

Journals

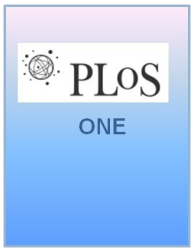

Á. Monteagudo and J. Santos. "Treatment analysis in a cancer stem cell context using a tumor growth model based on cellular automata". *PLOS ONE* doi: 10.1371/journal.pone.0132306, 10 (7), 2015 (Impact Factor: 3.234).

J. Santos and Á. Monteagudo. "Analysis of behaviour transitions in tumour growth using a cellular automaton simulation". *IET Systems Biology.* doi: http://dx.doi.org/10.1049/iet-syb.2014.0015 9(3):75 – 87, 2015 (Impact Factor: 1.059).

Á. Monteagudo and J. Santos. "Studying the capability of different cancer hallmarks to initiate tumor growth using a cellular automaton simulation. Application in a cancer stem cell context". *Biosystems* doi: 10.1016/j.biosystems.2013.11.001115, 115:46-58. 2014 (Impact Factor: 1.548).

Book chapters

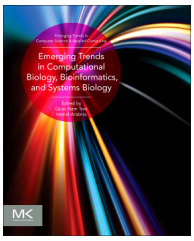

J.Santos and Á. Monteagudo. "Tumor growth emergent behavior analysis based on cancer hallmarks and in a cancer stem cell context". *Emerging Trends in Computational Biology, Bioinformatics and Systems Biology. Q-N. Tran & H.R. Arabnia (Eds.)* 2015 (In Press).

International conferences

Á. Monteagudo and J. Santos. "Evolutionary optimization of cancer treatments in a cancer stem cell context". *Proceedings of the 2015 Genetic and Evolutionary Computation Conference (GECCO 2015), ACM,* pages 233–240, 2015 (Best paper of the Biological and Biomedical Applications track) (Core A).

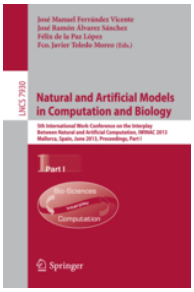

Á. Monteagudo and J. Santos. "Cancer stem cell modeling using a cellular automaton". *Proceedings IWINAC 2013 - International Work-Conference on the Interplay between Natural and Artificial Computation, Lecture Notes in Computer Science*, 7931:21–31, 2013.

Á. Monteagudo and J. Santos. "A cellular automaton model for tumor growth simulation". *Advances in Intelligent and Soft-Computing - Proceedings 6th International Conference on Practical Applications of Computational Biology & Bioinformatics*, 154:147–155, 2012.

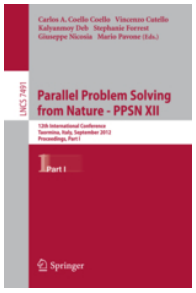

J. Santos and Á. Monteagudo. "Study of cancer hallmarks relevance using a cellular automaton tumor growth model". *Proceedings PPSN 2012 - Parallel Problem Solving from Nature-PPSN XII - Lecture Notes in Computer Science*, 7491:489-499, 2012 (Core A).

Appendix B

The graphical user interface

All the simulations and options commented in the thesis were incorporated in a simulation environment for the testing of the experiments. The whole project was programmed in the C# language using the Microsoft Visual Studio 2008 environment. Figure B.1 shows the main interface window of the environment. The interface was divided in two main parts: *Simulation* and *Evolution*.

In the *Simulation* panel the user can set the parameters of the simulation. Below the list of parameters is presented:

- *Simulation parameters* panel:
  - Grid size: it represents the total number of the cells of the grid.
  - Max iters: it represents the maximum number of iterations of the Cellular Automata. The simulation ends before this iteration if the event queue is empty.
- *Hallmark parameters* panel: in this panel the parameters that control the hallmarks can be set. The default parameters are presented as default values.
- *Visualization panel*: this panel has different options that allow the user set visual information. The user can set whether the tumor growth is displayed step by step (the graph is updated every 50 iterations by default) or at the end of the simulation. Moreover, in this panel, the user can save in a file an image in 3-D or 2-D in "PNG" format (figures B.2 and B.3). In the 3-D view, each cell is rendered as a small cube. The cube is colored according to the "genotype" of the cell it represents. There are 32 colors corresponding with the 32 possible combinations of mutations (hallmarks acquired) in the "genotype".

Once the parameters are filled the *Run* button is pressed to begin the simulation.

At the right side of the main window, the *Evolution environment* is located. In the panel *Differential Evolution parameters* the user can set the different parameters of the Differential Evolution optimization method. Here the list of parameters is presented:

- Population Size: the size of the population (must be greater than 4).
- Generations: optimization is ended by the specified number of generations set by user in this field.
- Grid size: it represents the total number of the cells of the grid.
- Max iters CA: it represents the maximum iterations of the Cellular Automaton.
- Num Evaluations CA: the number of evaluations applied to each individual of the population. Given the stochastic nature in each run of the cellular automaton and consequently in the fitness evolution, the fitness is averaged with that number of independent evaluations of the cellular automaton.
- DE Crossover probability (CR): the crossover probability parameter.
- DE Weight Factor (F): the differential weight parameter.
- Fitness Function. The user can select different objective functions to optimize: cancerous-healthy cells difference, number of total cells, average distance to the center, number of healthy cells, number of cancerous cells. In the thesis, only the fitness commented in Chapter 6 was used to optimize treatment applications.
- Type: the user can select maximize or minimize.

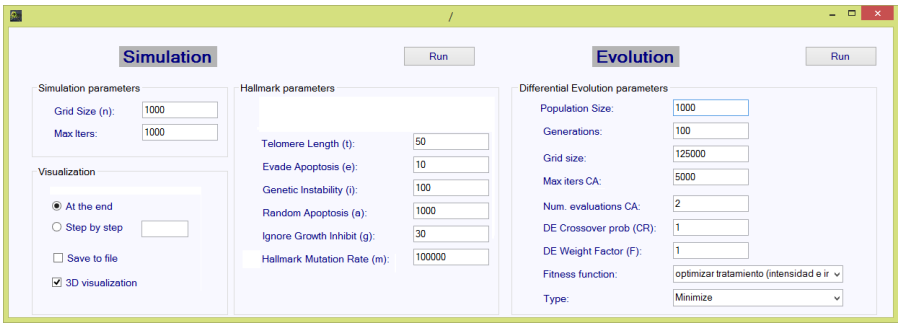

Figure B.1: Main panel of the simulator.

Figures B.2 and B.3 present the windows of the simulator that show the final result of the multicellular system after a cellular automaton run with a 3D and 2D representation respectively. To view the final grid state from a different angle the user can use the slider control *Rotations (X,Y,Z)* located at the lower part of the window. Moreover, for a better visualization, the user can zoom in by clicking the control slider *Zoom* and also can choose the type of cells displayed (all cells, only cancer cells or only healthy cells).

The environment allows to see graphically the evolution over time of different parameters as Figure B.4 shows. In the *Cellular system time evolution*

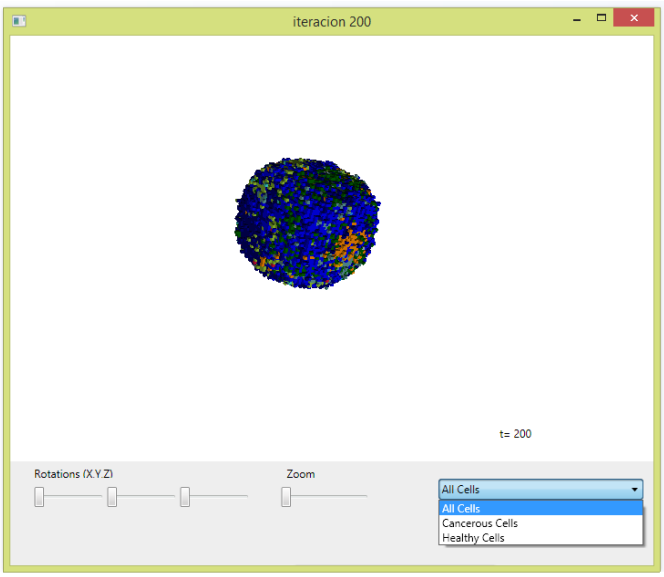

Figure B.2: Window of the simulator, that shows the final grid state with a 3D representation.

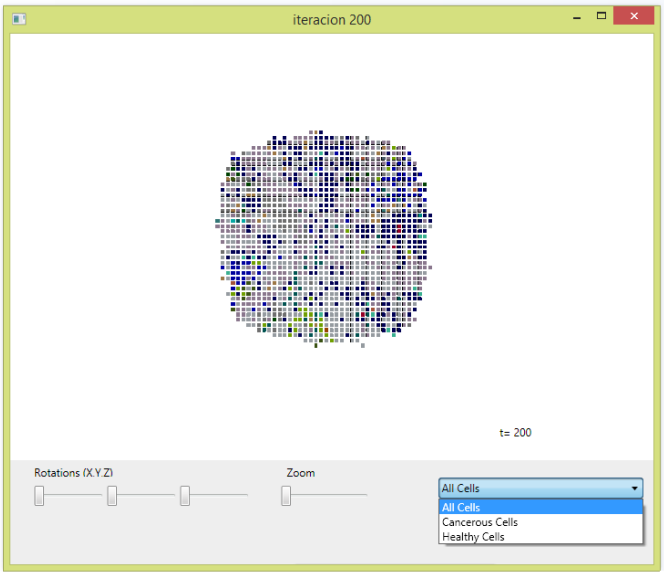

Figure B.3: Window of the simulator, that shows the final grid state with a 2D representation (plane that crosses the center of the grid).

panel the evolution over time of the hallmarks is shown (number of hallmarks acquired in all the cells) is displayed. In addition, if the checkbox *Show All* is checked then the evolution of the cancer and healthy cells is also shown. In the

Evolution graphics panel the evolution of the best fitness and average fitness over generations is displayed.

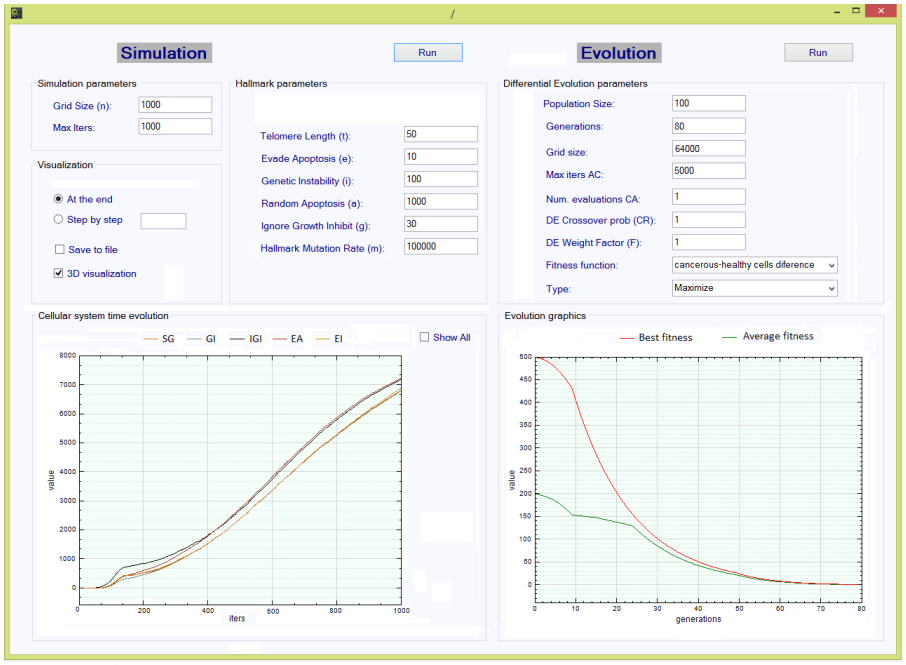

Figure B.4: Window of the simulator, that shows the evolution of hallmarks and cell types (associated to the Simulation part) and the evolution of the best and average fitness (associated with the Evolution part).

In accordance with the Regulations of the Ph.D. studies passed by the Governing Council of the University of A Coruña at its meeting of July 17, 2012, it is reproduced below a summary of this thesis in Spanish.

Appendix C

Resumen

C.1 Motivación

En esta tesis se ha realizado un modelado del crecimiento tumoral, considerando éste consecuencia emergente de las interacciones entre las células y su entorno. El modelado se ha considerado en el nivel de comportamiento celular, modelando los procesos de mitosis y muerte celular en función de la adquisición de una serie de rasgos característicos del cáncer (*hallmarks*) y del entorno inmediato de cada célula.

El cáncer es una enfermedad genética que, en el paradigma estándar, aparece como consecuencia de diversas mutaciones en células somáticas [33]. Estas mutaciones alteran el control de proliferación de las células que desemboca en una división celular descontrolada. Hanahan y Weinberg describieron las diferencias fenotípicas entre las células sanas y las cancerosas en un artículo titulado "The Hallmarks of Cancer" [39] y su revisión en 2011 [40]. Las seis alteraciones esenciales en la fisiología celular que colectivamente dictaminan el crecimiento maligno son: autosuficiencia en las señales de crecimiento, insensibilidad a las señales inhibidoras del crecimiento, la evasión de la muerte celular programada (apoptosis), potencial de replicación ilimitado, angiogénesis sostenida, e invasión de tejidos y metástasis, junto a la propiedad de inestabilidad genética que facilita la adquisición de los rasgos característicos.

Para el modelado hemos considerado la herramienta de Autómata Celular (AC), herramienta introducida por von Neumann para estudiar procesos de auto-replicación, y que ha sido aplicada además para estudiar el comportamiento emergente junto con la caracterización de sistemas complejos [2][46][51][52]. Un AC está formado por un espacio de n dimensiones dividido en un conjunto de celdas, en el que cada una de éstas puede encontrarse en dos o más estados. Las reglas que definen el AC determinan cuál es el siguiente estado de cada celda, en función del valor de las celdas consideradas en su "vecindad". Como indica Ilachinski [46], los ACs han sido el foco de atención por su habilidad de generar un amplio espectro de patrones de comportamiento en función de conjuntos de reglas definitorias relativamente simples, y además han mostrado la capacidad de capturar características esenciales de comportami-

entos cooperativos auto-organizativos complejos observados en sistemas reales.

La aproximación tradicional para modelar el crecimiento tumoral ha sido el uso de ecuaciones diferenciales para definir el estado previo al crecimiento vascular, e incluso en el estado de creación de nuevos vasos sanguíneos. Como indican Patel y Nagl [76], la utilización de ecuaciones diferenciales asume automáticamente que el estado actual del sistema es una consecuencia de su estado global previo. En realidad, una célula individual se comporta de acuerdo a su inmediata localidad, no de acuerdo con el estado general del tumor, y los entornos locales son diferentes. O, como indican Wodarz y Komarova [103], entre las ventajas del uso de ecuaciones diferenciales ordinarias está su simplicidad. Las desventajas incluyen la ausencia de detalle. Por ejemplo, no se pueden describir interacciones espaciales, imponiendo la asunción de interacciones del tipo masa-acción. Aun utilizando ecuaciones diferenciales parciales, estas aproximaciones tienden a representar las células tumorales de un modo colectivo, utilizando típicamente un término de proliferación y un término de muerte celular, incluyendo funcionalidades específicas opcionales como la interacción de las células tumorales con su entorno local. Además, muchos modelos de este tipo presuponen que todas las células cancerosas han adquirido los mismos *hallmarks* [24]. Por contra, éste no es el caso de las aproximaciones con autómatas celulares, en las cuales el estado de cada célula se define en función de su entorno o vecindad local.

La tesis considera el modelo de "hallmarks" para definir el estado de cada célula, situándonos por tanto en el estudio del comportamiento a nivel celular, sin entrar en los niveles inferiores molecular, genético o epigenético. En la intensa investigación en modelado de cáncer, como indica Savage [88], los investigadores han tenido una tendencia a centrarse en los genes y las proteínas pero, para entender y combatir la enfermedad, debe ser vista como un sistema, en lugar de simplemente como un conjunto de actividades celulares. Así, el autor indica que el reciente énfasis en la genética y en las vías de señalización celular en las células individuales ha causado que muchos investigadores olviden la visión sistémica.

Teniendo en cuenta estas consideraciones se ha utilizado la abstracción que representa la presencia de los *hallmarks* adquiridos por las células, que son a su vez consecuencia de los niveles inferiores (por ejemplo diversas mutaciones en oncogenes y genes supresores de tumores en las divisiones celulares), pero con una visión a nivel de interacciones celulares, permitiendo esa visión más integradora comentada por Savage. Pero dadas las interacciones entre los diferentes *hallmarks*, y la dependencia de estos de sus parámetros definitorios (probabilidades de aplicación, longitud inicial telómeros, ...), el comportamiento que se obtiene en el sistema multicelular es imposible de inferir intuitivamente o analíticamente. Es decir, estamos ante un ejemplo de comportamiento emergente, en el cual, aun conociendo las reglas de comportamiento e interacciones locales de los elementos constitutivos del sistema, no es posible inferir a priori el comportamiento resultante. Sin embargo, la simulación del comportamiento en cada célula, definido por un AC en función de los *hallmarks* adquiridos en cada célula, permite el análisis detallado de los posibles comportamientos emergentes mediante la iteración continua del AC a lo largo del tiempo y en cada célula individual.

Como indican Basanta y colaboradores [11], los modelos informáticos constituyen una herramienta exploratoria complementaria dada la complejidad de los procesos biológicos subyacentes y los requerimientos de tiempo involucrados en los experimentos biológicos tradicionales, a pesar incluso de que tales modelos computacionales son necesariamente una simplificación de la realidad. La biología computacional es una aproximación útil para el análisis de la dinámica evolutiva de los diferentes fenotipos en un tumor. En esta línea de utilización de las simulaciones en biología computacional se inscribe nuestro trabajo.

C.2 Estructura de las tesis

En el primer capítulo introductorio se ha explicado la motivación de la tesis, los trabajos previos con autómatas celulares en modelado de crecimiento tumoral y, particularmente, los pocos trabajos que han usado el modelo de *hallmarks* en la modelización. Se explican de modo somero los aspectos más representativos de la biología del cáncer, comentando los detalles más relevantes de cara a nuestra modelización, la explicación de los diferentes *hallmarks* considerados en la misma así como aspectos básicos sobre el ciclo celular y sobre rutas celulares. Se realiza también una introducción a la teoría de "Células madre del cáncer" (CMC), que sugiere que una minoría de células (CMC) es la responsable del desarrollo del inicio de un tumor y de su habilidad para metastizar y reaparecer (recidiva). El comportamiento y consecuencias de la presencia de CMC será incorporado en la modelización realizada en la tesis.

El segundo capítulo describe los detalles del modelado realizado con ACs para la simulación del comportamiento mitótico y apoptótico en cada célula. Se ha partido del modelo de eventos introducido por Abbot y colaboradores [1], aunque nuestro objetivo ha sido diferente al de esos autores, cuyo interés fue determinar las secuencias más probables de adquisición de *hallmarks* que terminan en un crecimiento tumoral. Nuestro interés se ha centrado siempre en el análisis de los diferentes comportamientos que se pueden obtener en el sistema multicelular. Se han considerado en la tesis cinco rasgos característicos: autosuficiencia en las señales de crecimiento, insensibilidad a las señales inhibidoras del crecimiento, la evasión del mecanismo de apoptosis, potencial de replicación ilimitado e inestabilidad genética. No se han considerado los rasgos característicos de angiogénesis y metástasis, ya que nuestra modelización siempre se ha focalizado en la primera etapa de crecimiento tumoral avascular. Los *hallmarks* están además determinados por parámetros definitorios que se explican en el capítulo. La simulación utiliza un modelo de retícula en 3D para situar espacialmente las células, y cada una de éstas tiene asociado un "genoma" artificial que determina si alguno de esos *hallmarks* considerados ha sido adquirido como consecuencia de mutaciones en la división celular.

El tercer capítulo estudia la aparición de posibles comportamientos en escenarios concretos que determinan la preponderancia de unos *hallmarks* sobre otros. Se eligen siempre escenarios característicos que conllevan un crecimiento tumoral. Se estudia y analiza la dependencia del comportamiento frente a condiciones de partida como el número de células iniciales consideradas en la retícula o el tamaño de retícula utilizado en la simulación. Se analiza el efecto de los principales parámetros que definen cada rasgo característico en

el comportamiento emergente, analizando la interdependencia entre diferentes *hallmarks* en el comportamiento final. Igualmente, se analiza la importancia relativa que puede tener un rasgo característico para obtener un comportamiento final de crecimiento tumoral, además del análisis de posibles transiciones en el comportamiento emergente cuando un agente terapéutico destruye células cancerosas (consideradas como tales cuando adquieren algún *hallmark*).

El cuarto capítulo incorpora la modelización de Células Madre del Cáncer. Las CMC tienen la capacidad de autorenovación y regeneración del tumor [34][98]. Si los tratamientos del cáncer no destruyen adecuadamente suficientes células madre cancerosas (como los tratamientos estándar actuales), el tumor puede reaparecer. Se ha analizado el comportamiento del crecimiento del tumor cuando las CMC se consideran en diferentes situaciones ambientales (que inducen la adquisición de diferentes *hallmarks*). El capítulo quinto analiza, en un contexto de presencia de CMC, diferentes estrategias de aplicación de tratamientos teniendo en consideración la capacidad de las CMC de regenerar un nuevo crecimiento futuro del tumor (recidiva).

Finalmente, el sexto capítulo considera la utilización de computación evolutiva para la optimización de un tratamiento contra células cancerosas diferenciadas (no CMC), teniendo de nuevo en cuenta el efecto futuro de regeneración del tumor por la presencia de las CMC. Se ha utilizado Evolución Diferencial [79] como método evolutivo robusto y contrastado en el campo, y se ha aplicado para la optimización de los tratamientos en cuanto a su periodo, intensidad y duración.

C.3 Conclusiones principales

Con la herramienta de simulación se han realizado diferentes pruebas. Primero, se ha chequeado si el comportamiento emergente es independiente de las condiciones iniciales del entorno celular en cuanto a su espacio libre disponible (capítulo 3). El comportamiento emergente depende solo de los parámetros asociados a los *hallmarks*, aunque las iteraciones temporales necesarias para obtener comportamientos estables dependen de esa condición inicial. Además, la experimentación muestra que el efecto de eliminación de los *hallmarks* es diferente dependiendo de la principal ventaja, con respecto a células sanas, de las células cancerosas para su proliferación, permitiendo un análisis cuantitativo de la relevancia relativa de los *hallmarks* en diferentes escenarios. Como se indicó en el capítulo 3, Hanahan y Weinberg [40] determinaron que, además de proveer una base sólida para la investigación en cáncer, los *hallmarks* han servido para identificar ciertas funciones celulares que se han convertido en dianas terapéuticas con la idea de que atacar simultáneamente dos o más vías de señalización celular puede ser un método más efectivo de terapia. En esta línea, el estudio en el capítulo 3 sobre la importancia relativa de los *hallmarks* en la proliferación de las células tumorales indica la importancia de terapias cuyas dianas sean las rutas moleculares y genéticas que controlan tales *hallmarks* más relevantes en cada situación ambiental del sistema multicelular. Butler [14], tomando como base nuestro trabajo, ha experimentado con la eliminación de los *hallmarks* en pares, tripletas y grupos de cuatro, también abstrayendo la eliminación de *hallmarks* por los efectos de drogas específicas y encontrando

que en algún caso la combinación incluso potenciaba el crecimiento, aunque en general, a más tratamientos aplicados, el crecimiento disminuía.

En el análisis de las posibles transiciones de comportamiento al eliminar células cancerosas, el modelo muestra que, en situaciones en las cuales la zona exterior del tumor dirige la expansión del mismo, no hay diferencias significativas entre la eliminación de cualquier célula cancerosa en el tumor y solo aquéllas del contorno exterior. Este análisis representa además una alternativa a los experimentos *in-vitro* focalizados en el estudio de los efectos comparativos de diferentes drogas o combinaciones de éstas [22][63], dado que indica que estos estudios *in-vitro* deben buscar también por posibles transiciones de comportamiento cuando se aplican diferentes drogas.

Cuando se incluye la simulación de CMC (capítulo 4), el modelado muestra cómo las CMC pueden regenerar un crecimiento tumoral cuando las células cancerosas diferenciadas (no CMC), con los *hallmarks* apropiados, encuentran escenarios ventajosos. Las simulaciones mostraron cómo el incremento de células cancerosas diferenciadas es más rápido después de un tratamiento que ataca a esas células diferenciadas, dado que las CMC tienen más oportunidades para diferenciarse. Esto está en consonancia con las observaciones clínicas que describen una regeneración posterior más rápida del tumor y una invasión acentuada de esa recidiva [93]. La importancia de las simulaciones es que éstas proveen la explicación sencilla en el análisis de ese comportamiento de regeneración más rápido del tumor.

El estudio de los efectos de diferentes estrategias de tratamientos, en el contexto de presencia de CMC, indica que la alternativa de tratamientos continuos de baja intensidad presenta una ventaja al no favorecer la proliferación y diferenciación de las CMC, lo que permite un control más fácil del posible recrecimiento futuro. Por contra, la aplicación de tratamientos periódicos y discontinuos con altas intensidades favorece la proliferación y diferenciación de las CMC en el futuro inmediato y, consecuentemente, favorecen el posible recrecimiento futuro del tumor. Por tanto, el análisis realizado en la tesis indica que dificultar la proliferación de las CMC es un punto importante a considerar, especialmente en el periodo inmediato después de un tratamiento estándar de cara a prevenir la expansión de células tumorales diferenciadas.

Los análisis de las estrategias de tratamientos aplicados en el contexto de presencia de CMC (capítulo 5) indican varios puntos clave:

1. La utilización de únicamente tratamientos estándar, que solo eliminan células diferenciadas que proliferan rápidamente, no solo elimina la posibilidad de posibles recrecimientos futuros como consecuencia de las CMC, sino que además facilita que la recidiva sea más rápida.

2. Un "tratamiento de diferenciación" de CMC en combinación con un tratamiento estándar puede controlar mejor el recrecimiento futuro, pero la planificación temporal de ambas estrategias es determinante, dado que la diferenciación de CMC produce células cancerosas diferenciadas que pueden promocionar rápidas proliferaciones de un tumor.

3. Finalmente, el tratamiento ideal debería dificultar la proliferación de CMC, especialmente después de la aplicación inmediata de un tratamiento estándar, y el análisis realizado indica que un tratamiento estándar de baja intensidad es mejor para dificultar la proliferación y diferenciación de las CMC.

Como indicaron Enderling y Hahnfeldt [25] "Si se detectan pronto, los tumores se pueden mantener potencialmente en un equilibrio de no avance por medio del reforzamiento de la habilidad de las células cancerosas diferenciadas de suprimir competitivamente la proliferación de las CMC". Por tanto, como han indicado Han y col. [38], atacando el nicho de las CMC y el estado quiescente de éstas es una posibilidad terapéutica ya que "Manteniendo las células en un estado quiescente por medio del bloqueo de receptores específicos y rutas metabólicas en el nicho de las CMC puede inhibir las funciones de iniciación tumoral y metástasis de las CMC". Nuestros análisis muestran que éste es uno de los factores más importantes a controlar y que no ha sido considerado intensivamente.

Finalmente, al utilizar computación evolutiva para la optimización de las estrategias de aplicación de un tratamiento en presencia de CMC (capítulo 6), teniendo en cuenta que la mejor estrategia de aplicación de un tratamiento estándar es aquélla que, con la menor intensidad posible minimiza en gran medida la futura capacidad de recrecimiento de las CMC, el análisis realizado indicó que, para dificultar la proliferación y diferenciación de las CMC, se deben evitar los tratamientos de alta intensidad. Estos promueven la proliferación y diferenciación de las CMC, haciendo más difícil el control del número final de células cancerosas diferenciadas como consecuencia de la capacidad de recrecimiento rápido de éstas. Los tratamientos optimizados mediante evolución simulada (para cada escenario particular) siguen este patrón de evitar altas intensidades, siempre con el objetivo de evitar la proliferación de las CMC y, por tanto, su diferenciación de cara a minimizar su futuro efecto de posible reaparición de un tumor. Además, los tratamientos optimizados especifican intervalos de mantenimiento de pocos días y con periodos de aplicación más espaciados que los de los tratamientos estándar.

Bibliography

[1] R.G. Abbott, S. Forrest, and K.J. Pienta. Simulating the hallmarks of cancer. *Artificial Life*, 12(4):617–634, 2006.

[2] C. Adami. *Introduction to Artificial Life*. Telos-Springer Verlag, 1998.

[3] A.V. Adamopoulos. CA2: In silico simulations of cancer growth using cellular automata. In *WSEAS Transactions on Systems 4(9)*, pages 1467–1473, 2005.

[4] M. Al-Hajj, M.S. Wicha, A. Benito-Hernández, S.J. Morrison, and M.F. Clarke. Prospective identification of tumorigenic breast cancer cells. *Proceedings of the National Academy of Sciences of the United States of America*, 100(7):3983–3988, 2003.

[5] T. Alarcón, H.M. Byrne, and P.K. Maini. A cellular automaton model for tumour growth in inhomogeneous environment. *Journal of Theoretical Biology*, 225:257–274, 2003.

[6] P. Anand, A.B. Kunnumakara, C. Sundaram, K.B. Harikumar, S.T. Tharakan, O.S. Lai, B. Sung, and B.B. Aggarwal. Cancer is a preventable disease that requires major lifestyle changes. *Pharmaceutical Research*, 25(9):2097–2116, 2008.

[7] A.R.A. Anderson, A.M. Weaver, P.T. Cummings, and V. Quaranta. Tumor morphology and phenotypic evolution driven by selective pressure from the microenvironment. *Cell*, 127:905–915, 2006.

[8] R.G. Bagley and B.A. Teicher. *Stem Cells and Cancer*. Humana Press, New York, USA, 2009.

[9] N. Bailon-Moscoso, J. C. Romero-Benavides, and P. Ostrosky-Wegman. Development of anticancer drugs based on the hallmarks of tumor cells. *Tumour biology*, 35:3981–3995, 2014.

[10] A. Bankhead and R.B. Heckendorn. Using evolvable genetic cellular automata to model breast cancer. *Genetic Programming and Evolvable Machines*, 8:381–393, 2007.

[11] D. Basanta, B. Ribba, E. Watkin, B. You, and A. Deutsch. Computational analysis of the influence of the microenvironment on carcinogenesis. *Mathematical Biosiciences*, 229:22–20, 2011.

[12] M. Baumann, M. Krause, and R. Hill. Exploring the role of cancer stem cells in radioresistance. *Nature Reviews Cancer*, 8:545– 554, 2008.

[13] J.H. Bielas, K.R. Loeb, B.P. Rubin, L.D. True, and L.A. Loeb. Human cancers express a mutator phenotype. *Proceedings of the National Academy of Sciences of the United States of America*, 103(48):18238–18242, 2006.

[14] J.L. Butler. *Using cellular automata and lattice Boltzmann. Methods to model cancer growth: Analysis of combination treatment outcomes.* PhD thesis, The University of Western Ontario, 2015.

[15] L.C. Cantley, W.S. Dalton, R.N. DuBois, O.J. Finn, P.A. Futreal, T.R. Golub, W.N. Hait, G. Lozano, J.M. Maris, W.G. Nelson, C.L. Sawyers, S.L. Schreiber, M.R. Spitz, and P.S. Steeg. AACR cancer progress report 2012. *Clinical Cancer Research*, 18(21):S1– 100, 2012.

[16] J.M. Chandler and E. Lagasse. Cancerous stem cells: deviant stem cells with cancer-causing misbehavior. *Stem Cell Research & Therapy*, 1(2), 2010.

[17] K. Chen, Y-H. Huang, and J-L. Chen. Understanding and targeting cancer stem cells: therapeutic implications and challenges. *Acta Pharmacologica Sinica*, 34:732–740, 2013.

[18] Colon cancer stages, http://www.cancer.gov/types/colorectal/hp/colon-treatment-pdq.

[19] S. Das and P.N. Suganthan. Differential evolution: A survey of the state-of-the-art. *IEEE Transactions on Evolutionary Computation*, 15(1):4–31, 2011.

[20] L.G. De Pillis and A. Radunskaya. The dynamics of an optimally controlled tumor model: A case study. *Mathematical and Computer Modelling*, 37(11):1221–1244, 2003.

[21] A. Dewanji, E.G. Luebeck, and S.H. Moolgavkar. A generalized Luria-Delbrück model. *Mathematical Biosciences*, 197(2):140–152, 2005.

[22] I. Dufau, C. Frongia, F. Sicard, L. Dedieu, P. Cordelier, F. Ausseil, B. Ducommun, and A. Valette. Multicellular tumor spheroid model to evaluate spatio-temporal dynamics effect of chemotherapeutics: application to the gemcitabine/chk1 inhibitor combination in pancreatic cancer. *BMC Cancer*, 12(15), 2012.

[23] M.M. Eisen. *Mathematical Models in Cell Biology and Cancer Chemotherapy.* Springer, Berlin-Heidelberg-New York, 1977.

[24] H. Enderling, M.A.J. Chaplain, and P. Hahnfeldt. Quantitative modeling of tumor dynamics and radiotherapy. *Acta Biotheoretica*, 58:341–353, 2010.

[25] H. Enderling and P. Hahnfeldt. Cancer stem cells in solid tumors: Is 'evading apoptosis' a hallmark of cancer? *Progress in Biophysics and Molecular Biology*, 106:391–399, 2011.

[26] V. Feoktistov. *Differential Evolution: In Search of Solutions*. Springer, New York, USA, 2006.

[27] S. Friberg and S. Mattson. On the growth rates of human malignant tumors: implications for medical decision making. *Journal of Surgical Oncology*, 65:284–297, 1997.

[28] S.N. Gardner. Scheduling chemotherapy: Catch 22 between cell kill and resistance evolution. *Journal of Theoretical Medicine*, 2(3):215–232, 2000.

[29] S.N. Gardner. Cell cycle phase-specific chemotherapy: computational methods for guiding treatment. *Cell Cycle*, 1:369–374, 2002.

[30] P. Gerlee and A.R.A. Anderson. An evolutionary hybrid cellular automaton model of solid tumour growth. *Journal of Theoretical Biology*, 246(4):583–603, 2007.

[31] J.L. Gevertz, G.T. Gillies, and S. Torquato. Simulating tumor growth in confined heterogeneous environments. *Physical Biology*, 5, 2008.

[32] M. Ghaemi, O. Naderi, and Z. Zabihinpour. A novel method for simulating cancer growth. *Lecture Notes in Computer Science*, 6350:142–158, 2010.

[33] W.W. Gibbs. Untangling the roots of cancer. *Scientific American*, 289:56–65, 2003.

[34] J. Gil, A. Stembalska, K.A. Pesz, and M.M. Sasiadek. Cancer stem cells: the theory and perspectives in cancer therapy. *Journal of Applied Genetics*, 49(2):193–199, 2008.

[35] D.A. Guertin and D.M. Sabatin. Defining the role of mTOR in cancer. *Cancer Cell*, 12(1):9–22, 2007.

[36] C. Guiot, P. Delsanto, and T. Deisboeck. Morphological instability and cancer invasion: a 'splashing water drop' analogy. *Theoretical Biology and Medical Modelling*, 4(4), 2007.

[37] G. Hamilton. Multicellular spheroids as an in vitro tumor model. *Cancer Letters*, 131(1):29–34, 1998.

[38] L. Han, S. Shi, T. Gong, Z. Zhang, and X. Sun. Cancer stem cells: therapeutic implications and perspectives in cancer therapy. *Acta Pharmaceutica Sinica B*, 3(2):65–75, 2013.

[39] D. Hanahan and R.A. Weinberg. The hallmarks of cancer. *Cell*, 100:57–70, 2000.

[40] D. Hanahan and R.A. Weinberg. Hallmarks of cancer: The next generation. *Cell*, 144(5):646–674, 2011.

[41] L. Hayflick. The limited in vitro time of human diploid cell strains. *Experimental Cell Research*, 37:614–636, 1965.

[42] T. Hillen, H. Enderling, and P. Hahnfeldt. The tumor growth paradox and immune system-mediated selection for cancer stem cells. *Bulletin of Mathematical Biology*, 75(1):161–184, 2013.

[43] S. Hosemann. Stage ii colon cancer: Adjuvant therapy? http://www2.mdanderson.org/depts/oncolog/sp/articles/10/10-oct/10-10-compass.html.

[44] Y. Hu and L. Fu. Targeting cancer stem cells: a new therapy to cure cancer patients. *American Journal of Cancer Research*, 2(3):340–356, 2012.

[45] J. Huang, L. Zhang, J. Greshock, T.A. Colligon, Y. Wang, R. Ward, D. Katsaros, H. Lassus, R. Butzow, A.K. Godwin, J.R. Testa, K.L. Nathanson, P.A. Gimotty, G. Coukos, B.L. Weber, and Y. Degenhardt. Frequent genetic abnormalities of the PI3K/AKT pathway in primary ovarian cancer predict patient outcome. *Genes Chromosomes Cancer*, 50:606–618, 2011.

[46] A. Ilachinski. *Cellular Automata. A Discrete Universe*. World Scientific, 2001.

[47] O.G. Isaeva and V.A. Osipov. Different strategies for cancer treatment: mathematical modeling. *Computational and Mathematical Methods in Medicine*, 40(4):253–272, 2009.

[48] A.R. Kansal, S. Torquato, G.R. Harsh, E.A. Chiocca, and T.S. Deisboeck. Simulated brain tumor growth dynamics using a three-dimensional cellular automaton. *Journal of Theoretical Biology*, 203:367–382, 2000.

[49] H. Korkaya, A. Paulson, F. Iovino, and M.S. Wicha. HER2 regulates the mammary stem/progenitor cell population driving tumorigenesis and invasion. *Oncogene*, 27(47):6120–6130, 2008.

[50] A.K. Laird. Dynamics of tumor growth. *British Journal of Cancer*, 18(3):490–502, 1964.

[51] C.G. Langton. Life at the edge of chaos. In *Artificial Life II, C.G Langton, C. Taylor, J.D. Farmer, S. Rasmussen (Eds.), Addison-Wesley*, pages 41–49, 1992.

[52] C.G. Langton. *Artificial Life: An Overview*. MIT Press, 1995.

[53] O. Lavi, M.M. Gottesman, and D. Levy. The dynamics of drug resistance: A mathematical perspective. *Drug Resistance Updates*, 15(1-2):90–97, 2012.

[54] A. Leary, E. Auclin, P. Pautier, and C. Lhomme. The PI3K/Akt/mTOR pathway in ovarian cancer: Biological rationale and therapeutic opportunities. In I. Díaz-Padilla, editor, *Ovarian Cancer - A Clinical and Translational Update*. Intech, 2013.

[55] K.R. Loeb and L.A. Loeb. Genetic instability and the mutator phenotype. *Am J Pathol.*, 154(6):1621–1626, 1999.

[56] J. Luo, N.L. Solimini, and S.J. Elledge. Principles of cancer therapy: Oncogene and non-oncogene addiction. *Cell*, 136(5):823–837, 2009.

[57] H. Ma, Q. Jiang, S. Han, Y. Wu, J.C. Tomshine, D. Wang, Y. Gan, G. Zou, and X. Liang. Multicellular tumor spheroids as an in vivo-like tumor model for three-dimensional imaging of chemotherapeutic and nano material cellular penetration. *Molecular Imaging*, 11(6):487–498, 2012.

[58] Hayat M.A. *Stem Cells and Cancer Stem Cells. Therapeutic Applications in Disease and Injury*, volume 11. Springer, New York, USA, 2014.

[59] M. Malumbres. Oncogene-induced mitotic stress: p53 and prb get mad too. *Cancer cell. doi: 10.1016/j.ccr.2011.05.023.*, 19(6):691–692, 2011.

[60] Everything maths & science. The cell cycle. http://everythingmaths.co.za/science/lifesciences/grade-10/03-cell-division/03-cell-division-02.cnxmlplus.

[61] M. F. McGuire, H. Enderling, D. I. Wallace, J. Batra, M. Jordan, S. Kumar, J. C. Panetta, and E. Pasquier. Formalizing an integrative multidisciplinary cancer therapy discovery workflow. *Cancer Research*, 73(20):6111 – 6117, 2013.

[62] R. Meza, J. Jihyoun, S.H. Moolgavkar, and E.G. Luebeck. Age-specific incidence of cancer: phases, transitions, and biological implications. *PNAS - Proceedings of the National Academy of Sciences of the United States of America*, 105:16284–16289, 2008.

[63] A.S. Mikhail, S. Eetezadi, and C. Allen. Multicellular tumor spheroids for evaluation of cytotoxicity and tumor growth inhibitory effects of nanomedicines in vitro: A comparison of docetaxel-loaded block copolymer micelles and taxotere®. *PLOS ONE*, 8(4), 2013.

[64] A.I. Minchinton and I.F. Tannock. Drug penetration in solid tumours. *Nature Reviews Cancer*, 6:583–592, 2006.

[65] Á. Monteagudo and J. Santos. A cellular automaton model for tumor growth simulation. *Advances in Intelligent and Soft-Computing - Proceedings 6th International Conference on Practical Applications of Computational Biology & Bioinformatics*, 154:147–155, 2012.

[66] Á. Monteagudo and J. Santos. Cancer stem cell modeling using a cellular automaton. *Proceedings IWINAC 2013 - International Work-Conference on the Interplay between Natural and Artificial Comutation, Lecture Notes in Computer Science*, 7931:21–31, 2013.

[67] Á. Monteagudo and J. Santos. Studying the capability of different cancer hallmarks to initiate tumor growth using a cellular automaton simulation. Application in a cancer stem cell context. *Biosystems*, 115:46–58, 2014.

[68] Á. Monteagudo and J. Santos. Evolutionary optimization of cancer treatments in a cancer stem cell context. *Proceedings of the 2015 on Genetic and Evolutionary Computation Conference, ACM*, pages 233–240, 2015.

[69] Á. Monteagudo and J. Santos. Treatment analysis in a cancer stem cell context using a tumor growth model based on cellular automata. *PlOS ONE. doi: 10.1371/journal.pone.0132306*, page 233–240, 2015.

[70] S. Moolgavkar and A. Knudson. Mutation and cancer: a model for human carcinogenesis. *Journal of the National Cancer Institute*, 66:1037–1052, 1981.

[71] C. I. Morton, L. Hlatky, P. Hahnfeldt, and H. Enderling. Non-stem cancer cell kinetics modulate solid tumor progression. *Theoretical Biology and Medical Modelling*, 8:48, 2011.

[72] National Cancer Institute. www.cancer.gov.

[73] L. Norton. Theoretical concepts and the emerging role of taxanes in adjuvant therapy. *Oncologist*, 6(3):30–35, 2001.

[74] L. Norton and R. Simon. Tumor size, sensitivity to therapy, and design of treatment schedules. *Cancer Treatment Reports*, 61(7):1307–1317, 1977.

[75] M. Osaki, M. Oshimura, and H. Ito. PI3K-Akt pathway: its functions and alterations in human cancer. *Apoptosis*, 9(6):667–76, 2004.

[76] M. Patel and S. Nagl. *The Role of Model Integration in Complex Systems Modelling. An Example from Cancer Biology.* Springer-Verlag, 2010.

[77] Y.T. Phung, D. Barbone, V.C. Broaddus, and M. Ho. Rapid generation of in vitro multicellular spheroids for the study of monoclonal antibody therapy. *Journal of Cancer*, 2:507–514, 2011.

[78] K.V. Price and R.M. Storn. Differential evolution - a simple and efficient heuristic for global optimization over continuous spaces. *Journal of Global Optimization*, 11(4):341–359, 1997.

[79] K.V. Price, R.M. Storn, and J.A. Lampinen. *Differential Evolution. A Practical Approach to Global Optimization.* Springer - Natural Comp. Series, 2005.

[80] K.A. Rejniak and A.R.A. Anderson. Hybrid models of tumor growth. *Wiley Interdisciplinary Reviews - Systems Biology and Medicine*, 3:115–125, 2011.

[81] M.W. Retsky, D.E. Swartzendruber, R.H. Wardwell, and P.D. Bame. Is Gompertzian or exponential kinetics a valid description of individual human cancer growth? *Medical Hypotheses*, 33:95–106, 1990.

[82] B. Ribba, T. Alarcon, K. Marron, P.K. Maini, and Z. Agur. The use of hybrid cellular automaton models for improving cancer therapy. *Proceedings, Cellular Automata: 6th International Conference on Cellular Automata for Research and Industry, ACRI 2004, Amsterdam, The Netherlands, P.M.A. Sloot, B. Chopard, A.G. Hoekstra (Eds.), Lecture Notes in Computer Science*, 3305:444–453, 2004.

[83] L. Ricci-Vitiani, D.G. Lombardi, E. Pilozzi, M. Biffoni, M. Todaro, C. Peschle, and R. De Maria. Identification and expansion of human colon-cancer-initiating cells. *Nature*, 445(7123):111–115, 2007.

[84] I.A. Rodríguez-Brenes, N.L. Komarova, and D. Wodarz. Tumor growth dynamics: insights into evolutionary processes. *Trends in Ecology and Evolution*, 28:597–604, 2013.

[85] J. Santos and Á. Monteagudo. Study of cancer hallmarks relevance using a cellular automaton tumor growth model. *Proceedings PPSN 2012 - Parallel Problem Solving from Nature - Lecture Notes in Computer Science*, 7491:489–499, 2012.

[86] J. Santos and Á. Monteagudo. Analysis of behaviour transitions in tumour growth using a cellular automaton simulation. *IET Systems Biology*, 9(3):75 – 87, 2014.

[87] J. Santos and Á. Monteagudo. Tumor growth emergent behavior analysis based on cancer hallmarks and in a cancer stem cell context. In *Emerging Trends in Computational Biology, Bioinformatics, and Systems Biology*. Q-N. Tran & H.R. Arabnia (Eds.) Elsevier/MK (In Press), 2015.

[88] N. Savage. Modelling: Computing cancer. *Nature*, 491:S62–S63, 2012.

[89] A. Seluanov, C. Hine, J. Azpurua, M. Feigenson, M. Bozzella, Z. Mao, K. Catania, and V. Gorbunova. Hypersensitivity to contact inhibition provides a clue to cancer resistance of naked mole-rat. *PNAS - Proceedings of the National Academy of Sciences of the United States of America*, 106(46):19352–19357, 2009.

[90] S.E. Shackney. A computer model for tumor growth and chemotherapy, and its application to l1210 leukemia treated with cytosine arabinoside (nsc-63878). *Cancer Chemotherapy Reports*, 54:399–429, 1970.

[91] R. Simon and L. Norton. The Norton-Simon hypothesis: designing more effective and less toxic chemotherapeutic regimens. *Natura Clinical Practice Oncology*, 3(8):406–407, 2006.

[92] R. Solé and B. Goodwin. *Signs of Life. How Complexity Pervades Biology*. Basic Books, 2000.

[93] A. Sottoriva, J. Verhoeff, T. Borovski, S.K. McWeeney, L. Naumov, J.P. Medema, P. Sloot, and L. Vermeulen. Cancer stem cell tumor model reveals invasive morphology and increased phenotypical heterogeneity. *Cancer Research*, 70(1):46–56, 2010.

[94] S.L. Spencer, R.A. Gerety, K.J. Pienta, and S. Forrest. Modeling somatic evolution in tumorigenesis. *Plos Computational Biology*, 2(8):939–947, 2006.

[95] G.W. Swan. Role of optimal control theory in cancer chemotherapy. *Mathematical Biosciences*, 101(2):237–84, 1990.

[96] A. Swierniak, M. Kimmel, and J. Smieja. Mathematical modeling as a tool for planning anticancer therapy. *European Journal of Pharmacology*, 625(1-3):108–121, 2009.

[97] A. Swierniak, A. Polanski, and M. Kimmel. Optimal control problems arising in cell-cycle-specific cancer chemotherapy. *Journal of Cell Proliferation*, 29(3):117–139, 1996.

[98] V. Vainstein, O.U. Kirnasovsky, Y. Kogan, and Z. Agur. Strategies for cancer stem cell elimination: Insights from mathematical modeling. *Journal of Theoretical Biology*, 298:32–41, 2012.

[99] M. Valcárcel, B. Arteta, A. Jaureguibeitia, A. Lopategi, I. Martínez, L. Mendoza, F. Muruzabaland, C. Salado, and F. Vidal-Vanaclocha. Three-dimensional growth as multicellular spheroid activates the proangiogenic phenotype of colorectal carcinoma cells via LFA-1-dependent VEGF: implications on hepatic micrometastasis. *Journal of Translational Medicine*, 6(57), 2008.

[100] F.J. Vara, E. Casado, J. de Castro, P. Cejas, C. Belda-Iniesta, and M. Gonzalez-Baron. PI3K/Akt signalling pathway and cancer. *Cancer Treatment Reviews*, 30(48):193–204, 2004.

[101] N.S. Vasudev and A.R. Reynolds. Anti-angiogenic therapy for cancer: current progress, unresolved questions and future directions. *Angiogenesis*, 17(3):471–494, 2014.

[102] D. Wodarz and N. Komarova. *Computational Biology of Cancer. Lecture Notes and Mathematical Modeling.* World Scientific, 2005.

[103] D. Wodarz and N. Komarova. Can loss of apoptosis protect against cancer? *Trends in Genetics*, 23(5):232–237, 2007.

[104] I.K.S. Yap, A. K. Radhakrishnan, and C.O. Leong. Current concepts in cancer research. *International e-Journal of Science, Medicine & Education*, 1(7):19–31, 2013.